INSTITUT FÜR VERFAHRENSTECHNIK DES INDUSTRIELLEN UMWELTSCHUTZES
Montanuniversität Leoben www.vtiu.com
Peter-Tunner-Straße 15 A-8700 Leoben

Diplomarbeit

# CIRCULATING FLUIDZED BED WITH EXTERNAL FLUIDIZED BED HEAT EXCHANGER

*BUILDING A COLD MODEL AND EXPERIMENTS*

Prepared for

**Austrian Energy and Evironment Co.**

**Authored by:**
Jungil KIM
9935260

**Supervisor/Reviewer:**
Dipl.-Ing. Dr.techn. Christian Weiß
O.Univ.Prof. Dipl.-Ing. Dr.mont. Werner L. Kepplinger

Leoben, 06.Oct. 2004

# EIDESSTATTLICHE ERKLÄRUNG

Ich erkläre an Eides statt, dass ich die vorliegende Diplomarbeit/Bakkalaureatsarbeit selbständig und ohne fremde Hilfe verfasst, andere als die angegebenen Quellen und Hilfsmittel nicht benutzt und die den benutzten Quellen wörtlich und inhaltlich entnommenen Stellen als solche erkenntlich gemacht habe.

# Abstract

This project was a joint venture between Austrian Energy and Environment Co. and the Institute of Process Technology and Industrial Environmental Protection. The aim was to build a downsized Circulating Fluidized Bed (CFB) cold model whose height is about 4.5 m based on the commercial CFB boiler at RV Lenzing of AVE Co. to investigate and optimize the current CFB boiler in Lenzing as well as any CFB boiler to be built in the future.
This paper includes the documentation of the installation and the sensoring system. Furthermore, the experimental results are documented, as there are the test operations of the built system, tests with a new designed siphon, bed material behavior in the external Fluidized bed Heat Exchanger (FHE) as well as in the CFB parts, the relationship of the mass rate of circulating particles with pressure drop in a riser and the influences of particle loading in the cyclone on the cyclone pressure drop.

# Kurzfassung

Dieses Projekt war ein Joint Venture zwischen Austrian Energy and Environment AG und dem Institut für Verfahrenstechnik des Industriellen Umweltschutzes. Das Ziel war ein kaltes Modell einer zirkulierenden Wirbelschicht (ZWS) zu bauen, dessen Höhe ca. 4.5 m beträgt, das auf dem kommerziellen ZWS-Dampfkessel in RV-Lenzing von AVE AG. basiert, um den gegenwärtigen ZWS-Dampfkessel in Lenzing sowie jeden möglichen zukünftig errichteten ZWS-Dampfkessel zu erforschen und weiter zu entwickeln.
Diese Diplomarbeit dokumentiert den Aufbau eines kalten Modells bzw. die Installation eines Messsystems. Ferner aber auch die experimentellen Resultate, wie Testbetriebe des errichteten Systems, Tests mit einem neu ausgelegten Siphon, Strömungsverhältnis des Bettmaterials im Fliessbettkühler sowie in der ZWS, die Beziehungen der Umlaufsmenge mit dem Druckabfall im Steigrohr, die Einflüsse der Partikelbeladung auf dem Zyklondruckabfall.

# Contents

# Introduction

The **C**irculating **F**luidized **B**ed (CFB) boiler with an external **F**luidized bed **H**eat **E**xchanger (FHE) has been successfully operating since 1998 at RV-Lenzing and can operate on various fuel resources and satisfies the flue gas emission limits.

However, some problems have been found since its start-up.

1. The function of siphon blocks, when the bed is operated with a high superficial velocity
2. Erosion and corrosion problems in the heat exchanging bundles by exhaust gas from the combustion chamber
3. Heat exchanging doesn't occur properly by the unwanted dead zone in the 2$^{nd}$ heating chamber of the FHE
4. Blockage of the gas distributor in the combustion chamber by foreign material in the fuel, such as stones, coins, wire etc.

To solve the number 1, a new siphon was designed, which is installed in our cold model for testing. For the number 4, Austria Energy and Environment Co.(AEE) has changed the design of the gas distributor in the combustion chamber in Lenzing. As a result, the nozzle shape and structure are changed. The newly designed nozzles are tested in our cold model by AEE but the results are not discussed in this paper, as they are not included in this project.

Beside the mentioned problems, in order to design a proper CFB boiler it is necessary to understand the flow behavior of the various fluidizing air flows in the combustion chamber (riser) as well as in the FHE, which cannot be changed arbitrarily in the commercial bed. The circulating amount of bed material is also important in order to adjust the system (e.g. temperature adjustment, heat exchanging etc).

For these reasons this project was conducted and focused on the building of a cold model to perform various experiments related with the particle flow in the CFB as well as in the FHE.

# Chapter 1.

# Theoretical background

## 1.1. Description of the commercial model in Lenzing

The consortium, AE&E and LEE, has installed a 110 MW CFB boiler for incinerating waste materials in Lenzing, Upper Austria and commercial operation started up in 1998. The plant can be operated not only with waste fuel such as a mixture of **R**efuse **D**erived **F**uel (RDF), packing material, rejects of paper mills, wood waste and sewage sludge but also with 100% bituminous coal, oil or natural gas. But the plant is normally operated only with waste material without any support fuels such as coal or oil. Due to the flexible fuel source and mixture, the calorific value of the fired fuel ranges from 6.5 up to 31 MJ/kg.

The combustion heat is removed in an external **F**luidized-bed **H**eat **E**xchanger (FHE) and a flue gas cleaning system is installed to meet emission requirements.

An interesting aspect of the plant is the use of exhaust air from the viscose fibre production plant, Lenzing Co., as combustion air, which contains $H_2S$ and $CS_2$.

### 1.1.1. Technical data

| | |
|---|---|
| Feed water temperature | 106 °C |
| Live steam temperature | 500 °C |
| Live steam pressure | 80 bar |
| Live steam mass flow | 129 t/h |
| Max. firing rate with waste fuels or hard coal | 110MW |
| Max. firing rate with natural gas or fuel oil | 55MW |
| Min. firing rate with a live steam temperature of 500 °C | 55MW |

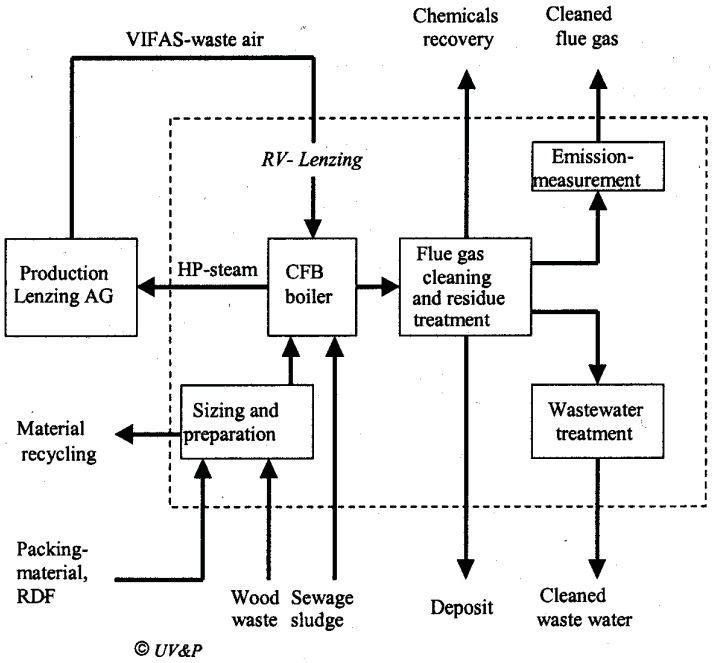


**Fig 1.1-1** Principle arrangement of the Lenzing plant [1]

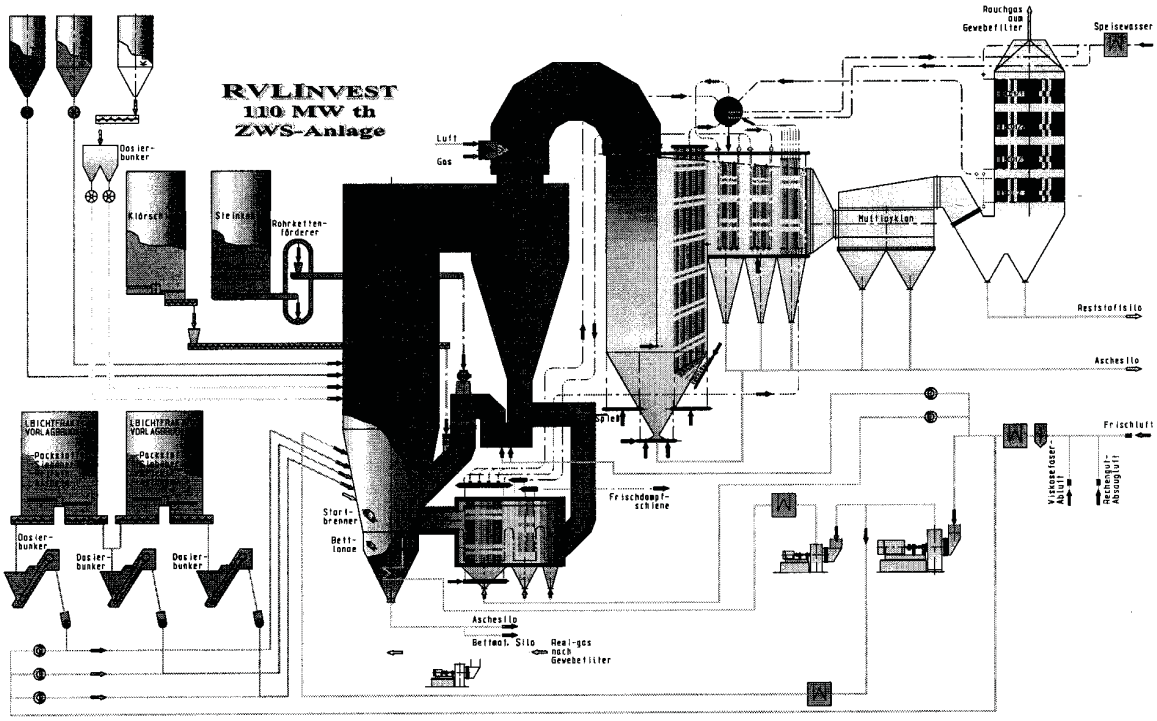


**Fig 1.1-2** Overview of the CFB-Boiler in Lenzing [1]

**Table 1.1-1** Properties of flue gas [1]

| Max. 0.5h mean value at all load cases | dimension | limit boiler exit | actual emission boiler exit | limit total plant | actual emission total plant |
|---|---|---|---|---|---|
| Dust (rel. to 11% $0_2$, dry) | $mg/Nm^3$ | | | | |
| $NO_x$ (rel. to 11% $0_2$, dry) | $mg/Nm^3$ | 300 | 70-120 | 70 | 35 |
| CO (rel. to 11% $0_2$, dry) | $mg/Nm^3$ | 45 | <1-10 | 50 | 2 |
| $C_{org.}$ (rel. to 11% $0_2$, dry) | $mg/Nm^3$ | 5 | 0.5 | 8 | 11 |
| $SO_2$ (rel. to 11% $0_2$, dry) | $mg/Nm^3$ | 2000 | 0-200 | 50 | 10 |
| $SO_3$ (rel. to 11% $0_2$, dry) | $mg/Nm^3$ | 40 | 5 | - | - |
| HF (rel. to 11% $0_2$, dry) | $mg/Nm^3$ | - | - | 0.3 | 0.02 |
| HCl (rel. to 11% $0_2$, dry) | $mg/Nm^3$ | - | 700-1600 | 7 | 1 |
| PCDD/PCDF (rel. to 11% $0_2$, dry) | $ng/Nm^3$ | 10 | <10 | 0.1 | 0.05 |

## 1.1.2. Components

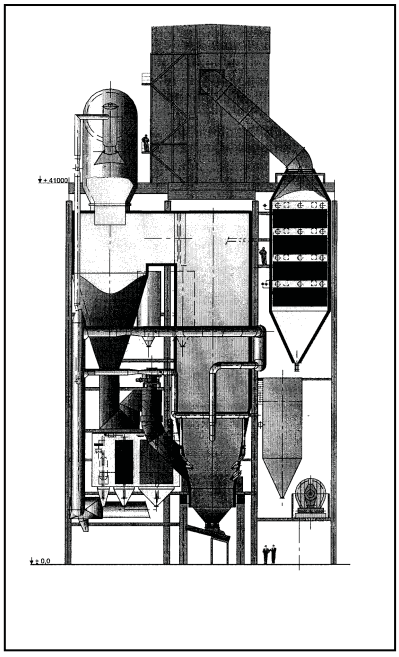

### CFB parts

By injecting the combustion air through a gas distributor at the bottom of the furnace, the bed inventory (nearly 100% quartz sand) forms a fluidized bed. High turbulence leads to an excellent combustion efficiency at relatively low temperatures of 870 to 880 °C.

A specific amount of bed material is carried out of the furnace with the flue gas. A cyclone separates the flue gas and the solid particles, which are re-circulated into the lower part of the combustion chamber.

Approx. 50% of combustion air is injected through the gas distributor at the bottom and the rest enters as secondary and tertiary air above the gas distributor. The operating temperature reaches 870-880 °C and therefore the formation of thermal NOx is inhibited. $SO_2$ in the flue gas can be captured by limestone dosing into the chamber.

The re-circulated flue gas, exhaust air from the viscose fibre production plant and cooled re-circulating bed material from FHE allow the compensation of different firing conditions according to different fuel conditions in the chamber

### External Fluidized bed Heat Exchanger part

The external **F**luid bed **H**eat **E**xchanger(FHE) cools down a branch flow of the circulating bed material before feeding it back into the combustion chamber. The heat of the bed material is transferred to the water-steam-path via a super heater and evaporator in in-bed tube banks.

The external fluidized bed exchanger consists of several refractory lined chambers, which are

working like small bubbling beds, separated by weirs. The hot branch flow of the circulating material from the loop seal first arrives in the so called empty chamber for equalizing the sand flow. In the next stage, the bed material flows into two heat exchanging chambers, wherein the in-bed heating surfaces of the water-steam-path are situated. Finally the cooled bed material returns to the combustion chamber via a fluidized canal.

## 1.2. Scale relationships

The main principle of scale relationships is based on the Pi-theorem. Through a dimensional analysis, different systems which share the same description by all of the independent dimensionless numbers are equivalent.

Consider the case where the bed in question is operated at an elevated temperature (e.g. 800°C) and at atmospheric pressure with air. The scale model is to be operated with air at ambient pressure and temperature. Then the air density of the cold bed is 3.5 times as large as the density of the hot bed. To maintain the ratio of particle to fluid interaction forces constant, the density of solid particles in the scaled cold bed must be 3.5 times as large as that of hot bed. With this calculated density of the model, the Archimedes number can be used to determine the particle diameter of the model. The Froude number is used to determine the superficial velocity. With the calculated particle diameter ($d_p$), the height (L) and diameter (D) of bed can be obtained, according to the ratio of $L/d_p$ or $D/d_p$; [2]

**Table 1.2-1** Scaling factors for proper modeling of hot bed performance [2]

| Variable | Hot Bed Variable ( 800°C ) | Scaled Cold Bed Variable ( 15°C ) |
|---|---|---|
| Superficial velocity | $u_{800}$ | 0.5 $u_{800}$ |
| Particle Diameter | $D_{p800}$ | 0.25 $d_{p800}$ |
| Particle Density | $\rho_{s800}$ | 3.5 $\rho_{s800}$ |
| Bed Dimension | $L_{800}$ | 0.25 $L_{800}$ |
| Bed Diameter | $D_{800}$ | 0.25 $D_{800}$ |
| Time | $t_{800}$ | 0.5 $t_{800}$ |

## 1.3. Bed material groups

The size of solid particles which can be fluidized varies greatly from less than 1 to 6 cm (2 1/2 in). It is generally concluded that particles distributed in sizes between 150 and 10 are the best for smooth fluidization (least formation of large bubbles). Large particles cause instability and give rise to slugging or massive surges. Small particles (less than 20 ) frequently, even though dry, act as if damp, forming agglomerates or fissures in the bed, or spouting. Adding finer sized particles to a coarse bed or coarser-sized particles to a bed of fines usually results in better fluidization. [4]

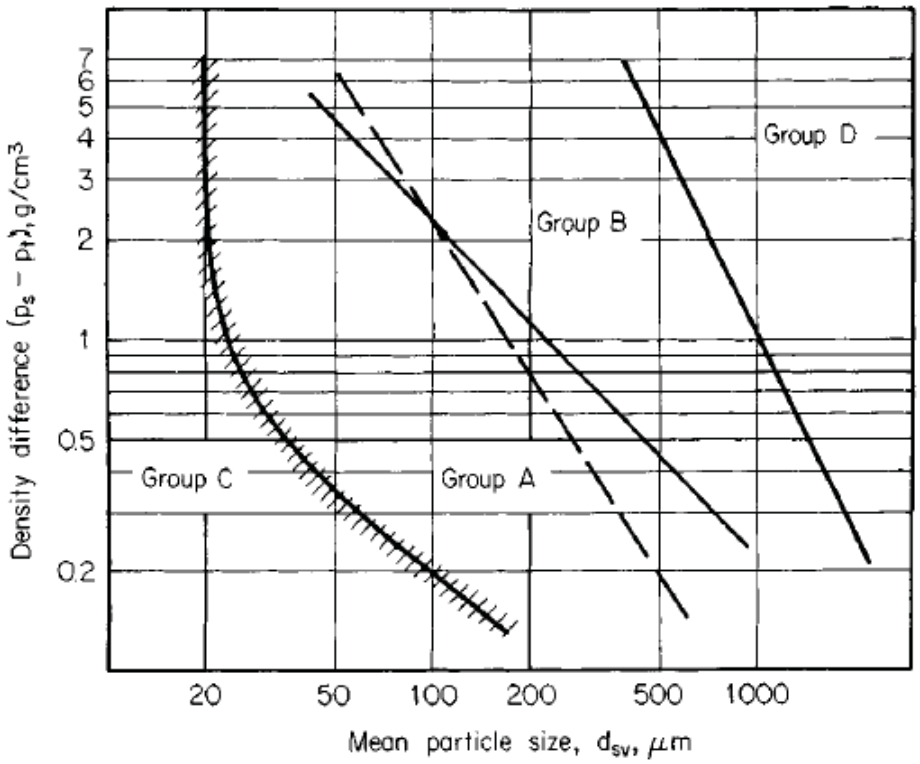


**Fig 1.3-1** Powder groups diagram for fluidization by air (ambient conditions); [4] from [3]

The properties of each group according to Geldart are following; [5] from [6], [7], [8].

### Group A

The particles have an average solid size between typically 20 - 100 and relative low density smaller than 1400 kg/m$^3$. The Bed expands to 2 – 3 times that of the minimal fluidized level before bubbles build up. At higher speeds, gas streams in the form of bubbles through the bed. The bubble rising speed for fluidized powders belonging to group A is larger compared to other gourps. The smaller and specific lighter the particles are, the bigger the cohesive forces between particles.

### Group B

The particles are about 40 – 500 and 1400 – 4500 kg/m$^3$ typically. After exceeding the minimal fluidized point, bubbles build up. They join together fiercely so that the bubbles with rising and increasing velocity accumulate. The cohesive forces between particles can be neglected as compared with streaming force.

### Group C

These consist of very small particles under 20 – 30 and are remarkably cohesive. The influence of cohesive force is greater than streaming force. Most of case, the complete bed is raised or some canals built up wherein the gas streams upward. In this case, the total pressure drop could be

remarkably smaller than the theoretical value.

**Group D**

Fluidized beds with coarse particle size, > ca. 600 , and high density need relative high gas velocity for fluidization. Although particle injection conditions are turbulent, bubbles rise with smaller velocity as void gas. i.e. gas flows throughout voids in the bed with slower velocity. The mixing of the particles is relatively bad and abrasion risk exists.

# 1.4. Fluidized bed

The introduction of gas from the bottom of a column containing solid particles via a gas distributor can cause the particles to be fluidized. As shown in **Fig 1.4-1**, the regimes are different according to supplied superficial velocity of fluidizing gas, which equals that of the volumetric flow rate of supplied fluidizing air divided by the cross-sectional area.

## 1.4.1. Regimes of particle fluidization

When gas is passed upward through a bed of particles of groups A, B, or D, friction causes a pressure drop expressed by the Carman-Kozeny fixed-bed correlation. As the gas velocity is increased, the pressure drop increases until it equals the weight of the bed divided by the cross-sectional area. This velocity is called minimum fluidizing velocity, $u_{mf}$. When this point is reached, the bed of group A particles will expand uniformly until at some higher velocity gas bubbles will form (minimum bubbling velocity, $u_{mb}$). For group B and group D particles $u_{mf}$ and $u_{mb}$ are essentially equal. Group C particles exhibit cohesive tendencies, because these are small enough that inter-particle forces play a significant role; [4]. The $u_{mf}$ can be calculated representatively from the Wen and Yu equation, which is derived from Ar and Re number co-relations; [9], or the modified equation by Grace; [10]. When the superficial gas velocity is increased further, gas bubbles become larger. Slugging is said to occur when the bubbles grow to sizes comparable with the column diameter. The minimal slugging velocity, $u_{ms}$, can be estimated by an equation from Steward and Davison.

$$u_{ms} = u_{mf} + 0.07\sqrt{gD} \qquad (1.4\text{-}1)$$

However, slugging is not encountered for shallow beds (e.g. H/D<1), in columns of very large diameter or for fine particles (e.g. $d_p$<60 ) because bubbles are then unable to grow to be comparable size to the column diameter. [10]

As the gas flow is further increased, “ratholes” appear; the gas opens channels that extend from the gas distributor to the surface. If channels are not formed, the whole bed will lift as a piston. [4]

**Table 1.4-1** Characteristics of gas-solid flow regimes; [10]

| Velocity range | Regime | Appearance and principal features |
|---|---|---|
| $0<u<u_{mf}$ | Fixed bed | Particles are stationary; gas flows through interstices. |
| $u_{mf}<u<u_{mb}$ | Bubble-free fluidization | Bed expands smoothly and uniformly; top surface is well defined; some small-scale particle motion; little tendency for particles to aggregate; very little pressure fluctuation. |
| $u_{mb}<u<u_{ms}$ | Bubbling fluidization | Voids form near the distributor, grow mostly by coalescence, and rise to the surface; top surface is periodically; irregular pressure fluctuations of appreciable amplitude. Bubble size increases as U increases. |
| $u_{ms}<u<u_c$ | Slugging fluidization | Voids fill most of the column cross-section; top surface rises and collapses periodically with a reasonably regular frequency; large and regular pressure fluctuations. |
| $u_c<u<u_{se}$ | Turbulent fluidization | Small voids and particle clusters; top surface difficult to distinguish; small amplitude pressure fluctuations only |
| $u_{se}<u$ and max ($v_{CB}$, $v_{CC}$, $v_C$)$<u<v_{CA}$ | Fast fluidization | No distinguishable upper bed surface; particles are transported out at the top and must be replaced by adding solids near the bottom. Clusters or strands of particles move downward, mostly near the wall, while gas and entrained widely dispersed particles move upward in the interior. Increasingly dilute as U is increased at a fixed solid feed rate. |
| $v_{CA}<u$ | Dilute-phase transport | No axial variation of solids concentration except in the bottom acceleration section. Some particle strands may still be identified near the wall. |

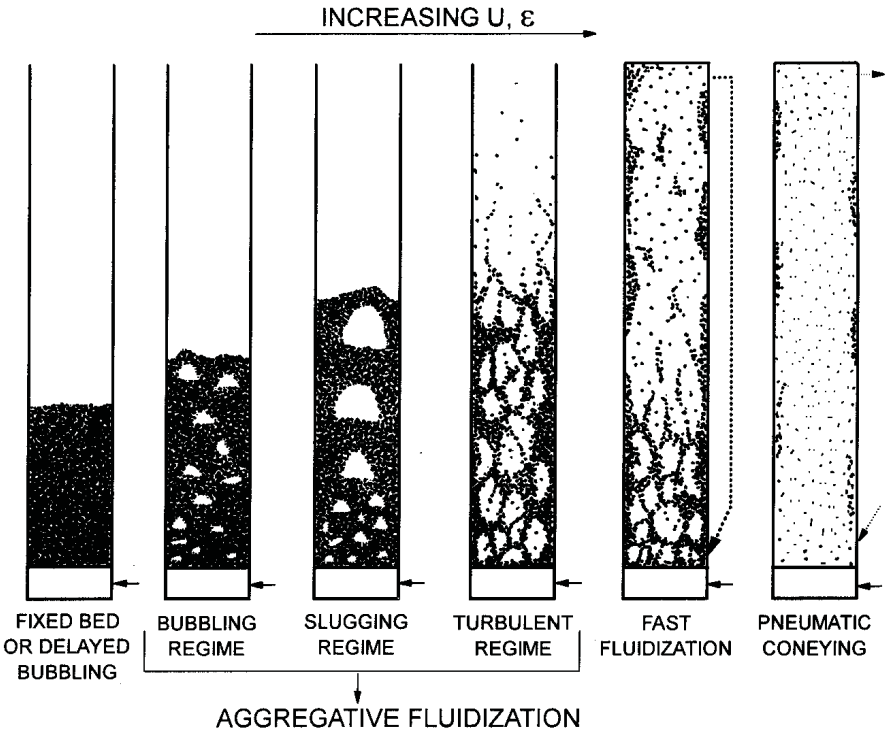


**Fig 1.4-1** Flow pattern in gas-solids fluidized beds [10]

### 1.4.2. Phase diagram

The phase diagram for a fluidized bed can be a useful tool, to help design a new fluidized bed or optimize an existing bed.

**Phase Diagram (Reh)** Reh; [11] has correlated the various types of gas-solid systems in which the gas is flowing counter to gravity in a status graph using the parameters of particle-Reynold number and particle-Froude number. Here, the Archimedes number, Ar, is dependent not on the superficial velocity but on the particle diameter and some physical properties of the fluid. On the other hand, the M number is independent of the particle diameter. Therefore, with given variables, the minimum fluidization velocity, proper superficial velocity for the bed, particle diameter, void fraction (ε), and so on, can be calculated. In this way, a new system can be designed and it helps to solve some possible problems in the fluidized bed.

**Phase Diagram (Grace)** Grace [12] has applied and simplified the status graph from Reh using the parameters of the Archimedes number (Ar) for the particle size and a non-dimensional velocity ($U^*$) for the gas effects.

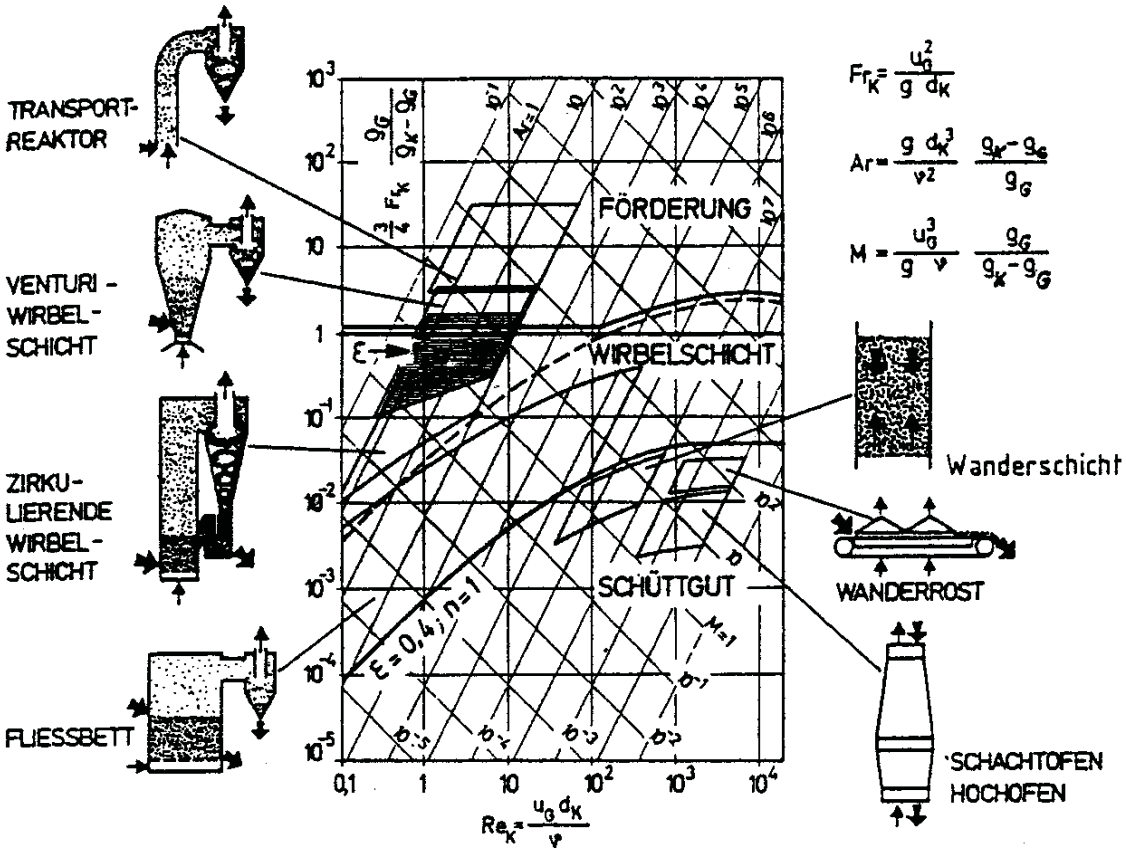


**Fig 1.4-2** Reh-diagram; [31]

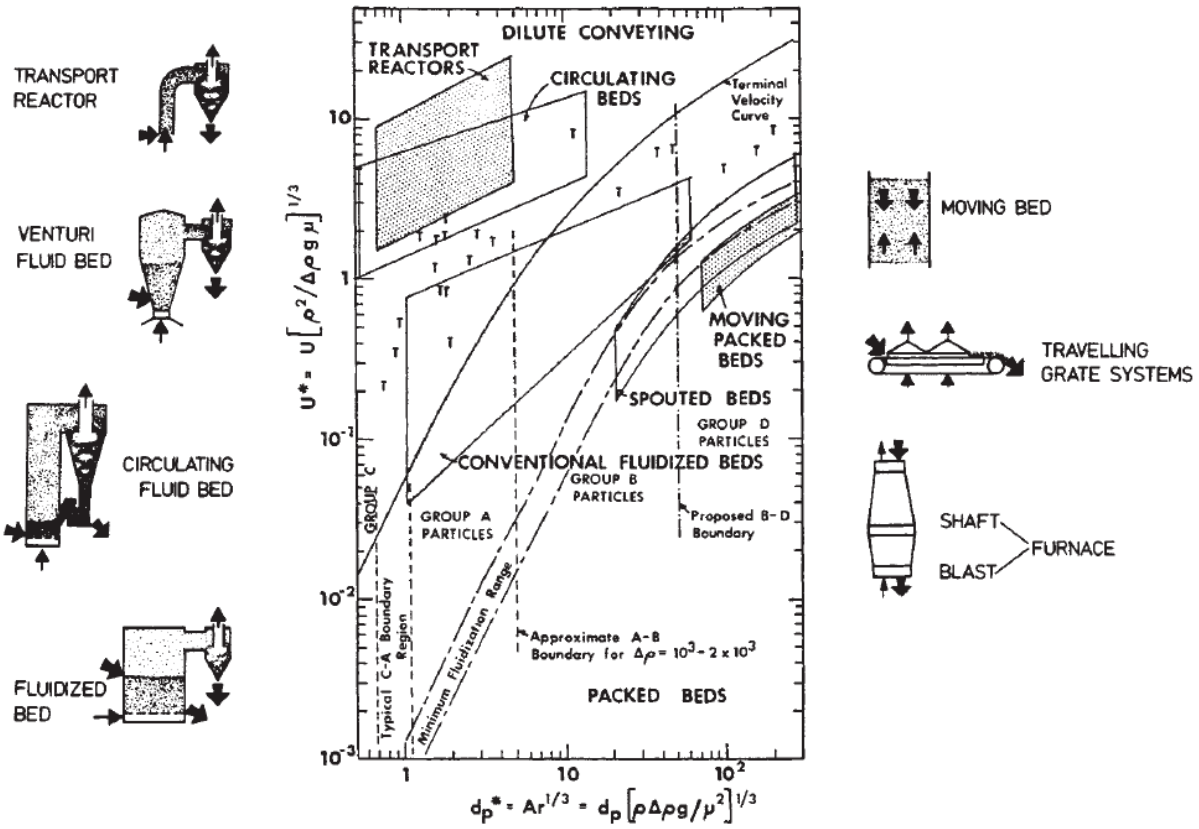


**Fig 1.4-3** Applied Reh-diagram from Grace; [10] from [12]

**Table 1.4-2** Key features of fluidized bed reactors; [10]

| | **Low velocity fluidized bed reactors** | **CFB reactors** | **Dilute-phase transport reactors** |
|---|---|---|---|
| Particle retension time | minutes - seconds | seconds per circulation | once-through system |
| Regime | bubbling, slugging or turbulent fluidization | upper part is usally fast fluidization; Bottom of the reactor may be turbulent fluidization or even bubbling condition | |
| Superficial gas vel. | < 2 m/s | 3 – 16 m/s | 15 – 20 m/s |
| Particle diameter | 0.03 to 3 mm | usually 0.05 to 0.5 mm | typically 0.02 to 0.08mm |
| Net circulating flux | 0.1 – 5 kg/m$^2$s | 1 – 1000 kg/m$^2$s | up to about 20 kg/m$^2$s |
| Void fraction | 0.6-0.8 in bed much higher in freeboard above bed | 0.8 – 0.98 on an average over riser | >0.99 |
| Gas mixing | substantial axial dispersion; complex two-phase behavior | some gas downflow near walls typically results in intermediate gas mixing | very little axial dispersion |

### 1.4.3. Representative types of fluidized beds

Fluidized beds can be classified into mainly three types, bubble bed, circulating fluidized bed and transport reactors, according to superficial velocity of gas and particles' flow pattern. The features of each bed are detailed in **Table 1.4-2**.

## 1.5. Description of (external) CFB

A number of possible configurations are available for carrying out solid particles / fluid reactions and contacting operations: (e.g. chemical process industry, mineral processing, pharmaceutical production, energy-related processes, and so on). The CFB among these systems has come to prominence in the past two decades in terms of major applications.

As noted before, Grace has classified several patterns of regimes, which appears in the fluidized bed according to various superficial velocities. (**Fig 1.4-1**) The earlier researches were under the strong influence of catalytic reactor developments and the experiments of that time were conducted in tall columns with a large length to diameter ratio, L/D, with smooth recycle of solids into their risers; [13] from [14], [15]. The difference between catalytic reactors and boilers are not only limited by riser conditions, but a big difference may also exist in the downcomer. Rapid catalytic reactors contain most of the catalyst inventory since regeneration is done rather slowly in the bubbling-bed mode. In combustors, the downcomer may have a much smaller volume compared to the riser unless it has an external heat exchanger; [13].

CFBs obtain the best efficiency in the mass- and heat exchanging systems, as a large slip velocity between gas and solids can be used. See **Fig 1.5-1**; [16].

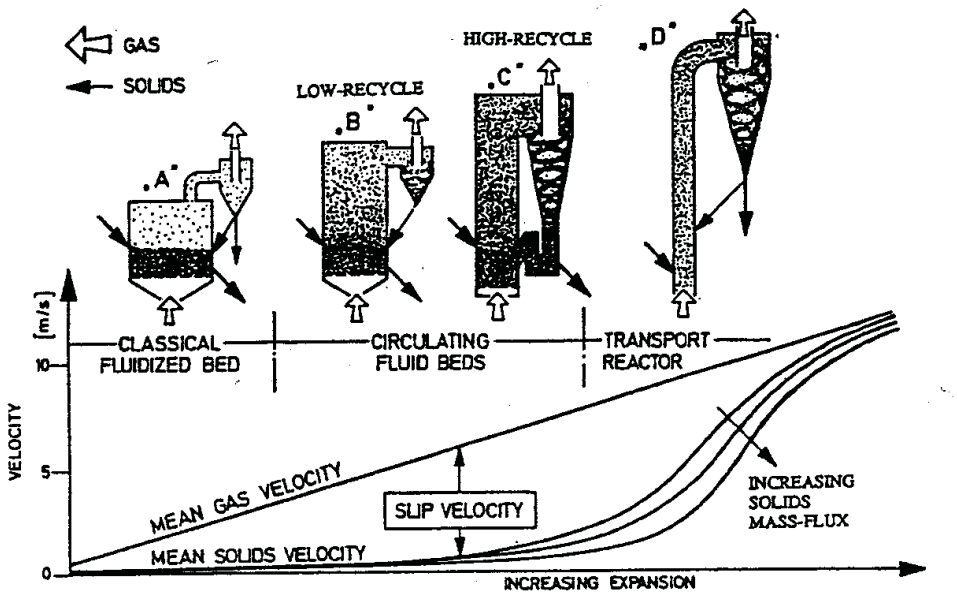


**Fig 1.5-1** Gas and particles velocities in fluidized beds; [16]

### 1.5.1. Hydrodynamics in the CFB

CFB exhibit very complex hydrodynamics, caused by interactions between the gas and solid phase. The motion of gas and solids is driven by many mechanisms that are difficult to identify and describe.

In a CFB the introduced gas from the bottom of the bed with relative high superficial velocity fluidizes particles in the bed and transfers them into a cyclone. The particles are then separated from gas in the cyclone and re-enter into the riser through re-circulated particles return seals (e.g. siphon, L-valve).

In the present chapter, investigated flow regime in the riser and the donwcomer are discussed, whereas gas and solid separation will be discussed in the next section

#### 1.5.1.1. Riser

The Riser is a tall reactor vessel or column used to provide a principal reaction zone. On average, particles travel upwards in the riser core, on the other hand, the motion near the wall may be downwards; [10]. This phenomenum is caused by exit, wall and entrance effect (it is concerned with the re-circulated particles return seal). As a result, the regime in the actual CFB is different from Grace's pattern in **Fig 1.4-1**, as shown in **Fig 1.5-2**.

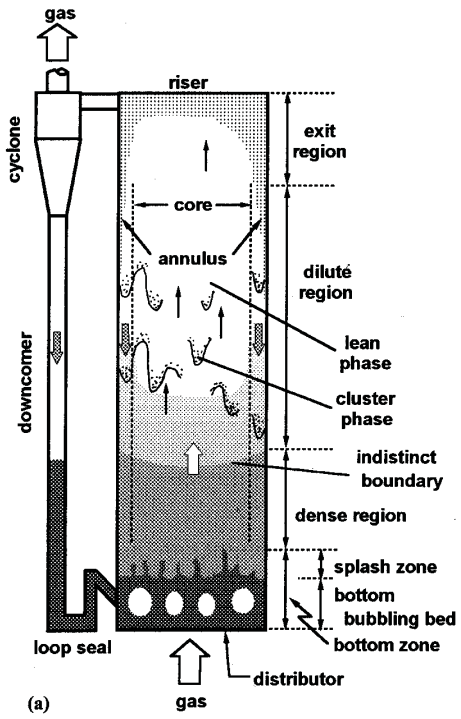


**Fig 1.5-2** A typical flow structure in circulating fluidized bed; [13] from [17]

## Exit effect

The actual CFB combustors are restricted by the end of columns, whose exit structure affects the behavior of bed material strongly. Most of CFB combustors are designed with abrupt exit, where the solids exit through a sharp 90 take-off just below the riser top. The heavier particles that cannot follow the gas streamlines into the exit port are reflected at the top of the riser and causes the increase of solid concentration at the top; [18] from [19].

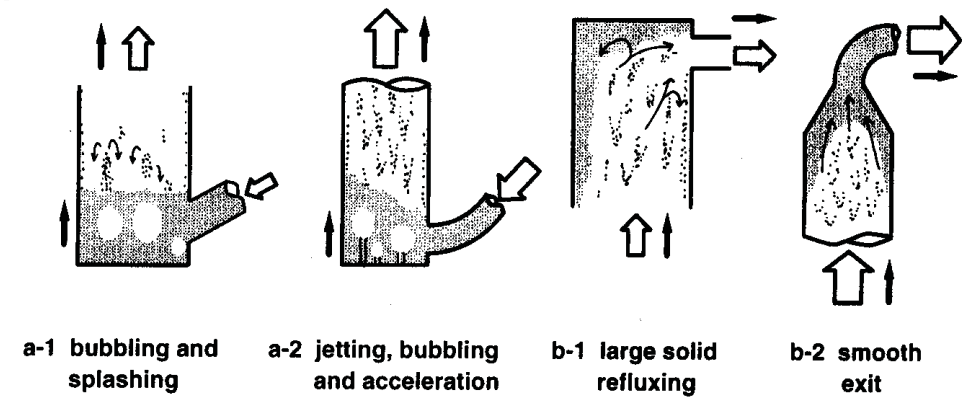


**Fig 1.5-3** The particle motion at entrance and exit regions, a-1 and b-1 are typical combustor type designs, and a-2 and b-2 are for catalytic reactors [13]

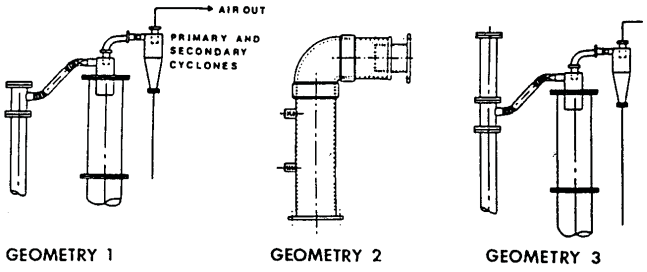


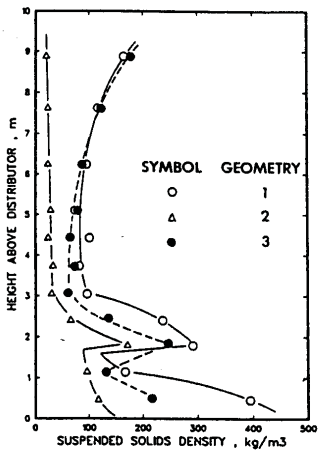


**Fig 1.5-4** Effect of exit structure on the axial bed density profile; [13]

### Cluster

The collisions among particles are not elastic, as the energy is lost by fluid friction, inter-particle frictions, plastic deformation of solids, etc, and these non-elastic collisions with attractive inter-particle forces give a definite tendency to gather; [20].

### (Core-) Wall effect

The velocity along the wall in a cylinder is smaller than in the so called core. As a result, the boundary layer along the wall has the capability to hold more particles than the central part and the particles flows downward. In the region of axially constant suspension density, the intermittent refluxing of the dense phase from the wall keeps their macroscopic density profiles in equilibrium; [13].

#### 1.5.1.2. Downcomer

The particles separated in the cyclone are transferred from a lower pressure to a higher pressure region. Solids can be transferred by gravity against an adverse pressure gradient if gas flows upward 'relative' to the downward flowing solids. This relative gas-solids flow is then able to generate the required 'sealing' pressure drop. Irrespective of actual gas flowing direction, upward or downward, the relative gas-solids velocity, $v_r$, is directed upward. Here the relative gas-solids velocity is defined as :

$$v_r = |v_p - v_g| \qquad (1.5\text{-}1)$$

where $v_p$ is the solids velocity and $v_g = U/\varepsilon$ is the interstitial velocity; [21].

However, the packed particles in the downcomer can really block the flow of particles according to the shapes of return systems, the designs of reservoirs or the pressure distribution in the column. Therefore, extra aeration for a downcomer is needed sometime.

Three types of regime in the downcomer can be distinguished; [21].

### Packed-bed flow

$v_r < u_{mf}$, The voidage is relatively constant. As $v_r$ is increased, $\Delta P/L$ increases. It should be avoided that the downcomer vibrates or radiates a loud 'chattering'.

### Fluidized-bed flow

$v_r \geq u_{mf}$, $\Delta P/L$ is relatively constant.

According to the particle group, the regime shows different patterns. Usually, group A and B are used for CFB. In both cases, bubbles to be formed must be avoided, as the bubbles can coalesce and rising bubbles hinder the solid downflowing, when the bubble rise velocity, $v_b$, is larger than $v_p$; [22].

The proper relative velocities in Group A and B are suggested in **Fig 1.5-5**.

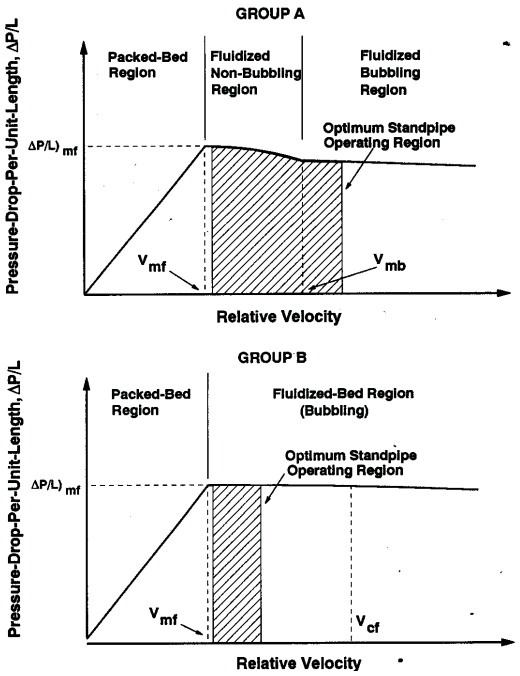


**Fig 1.5-5** Optimum downcomer operating regions for Group A and B particles

## Streaming flow

Underflow downcomers operate sometimes in a dilute-phase streaming flow which is characterized by high voidage. A substantial amount of gas can be carried down the stand pipe when operating in this mode; [23].

### 1.5.1.3. Return systems (re-circulated particles return seals)

The pressure at the bottom of the riser is high in order to fluidize particles. The pressure is lost, as height increases, and finally remarkable pressure drop occurs at the cyclone in a CFB. The particles which are separated in the cyclone must be re-circulated into the riser in a external CFB for a continuos operation. As the pressure at the bottom is higher than that at the top, as noted before, it is possible for the particles in a downcomer to settle down and not to be re-injected into the riser. To prevent the influence of this higher pressure at the bottom of the riser and for particle settling, a solid return system is needed; see **Fig 1.5-6**.

Various types of solid return systems are available and some of them are shown in **Fig 1.5-7**. In any case, the return system must satisfy the following conditions.

- Downcomer (downleg) must be large enough to carry momentarily high rates of solids and
- must provide seals to overcome cyclone pressure drops as well as
- to allow for differences in fluid density of bed and cyclone products.

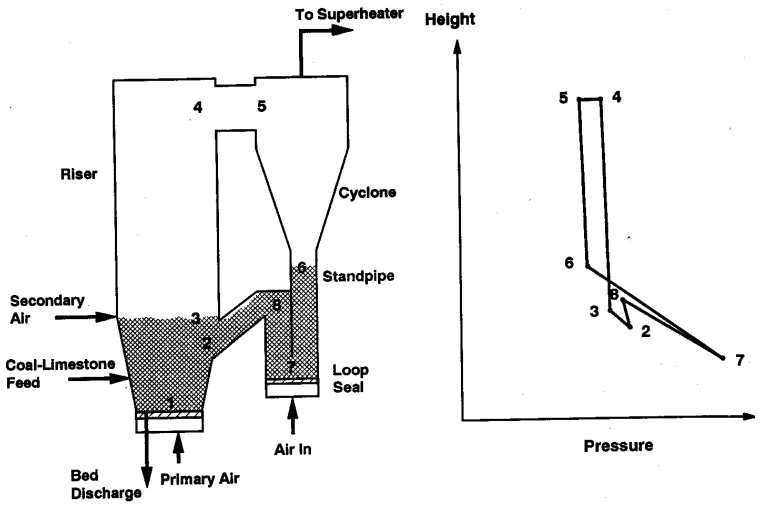


**Fig 1.5-6** Pressure profile in a CFB with a siphon

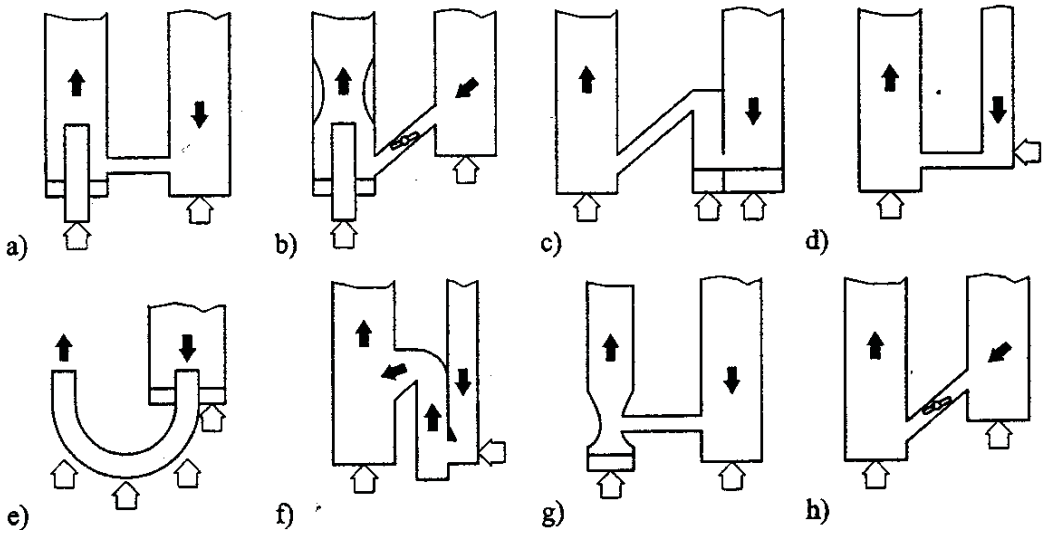


**Fig 1.5-7** Various solids return types a) inflow with inner grid in riser b) inflow with inner grid in the riser and control valve c) siphon d) L-valve e) J-valve f) H-valve g) venturi inflow h) inclined inflow with mechanical valve

## 1.6. Cyclone

Cyclones are most widely used for a dust collection equipment, as they have no moving parts, are relatively inexpensive to construct, and maintenance costs are low. The dust-laden gas enters into a cylindrical or conical chamber and the flow changes into centrifugal movement in the chamber. The dust in the gas is separated by centrifugal force from the gas and the separated gas leaves through an opening at top of the cyclone. Cyclones can be classified into three types according to the gas inlet types. See **Fig 1.6-1**.

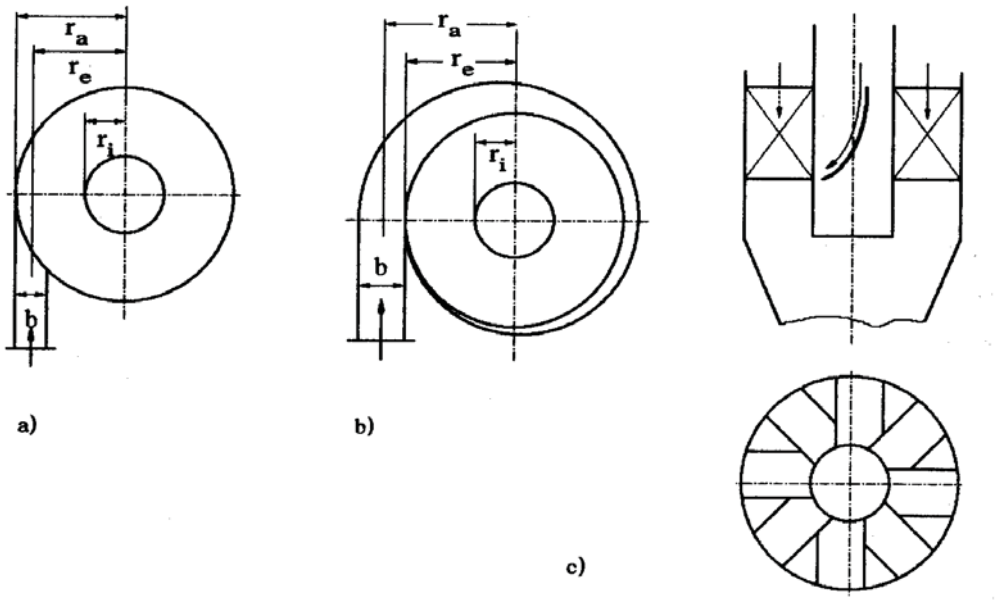


**Fig 1.6-1** a) slit inflow b) spiral inflow c) axial inflow; [24]

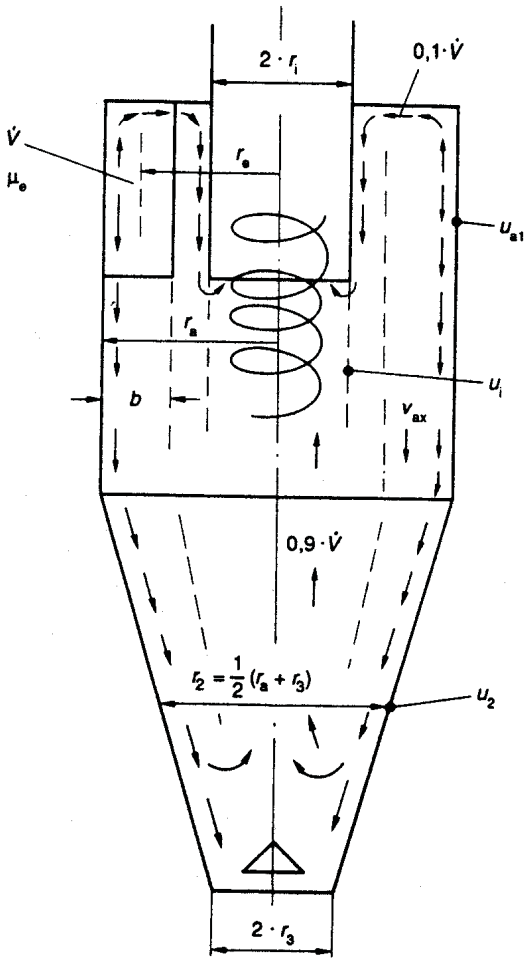


**Fig 1.6-2** Nomenclature for cyclone dimension and velocities; [25]

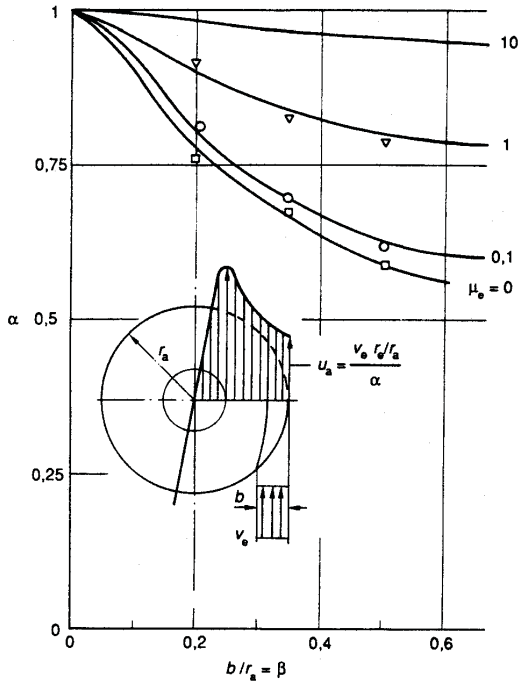


**Fig 1.6-3** The relationships between α and β; [25]

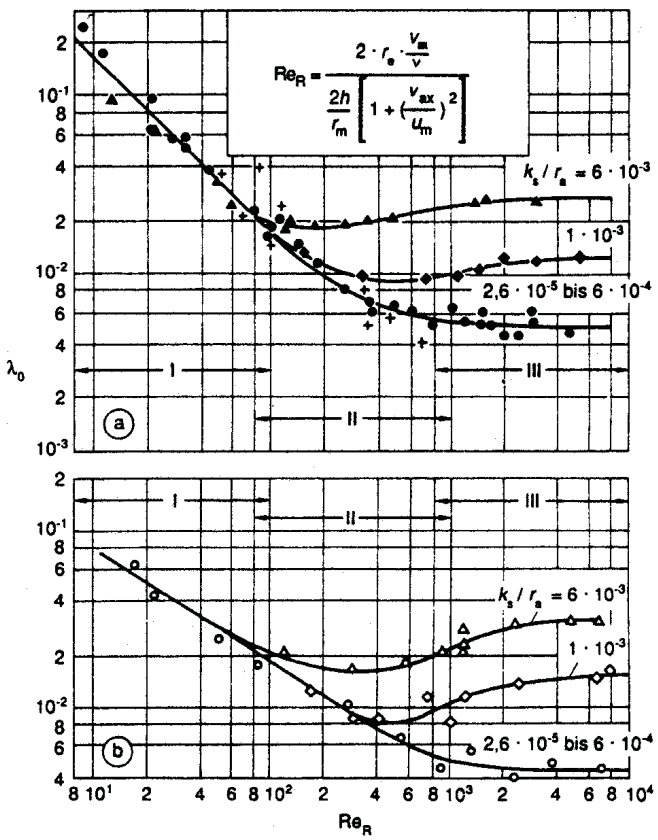


**Fig 1.6-4** Friction coefficient change for lean gas in a a) cylindrical- b) conical- cyclone body according to $Re_R$, where ks is roughness of material. e.g. 0.007≤steel≤6 [mm]; [25]

**Table 1.6-1** Required equations for pressure drop calculation in a cyclone

| | | | |
|---|---|---|---|
| Mean inlet radius | | | $r_e = r_a - \frac{b}{2}$ |
| Radius of the cone at half height | | | $r_2 = \frac{r_a + r_3}{2}$ |
| Relative width of cyclone inlet | | | $\beta = \frac{b}{r_a}$ |
| Expansion/contraction coefficient (See **Fig 1.6-3**) | | | $\alpha = \frac{1 - \sqrt{1 + 4\left[\left(\frac{\beta}{2}\right)^2 - \frac{\beta}{2}\right]\sqrt{1 - \frac{1-\beta^2}{1+\mu}\left(2\beta - \beta^2\right)}}}{r_a}$ |
| Solid friction coefficient (See **Fig 1.6-4**) | general | | $\lambda = \lambda_0 + 0.25\sqrt{\eta_{total}\,\mu Fr_i \frac{\rho_g}{\rho_p(1-\varepsilon_{str})}}\left(\frac{r_a}{r_i}\right)^{-\frac{5}{8}}$ |
| | For simplified calculation (assumption : for unladen gas $\lambda_0$=0.005) | μ<1 | $\lambda = 0.005(1 + 2\sqrt{\mu})$ |
| | | μ>1 | $\lambda = 0.005(1 + 3\sqrt{\mu})$ |
| Dimensionless numbers for solid friction | Froude number | | $Fr_i = \frac{v_i}{\sqrt{2gr_i}}$ |
| | Reynolds number | | $\mathrm{Re}_R = \frac{2r_e v_{ax}/\nu}{2\frac{h}{r_m}\left[1 + \left(\frac{v_{ax}}{u_m}\right)^2\right]}$ where ν is the kinematic viscosity of gas ($\eta_g$ / $\rho_g$) |
| | Voidage in the strand | | $\varepsilon_{str} = \frac{1 + \varepsilon_{sch}}{2}$ |
| Velocities (See **Fig 1.6-2**) | tangential velocity at $r_x$ | | $u_x = \frac{v_e r_e / r_x}{\alpha}$ e.g. x=a(outer vessel), 2(the middle of conical part). |
| | gas velocity in gas inlet | | $v_e = \frac{\dot{V}}{h_e b}$ |
| | tangential velocity at $r_i$ | | $u_i = \frac{u_a r_a / r_i}{1 + \frac{\lambda}{2}\frac{A_R}{\dot{V}} u_a \sqrt{r_a / r_i}}$ |
| | mean radial velocity at $r_i$ | | $v_{ri} = \frac{\dot{V}}{2\pi r_i h_i}$ |
| | mean tangential velocity at inflow surface ($r_e$) | | $u_{e1} = \frac{u_a r_a / r_e}{1 + \frac{\lambda}{2}\frac{A_{e1}}{0.9\dot{V}} u_a \sqrt{r_a / r_e}}$ |

To be continued

| | | |
|---|---|---|
| | tangential velocity at $r_2$ | $u_{e1} = \dfrac{u_a r_a / r_2}{1 + \dfrac{\lambda}{2}\dfrac{A_{e1}}{0.9\dot{V}} u_a \sqrt{r_a / r_2}}$ |
| | mean axial velocity in separation chamber | $v_{ax} = \dfrac{0.9\dot{V}}{\pi(r_a^2 - r_m^2)}$ |
| | Mean axial velocity in a vortex tube | $v_i = \dfrac{\dot{V}}{\pi r_i^2}$ |

$A_R$ = total inner surface area of a cyclone included vortex tube outer surface area

$A_{e1}$ half of the surface area during first rotation of solids, $A_{e1} = (2\pi r_a h_e)/2$

Assumption : the secondary flow in a cyclone is 10%. This value can vary 5-15%; see **Fig 1.6-2**

**Pressure drop**

The pressure drop in a cyclone can be calculated by the sum of the pressure drop contributions at the barrel ($\Delta p_e$) which is dependant on friction and vortex tube pressure ($\Delta p_i$) which is dependent on the spin ratio $u_i/v_i$. Most of the pressure drop occurs at the vortex tube and the pressure drop at vortex tube is about ten times as large as that at the barrel.

$$\Delta p_{total} = \Delta p_e + \Delta p_i \qquad (1.6\text{-}1)$$

where

$$\Delta p_e = -\lambda \frac{A_R}{0.9\dot{V}} \frac{\rho_g}{2} (u_a u_i)^{3/2} \qquad (1.6\text{-}2)$$

and

$$\Delta p_i = -\left[ 2 + 3\left(\frac{u_i}{v_i}\right)^{4/3} + \left(\frac{u_i}{v_i}\right)^2 \right] \frac{\rho_g}{2} v_i^2 \qquad (1.6\text{-}3)$$

# Chapter 2.

# Description of the pilot plant

A cold bed model was designed for tests at ambient conditions, in order to solve some already known problems in the commercial bed and to improve them. The cold bed model is based on Lezing's hot bed model and scaled down according to L.R. Glicksman's theory; [2] and his experiments; [26]. Copper particles whose density is 3.5 times as large as that of quartz sand are used as bed material to maintain a constant ratio of particle to gas density due to the temperature difference between the cold and hot bed.

The system consists mainly of three parts – **C**irculating **F**luidized **B**ed (CFB) with a solid separator – cyclone - and a newly designed siphon, external **F**luidized bed **H**eat **E**xchanger (FHE) and secondary parts such as filter and air blowers.

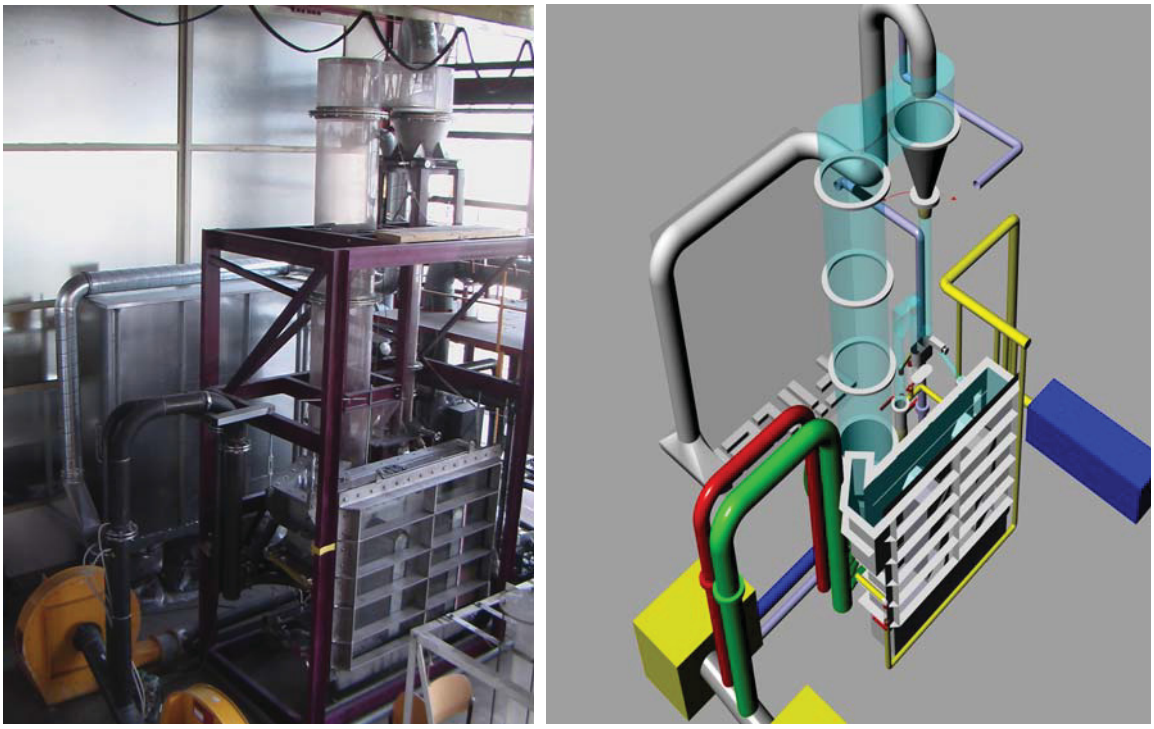

**Fig 1.6-1** Photo from the cold model and its simplified 3D-model.

# 2.1. Circulating Fluidized Bed (CFB) parts

## 2.1.1. Combustion chamber and cylinder

The combustion chamber is made of stainless steel to support the cylinder (riser) and to connect with other steel structures, whilst the cylinder parts (riser) are Plexiglas to observe the behavior of particles. The inner diameter of the (Plexiglas-)cylinder and the steel cylindrical part in the combustion chamber is 480 mm and the height from the gas distributor is about 4500 mm.

A wind box wherein fluidizing air is supplied is attached under the combustion chamber and a gas distributor is installed between the wind box and the combustion chamber. The gas distributor is simplified in our cold model and consists of drilled stainless steel plates with a 40 μm steel screen with about 1-2 mm gap between the screen and the steel plate to distribute gas uniformly.

On the conical combustion chamber, there are two re-circulated bed material inlets from siphon and FHE exits and 6 secondary air inlets whereby three are of smaller diameter (secondary air-1) and the remaining three are of larger diameter (secondary air-2) above the inlets of secondary air-1. See details for secondary air connections in section 2.4.2 .

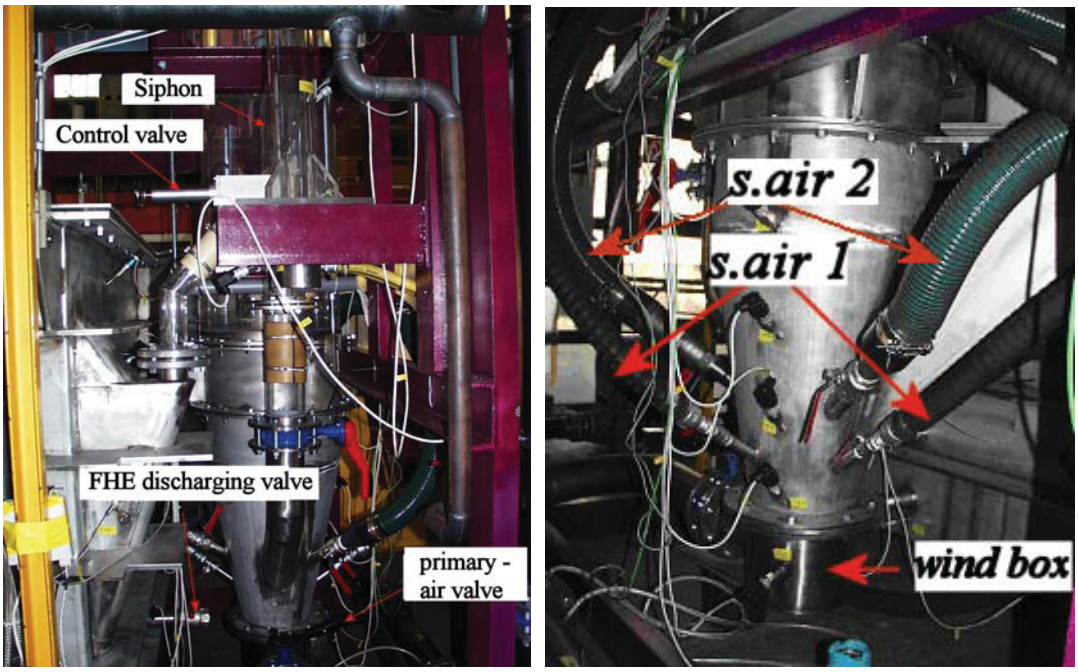


**Photo 2.1-1** Combustion chamber

6 mm inner diameter taps to mount the pressure sensors and temperature sensors are installed in the combustion chamber and cylinder. One tap for a pressure sensor in the wind box, four for pressure sensors at the conical part and five pressure sensors and a temperature sensor for the cylindrical part are installed. See details for sensors in section 3.2.

### 2.1.2. Siphon

A siphon maintains a specified level of bed material between cyclone downcomer and combustion chamber. When the siphon isn't filled with bed material up to the specified level, the fluidizing air from combustion chamber flows through the siphon and increases pressure in the downcomer. This will induce an entrainment of particles in upward direction through the downcomer.
Our model also has an external FHE and an intermediate reservoir is needed to supply a small flux of circulating bed material into the FHE. To adjust the bed material flux into the FHE, a control valve is installed between the siphon and the FHE; (see valves section and **Photo 2.1-1**).
Bed material which stays in the siphon must be externally forced in order to flow spontaneously. Therefore, the wind box which is separated into two sections is attached under the siphon with a gas distributor, which consists of a porous steel plate and a stainless steel screen. Compressed fluidizing air from a roots pump is injected into the wind box to fluidize the bed material in the siphon a rate of approx. 15m$^3$/h in the cold model.

**Fig 2.1-1** Current installed siphon in the cold bed model

### 2.1.3. Cyclone

The cyclone is the most widely used type of dust separating equipment.
To observe the behavior of bed material, many parts of the cyclone are made of Plexiglas. The inlet which is also made of Plexiglas is connected with the cylinder on the combustion chamber, whilst the cone in the cyclone is stainless steel. These parts (not only the cyclone but also riser parts) which are made of Plexiglas expand according to the temperature during operation. Therefore, the connecting Plexiglas between the riser and the cyclone is under stress to support the weight of

cyclone, in case of the expanded cylindrical Plexiglas part in the riser by the thermal effect. This can cause serious problems such as fracture of the Plexiglas.

The solution was to install weight compensators; see **Photo 2.1-3**. The plate which is attached to the cone is raised by two crowbars and a spring scale is installed between the frame for the system and the bar. The length adjustable bar which has two different threaded bars, one right and the other left, is attached under the scale to adjust the engaged force. The other end of this bar is welded to the main frame for the system. The engaged force raise the plate on the cylinder and minimizes the stress in the connecting Plexiglas which is connected between the cylinder in the riser and the cyclone. The force added by the length adjustable bar for weight compensation can be read on the spring scale.

**Photo 2.1-2** Cyclone

**Photo 2.1-3** Stress compensator

## 2.2. External Fluidized bed Heat Exchanger (FHE)

The FHE is the most characteristic part in comparison with other CFB (Circulated Fluidized Bed) installations. The FHE in RV-Lenzing consists of several refractory lined chambers, which are working like small bubbling beds, separated by weirs. The hot branch flow of the circulating material from the loop seal (Siphon) first arrives in the so called empty chamber (the chamber without any heat exchanging surfaces) for equalizing the sand flow. In the next stage, the bed material flows into two cooling chambers, wherein the in-bed heating surfaces of the water-steam-path are situated. Finally the cooled bed material is transported back into the combustion chamber via a fluidized recycle canal.

The chambers are fluidized with (combustion) air. Each chamber is equipped with a separate positive displacement fan to prevent bed material interaction between the chambers; [1].
The FHE which is installed in the cold model has no refractory lined wall and the gas distributor at the bottom is simplified, comprising a steel screen on a porous steel plate. Moreover the front side wall is assembled with safety glass to observe the behavior of bed material. The top cover is made of Plexiglas and steel frames are laid on it to mount the Plexiglas. These two – front side and top – parts are assembled with nuts and bolts and sealed with rubber, as the FHE must be re-opened to move the weirs or to fill up bed material from time to time.

**Photo 2.2-1** FHE on assembly (left) and in operation (right)

**Photo 2.2-1** shows the operating FHE with sand filled up and the empty FHE without weirs. A flute at right side on the rear plate is the entrance for bed material from the siphon.
**Photo 2.2-2** shows the porous plate for gas distributing in the delivering chamber. The bed material from the FHE is fluidized here and then transferred via gravity into the combustion chamber (riser) through the downward inclined canal which is shown in the bottom right edge of in the photo.
**Photo 2.2-3** shows the three so called "wind boxes" under the main porous plate of the 1st and 2nd heating chamber for gas distributing and bed material fluidizing in the FHE. The fluidizing air streams of the chamber are separated from each other.
In the wind box, the three frames to assemble the separating plates are shown. These are used when the weir is moved for the bed material behavior test according to various weir conditions. The separating plate in the wind box must be fixed according to the position of the weir.

**Photo 2.2-2** Delivering chamber for the bed material passage from the 2nd heating chamber to the combustion chamber; the porous steel plate before mounting of steel screen on it

**Photo 2.2-3** Wind boxes under the gas distributor in the FHE (The direction of view is vertically downward)

# 2.3. Bed material

## 2.3.1. Sand

The second stage of our investigation was conducted with quartz sand to optimize the system. Quartz sand is also used currently in Lenzing as bed material. See **Table 2.3-1** for the sand properties used in our cold model, as detailed by supplier.

**Table 2.3-1** Quartz sand data from supplier

| **Diameter [mm]** | **Sieve residue [%]** |
|---|---|
| 0.355 | 0 |
| 0.25 | 0 |
| 0.18 | 0.5 |
| 0.125 | 21 |
| 0.09 | 41.8 |
| 0.063 | 20.9 |
| <0.063 | 15.8 |

| **Chemical analysis** | |
|---|---|
| Element | [%] |
| $SiO_2$ | 98 |
| $Al_2O_3$ | 0.7 |
| $Fe_2O_3$ | 0.2 |

| **Physical properties** | |
|---|---|
| Bulk(piled) density | 1.4 t/m$^3$ |
| Density | 2.65 t/m$^3$ |
| Hardness | 7 Mohs |
| Average diameter | 0.09 mm |
| AFS-Number | 163 |
| Loss on ignition | < 0.2% |
| Sinter beginning | >1550 °C |

## 2.3.2. Copper (Cu) particles

The density of Cu is about 3.3 times larger than that of quartz sand. Therefore, copper is a suitable bed material for the similarity study for the industrial plant's operating point (850°C) in our cold model; for the basic reason in the estimation of the model bed material properties according to similarity considerations; see section 1.2

Cu bed material is supplied from Ecka granulate MicroMet GmbH and has the following properties.

**Table 2.3-2** Properties of Cu bed material according to the manufacturer

| Sieve analysis | Dimension | Actual value |
|---|---|---|
| > 250 | % | 0.0 |
| > 200 | % | 0.6 |
| > 160 | % | 3.4 |
| > 100 | % | 20.7 |
| > 63 | % | 31.3 |
| < 63 | % | 44 |
| Mean particle diameter | | 68 |
| density | $g/cm^3$ | 8.95 |
| Piled density | $g/cm^3$ | 3.22 |
| **Chemical analysis** | | |
| Oxygen | % | 0.37 |

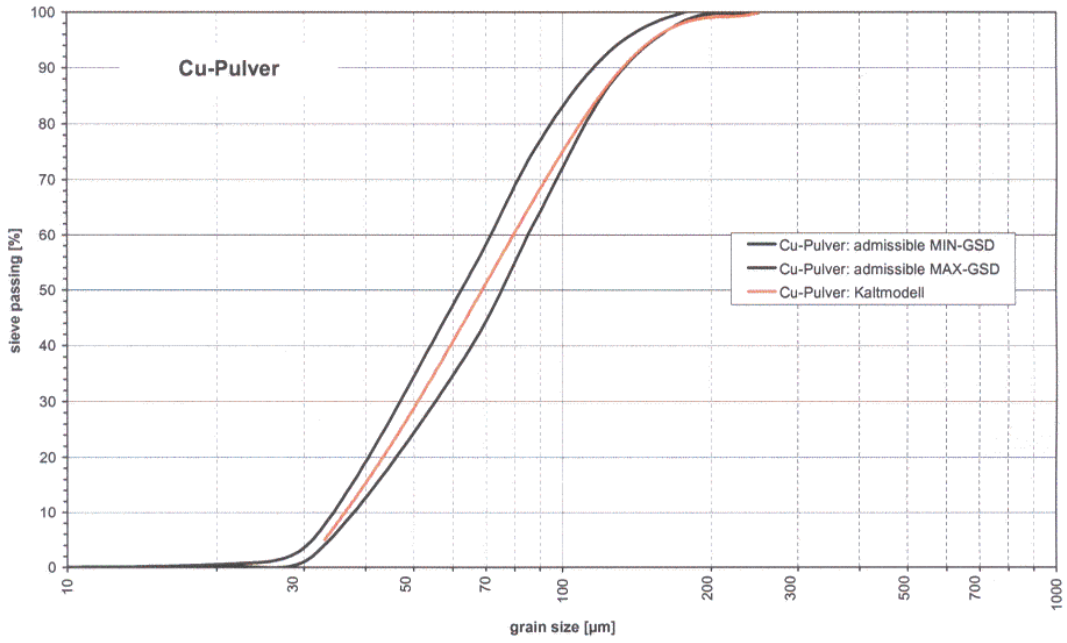


**Fig 2.3-1** Cu particle size distribution; tested in the AEE Lab.[33]

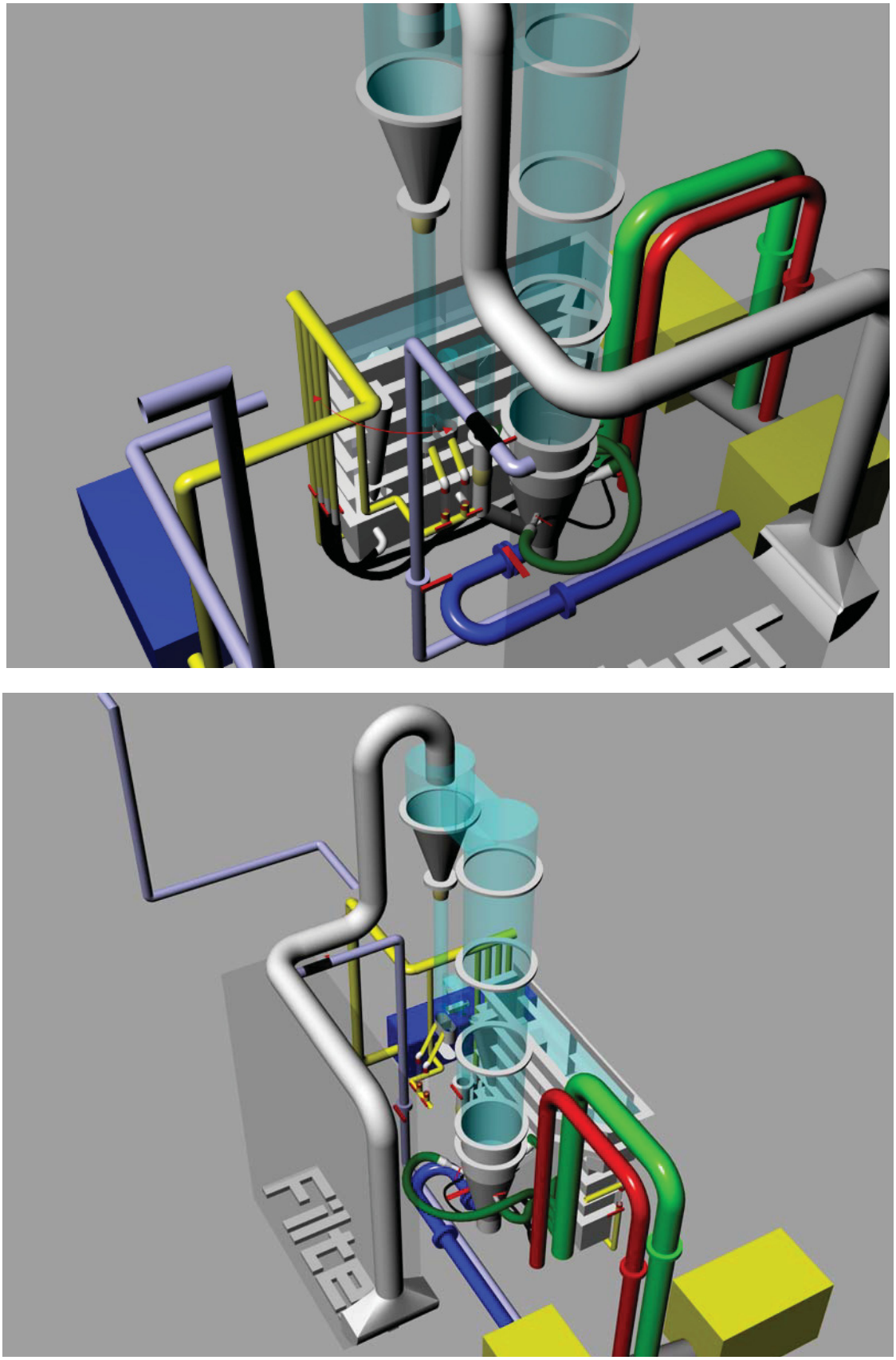

**Photo 2.3-1** Whole system as a 3D model from different viewpoints

## 2.4. Hose, pipes and valves

The connections for fluidized air to various parts in the cold model are explained in this section. To improve understanding, the 3D-model is illustrated with various colored pipes and hoses according to their functions. Remaining parts such as air blowers and filter are simplified. (**Photo 2.3-1**, **Table 2.4-1**)

**Table 2.4-1** Dimensions of pipes and their color in the 3D-model.

| Name | Dimension | Color |
|---|---|---|
| Primary air | DN 125 | dark blue |
| By-pass from booster (for emergency) | DN 80 | sky blue |
| Secondary air-1(small) | DN 125 | red |
| Secondary air-2(Big) | DN 180 | green |
| Pipes from roots pump | DN 100 | yellow |
| Pipes from roots pump to siphon | DN 50 | yellow |
| Pipes from roots pump to FHE | DN 50 | yellow |

### 2.4.1. Primary air and by-pass system

The primary air pipe from the booster to the wind box under the combustion chamber is the blue colored pipes in the 3D-model. To control the volumetric flow rate of primary fluidizing air, a butterfly valve is installed at the upstream for the wind box under the combustion chamber. In the middle of the primary air pipe line from the booster, an orifice plate is assembled between flanges. Three 6 mm-taps are located before and after the plate, in order to measure the temperature of air and the pressure difference. For the static pressure measurement the holes located one pipe diameters upstream and a half pipe diameters downstream from the plate.

The emergency by-pass pipe is colored in sky-blue. The emergency and primary air pipes are connected with a divider. The emergency valve is in the near of the siphon valves on the vertical pipe along the frame. Opening of the valve lets the fluidizing air from ventilators flow to the outside of the lab and decrease the pressure in the riser. The by-pass is currently connected to the filter for the purpose of cleaning for the filter; see **Photo 2.4-1**.

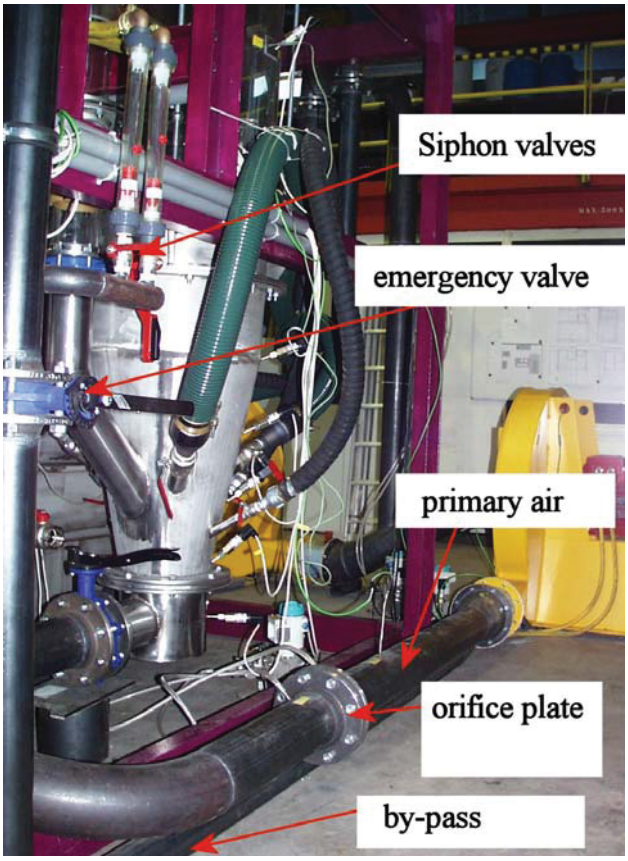


**Photo 2.4-1** Primary air pipe line

## 2.4.2. Secondary air (pipes, hose size, valves, reducers)

Secondary air is distributed from the radial ventilator through two pipes. One is for the secondary air-1 (smaller diameter) and the other is for the secondary air-2 (larger diameter). Each pipe has 3 taps for the hoses which connect between the secondary air pipes and the secondary air inlets on the combustion chamber. As can be seen in **Photo 2.4-1**, the secondary air inlets are spread out on the combustion chamber, in order to promote turbulence in the chamber.

Secondary air-1 (smaller diameter) pipe is a DN125 (red in **Photo 2.4-2**). To measure the volumetric flow rate, the orifice plate is installed between flanges and two 6 mm-taps for the pressure difference sensor located according to radius taps. See details for radius taps in section 3.3 . The hose diameter is 40 mm and black color. It connects between secondary pipe-1 and the reducer at the secondary air inlets. The reducers reduce the diameter of secondary air-1 hoses from 40mm to 20mm, which is assembled with secondary air-1 ball valves; see also **Photo 2.1-1**

Secondary air-2 (larger diameter) pipe is DN 180 (green in **Photo 2.4-2**), the diameter of the hoses (dark green in **Photo 2.4-2**) is 80 mm and the reducers reduce from 80 mm to 40 mm. The valve type is a ball valve and the orifice plate between flanges in the pipe for measuring the volumetric flow rate via the pressure difference is also installed.


**Photo 2.4-2** Top view (left) and bottom view (right) for secondary air connections

### 2.4.3. Compressed air connections from roots pump for FHE

Compressed air is supplied by the roots pump, in order to overcome the weight of Cu particles in the FHE, which weighs about 2.5 ton. DN100 pipe is connected with the roots pump and five DN50 pipes branch off from it. They are for the empty- , first- , second heating, delivering and Siphon fluidizing chamber respectively.

In three pipes for the empty, first - and second heating chambers, orifice plates are installed to measure and record the flow rate of fluidizing air, whilst the remaining two pipes have just flow indicators. The three pipes for the chambers in the FHE have ball valves to adjust the flow rate which is supplied into each chamber and the downstream sides of the valves are joined with hoses (black in **Photo 2.4-3**). Their diameter is 50 mm. The pipe to the siphon splits into two and these are connected to separate chambers in the wind box under the siphon via flow indicators and hose.

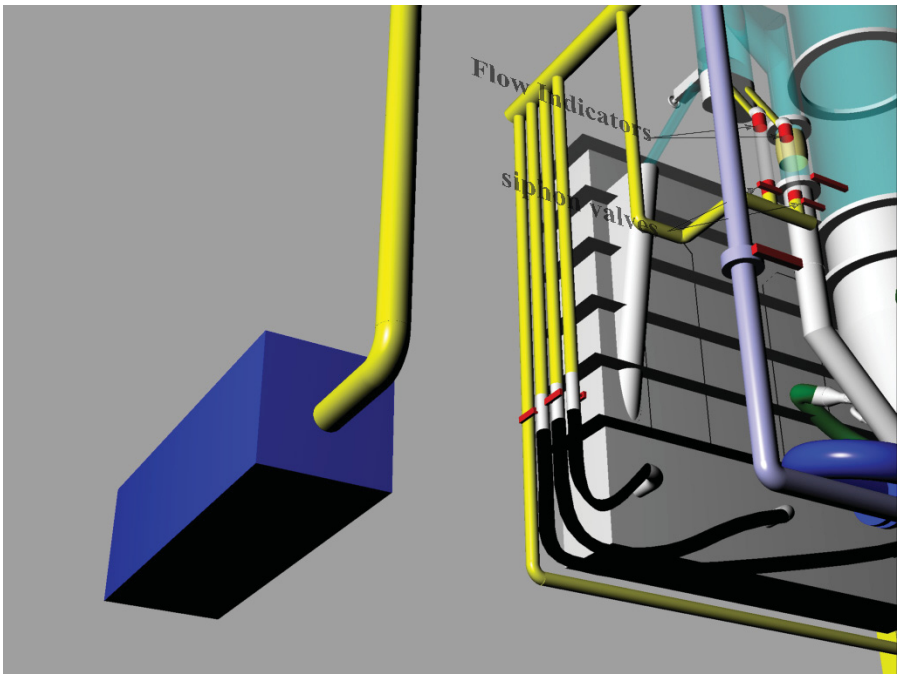


**Photo 2.4-3** Roots pump connections

### 2.4.4. Other valves and pipes

Three discharging valves are on the exterior wall of the FHE at the bottom of each chamber.
A control valve which can adjust the amount of bed material from the siphon to the FHE is installed at the siphon. See **Photo 2.4-3** and **Photo 4.4-2** as well as **Photo 4.4-1**.
The gas outlet in the cyclone is connected with the 200 mm diameter pipe and goes into the filter via a 180 ° bent connector.

## 2.5. Air blowers

The fluidizing air is supplied by two ventilators which blow into the combustion chamber; i.e. riser, and one roots pump which blows high pressure fluidizing air into the FHE. They are colored by yellow and blue respectively in the 3D model. The reasons for the use of the two different types of blowers are as follows:
To fluidize the bed material, the riser needs a higher volumetric flow rate rather than higher pressure. In contrary, a higher pressure is required to overcome the weight of piled bed material in each chamber of the FHE. The first blower which blows air into the following blower is named 'radial ventilator' and the other one is named 'booster'. The blower for FHE is named roots pump.
The specifications for the two ventilators and the roots pump are detailed in the following table

**Table 2.5-1** Specifications for ventilators

| | |
|---|---|
| Volumetric flow rate | 3000 $m^3$/h |
| Pressure(p total / p static) | 118.84 / 107.36 mbar |
| Electrical power | 18.5kW<br>(2 poles, 400V, 50Hz, IP55) |
| Max. temperature | 80 °C |

For more information: http://www.gtg.at

**Table 2.5-2** Specifications for roots pump

| | |
|---|---|
| Volumetric flow rate | 13.7 $m^3$/min |
| Positive operational pressure | 1.05 bar |
| Max. pressure difference | 800 mbar |
| Electrical power | 23.9 kW |
| Max. temperature | 140 °C |

For more information: http://www.aerzener.de

**Photo 2.5-1** Ventilators (left) and roots pump (right)

# Chapter 3.

# Sensors and data acquisition

The measuring system consists of three main parts.

- ✓ **Software**: HP Basic program, Excel file with **V**isual **B**asic for **A**pplications (VBA) and Lookout from National Instruments
- ✓ **Data acquisition system** which amplifies and sends the measured signal from the sensors to the computer, such as current transformers (from AC to 24V AC) with 100 Ohm resistors for 4-20 mA current, Amplifier, Transmitter, GPIB card
- ✓ The **sensors** for measuring pressure, temperature and pressure difference for volumetric flow rate

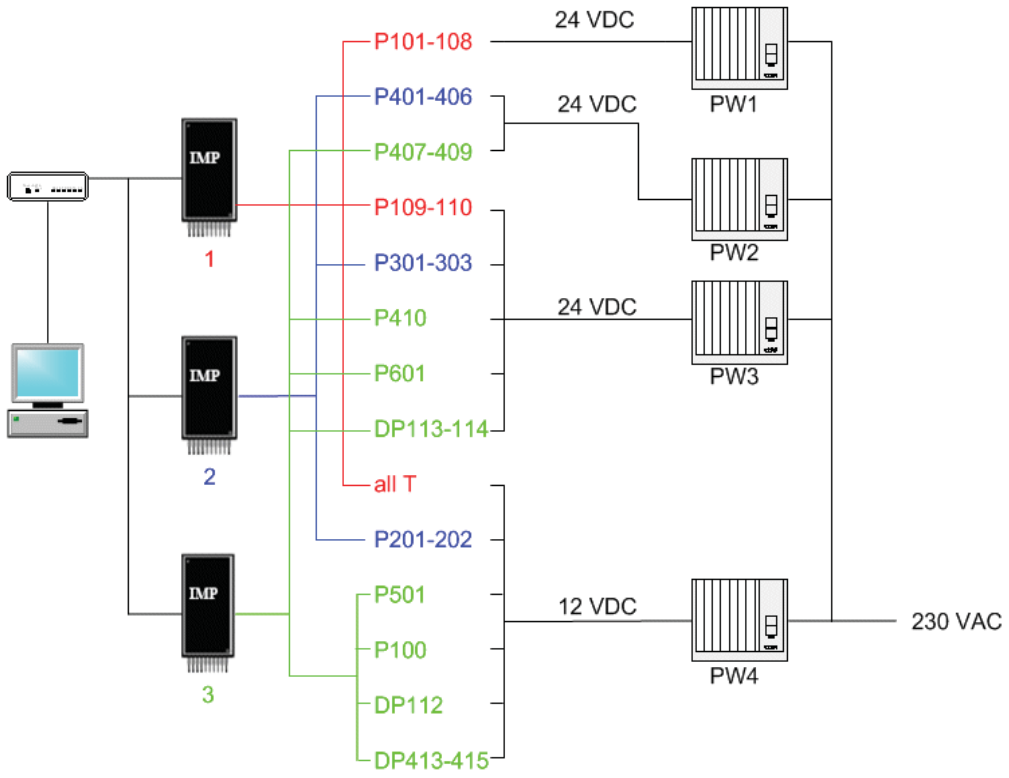


Fig 2.5-1 Layout for the measurement

In a preliminary step, only the Basic program which was written by Dip.-Ing. Rob was installed as the data acquisition software. This text-based Basic program has some useful functions such as

recording data, making graphs, calculating average values, etc. However, it has some problems because of the outdated text-based program. The problems are as follows:

- ✓ Measured data cannot be shown in real time
- ✓ Just one measured value can be shown on screen. This makes it very difficult to adjust the valves for a proper amount of fluidizing air.
- ✓ To change some parts or install new devices, the code must be partly changed.
- ✓ Therefore, basic programming ability is needed or a programmer must be at hand, whenever any set-up is changed.
- ✓ There is no manual for this program.

For these reasons, an alternative program was constructed, based on Lookout from National Instruments.

# 3.1. Software

## 3.1.1. HP Basic

BASIC (standing for **B**eginner's **A**ll Purpose **S**ymbolic **I**nstruction **C**ode) was written (invented) in 1963, at Dartmouth College, by mathematicians John George Kemeny and Tom Kurtzas as a teaching tool for undergraduates. BASIC's popularity was spread by both Paul Allen and William Gates, in 1975. Gates and Allen (both Microsoft founders) wrote a version of BASIC for the Altair personal computer; [27].

Basic language is a representative interpreted language and any source code is needed to run in the Basic interpreting program (‘HP Basic for windows’ in our case). This means that source code must be re-coded to change a value. For example, if the orifice plates for measuring flow rate were changed to a different diameter, the source code must be edited.

It has a lot of functions needed in data acquisition such as to display data, to save, to display graphs etc. However, this application is based on old type Basic language, making it difficult and inflexible to use.

The source code of Dip.Ing. Rob is located in the ‘c:\hpbasic\programme’ folder and the filename is ‘dtu_zws’. This path and filename must be initialized and loaded to run the application.

In a Basic source code, the line or a part of line beginning with ‘!’ is for comments and it is not interpreted by the interpreting program. To break a procedure, ‘ctrl + break’ on a keyboard must be pressed.

### 3.1.1.1. The locations of important folders/files and their roles

**‘programme’ folder:**

The source code files of the measuring application on Basic is located in the folder

'c:\hpbasic\programme', where 'DTU_zws' is the original source code file and 'DTU_res' is restored file. These two files hold the source code of the application.

To save this file, when the code is changed in the edit mode, delete the text block from the line number to the '!' sign on each the line (e.g. 10, 20..) and press enter. For the restoring, repeat it on the line 11.

```
Source code:
10   ! RE-STORE "\HPBASIC\PROGRAMME\DTU_zws"
11   ! RE-STORE "\HPBASIC\PROGRAMME\DTU_res"
20…
```

**Fig 3.1-1** Basic source code for saving, line 10 and 11

**'Daten' folder:**

The configured data and measured data files are saved in this folder.

**'Exceldat' file:**

This is the text based DB (Data Base) file and works like a buffer. The measured data which is read from **I**solated **M**easurement **P**od (IMP) by the Basic program is saved temporarily for Excel to read it.

**'Exceldat2' file:**

converts a DB file from Exceldat, to change into the suitable format for Excel. This converting is executed by VBA in Excel.

See also VBA program.

**'Speicher' file:**

Configured data such as sensor name, matrix number, dimension, correction curve, IMP number and its channel is saved as Basic DB format. See also MAT-NR and '–end– werte'.

#### 3.1.1.2. Loading the source code

The screen shot after starting the HP Basic for windows, a Basic program interpreter, is shown in **Photo 3.1-1**. To load the measure program for Basic follow the next steps.

```
Start HP Basic for windows
msi "\hpbasic\programme" [Enter]
load "dtu_zws" [Enter] (or F5 for shortcut )
run [Enter] (or F3 for shortcut)
```

**Fig 3.1-2** Steps for loading and running of basic program

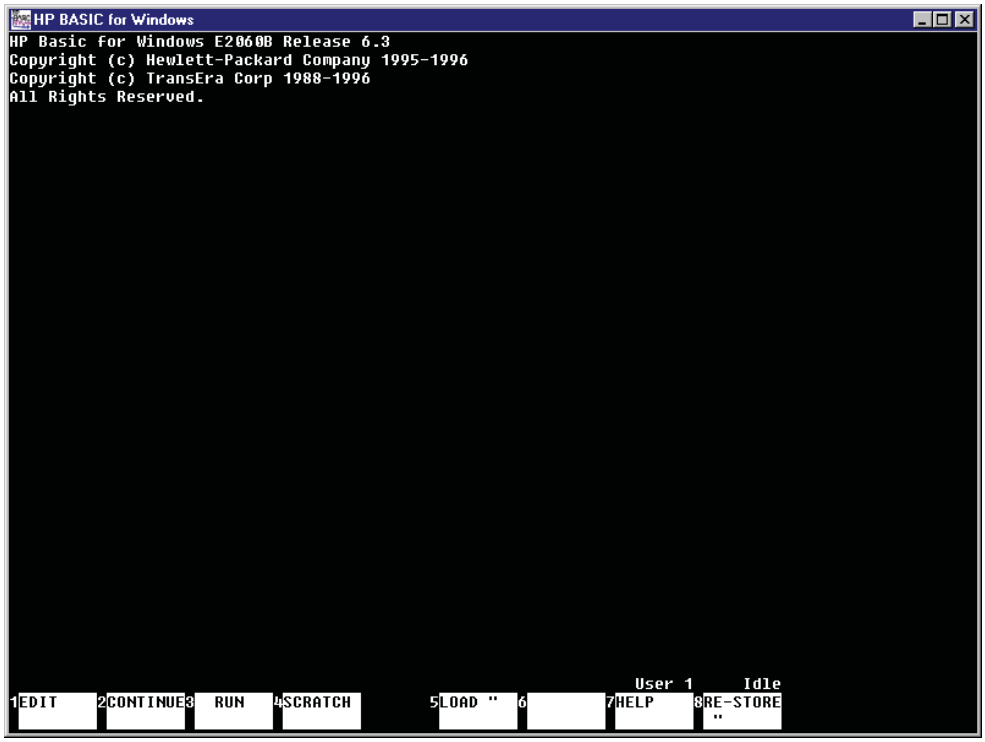


**Photo 3.1-1** Starting screen of HP Basic for Windows

#### 3.1.1.3. Menus and configuration displays on the screen after RUN command

### Test Scan on/off

**OFF**:

The actual measured data are read for normal measuring.

**ON**:

The sample data on the source code is used for program itself tests.

ON/OFF can be changed by deleting '!' on one of the lines 726 or 730 in the source code.

### information for configuration

These lines show the configuration for the print option and the store option in the Rob's basic program for the data acquisition. These functions (such as storing and printing measured values) can be executed on the Lookout.

### installed orifice plates for volumetric flow rates

This paragraph shows the information for installed orifice plates. The configuration can be changed on the lines 713 – 720 in the source code in Edit mode by replacing '!'.

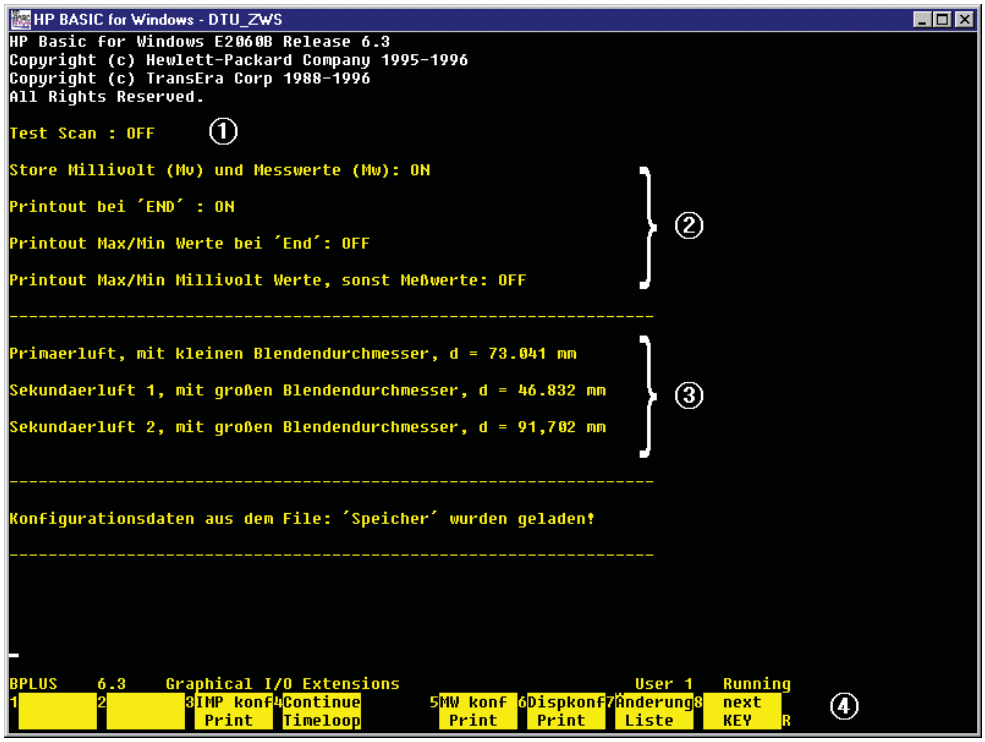


**Photo 3.1-2** Screen shot after RUN command

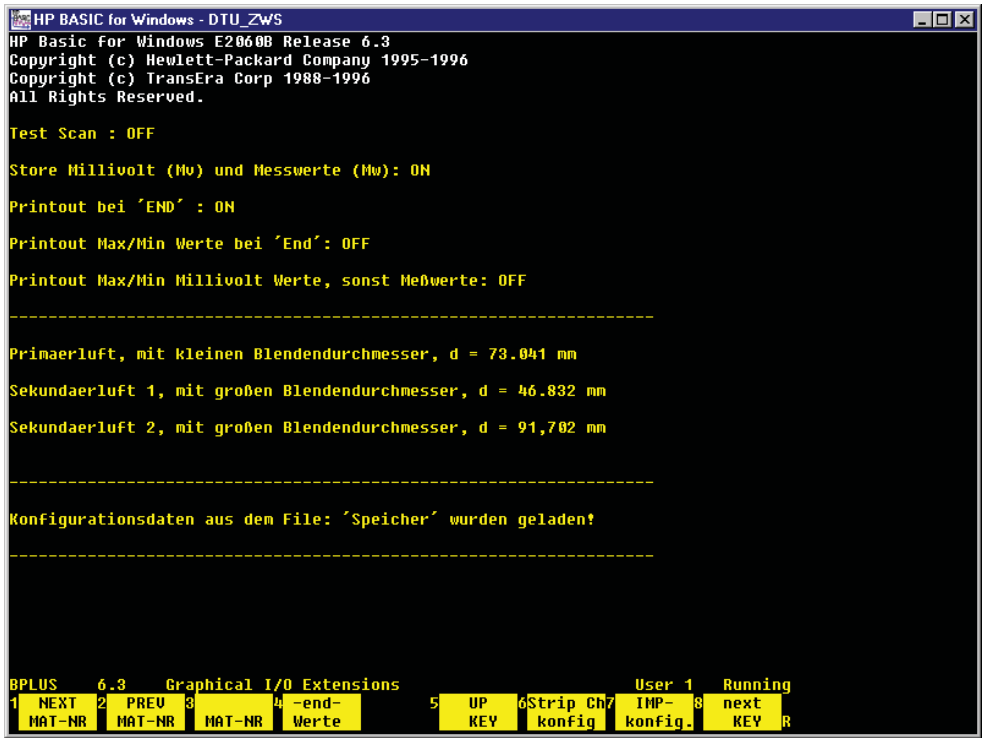


**Photo 3.1-3** Next menus

**menus**

These menus can be executed by either the function keys (F1 – F8) on a keyboard or by mouse clicking:

**IMP konf Print :**

prints IMP configuration data (IMP No., Channel, Mode, Matrix No.)

**Continue Timeloop :**

loads IMP configurations and then scans the measured values from IMPs see also the screenshot on operation (**Photo 3.1-6**)

On the occasion of any print command, a dialog window is opened and Times New Roman font and font size 8 should be selected.

**MW konf Print :**

prints the configuration data such as measuring points, Matrix numbers, IMP numbers, correction curves, dimensions, and modes. This command has two options. One is sorted by Matrix number and the other is by DTU and channel. See also MAT-NR

**Next KEY :**

shows next menus

In **Photo 3.1-3**, which is the screen shot for the next menus as the result of 'next menu' command.

**MAT-NR:**

Configurations for sensors (their name, Matrix No., mode (volt/resistor), dimension, correction curve), IMP and their channel can be set up. After the command, the number of the sensor which is configured must be specified.

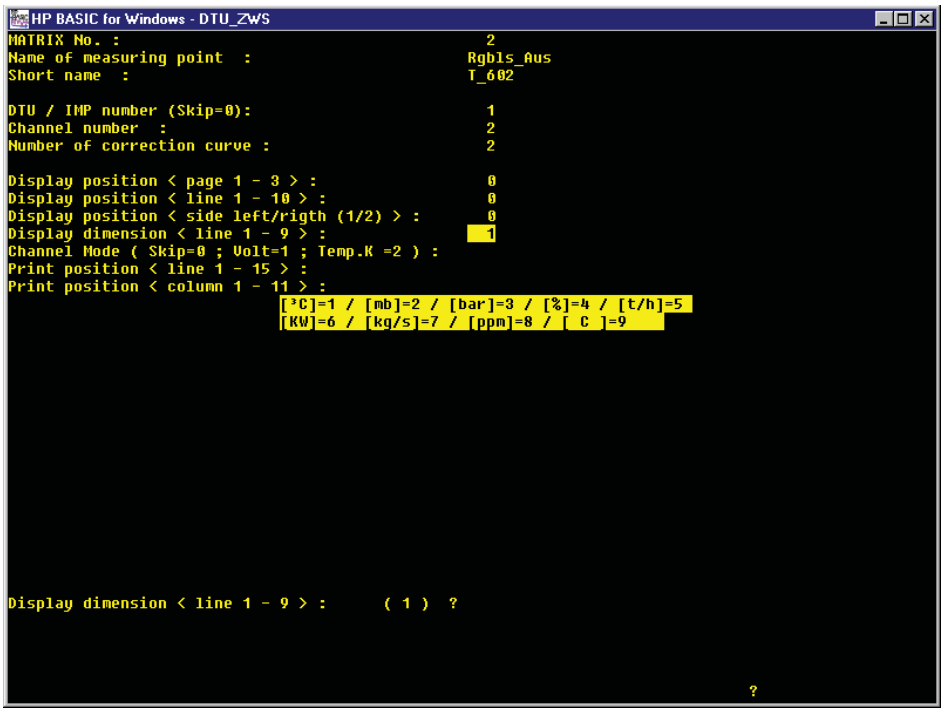


**Photo 3.1-4** Sensor configuration menus after MAT-NR command

Thereafter, information according to **Photo 3.1-4** can be shown on the screen. Display positions and print positions don't have to be entered. Leave them as 0. Input the number of suitable dimensions for the sensor on the display's dimension < line 1- 9> menu.

**NEXT/ PREV MAT-NR:**

Configurations for next or previous sensor. The matrix number for a sensor is required.

**-end- Werte:**

After sensor configuration or new sensor installation, the number of milli-volt signals (from e.g. pressure sensors) and from resistors (e.g. thermocouples) must be registered here respectively, when the total number of sensors according to the kind of output signals is changed.

The number of temperature sensors must not be changed (default is 1) in our case, because Pt-100 sensors are used for measuring temperature in stead of thermocouples and reference temperature is also not used. If any thermocouple is installed in the system, it must be changed to the last number without reference number. See also section dealing with temperature measuring

**Next KEY:**

Back to first menus

### 3.1.1.4. Edit mode

During running the measuring program or in a case of program interruption, it can be changed into Edit mode or stopped by 'ctrl + break' on a keyboard. The screenshot after breakage is shown in **Photo 3.1-5**.

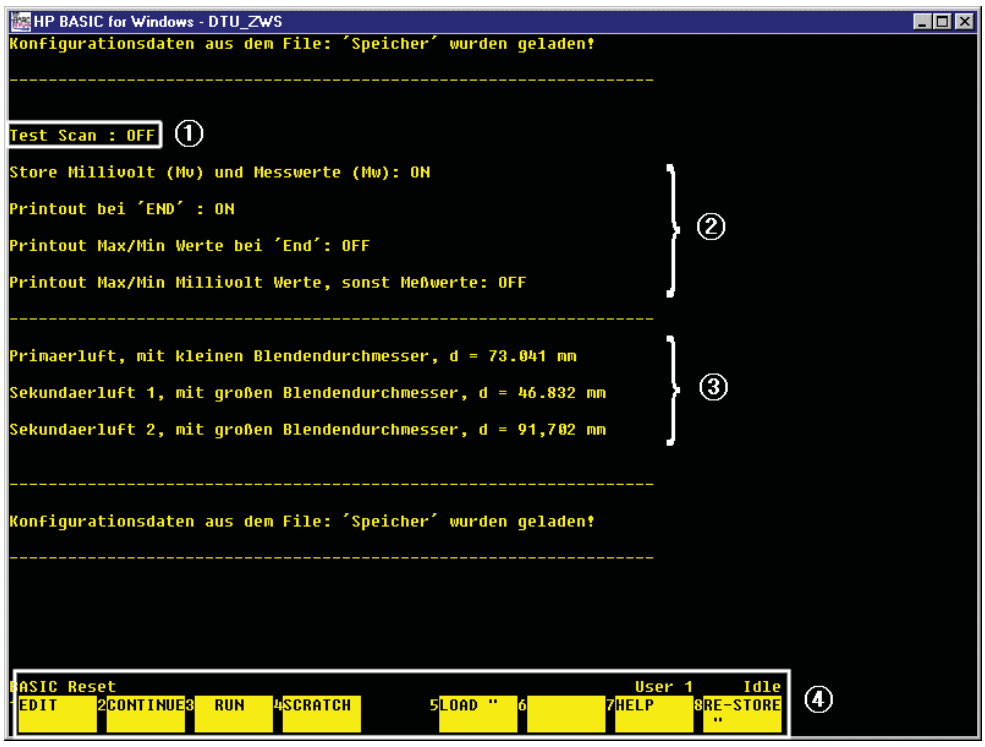


**Photo 3.1-5** Screen shot after breaking the procedure

The menus in the photo can be executed by either the function keys (F1 – F8) on a keyboard or by typing the command.

**EDIT:**

The source code can be edited in Edit mode. In case of editing a certain line, type 'edit [line No.]'

**CONTINUE:**

continues the paused procedure.

**RUN:**

runs the initialized program file.

**LOAD:**

is a shortcut key loading a source code (program).

**HELP:**

opens help window.

Usage : help [command]

#### 3.1.1.5. Menus on running

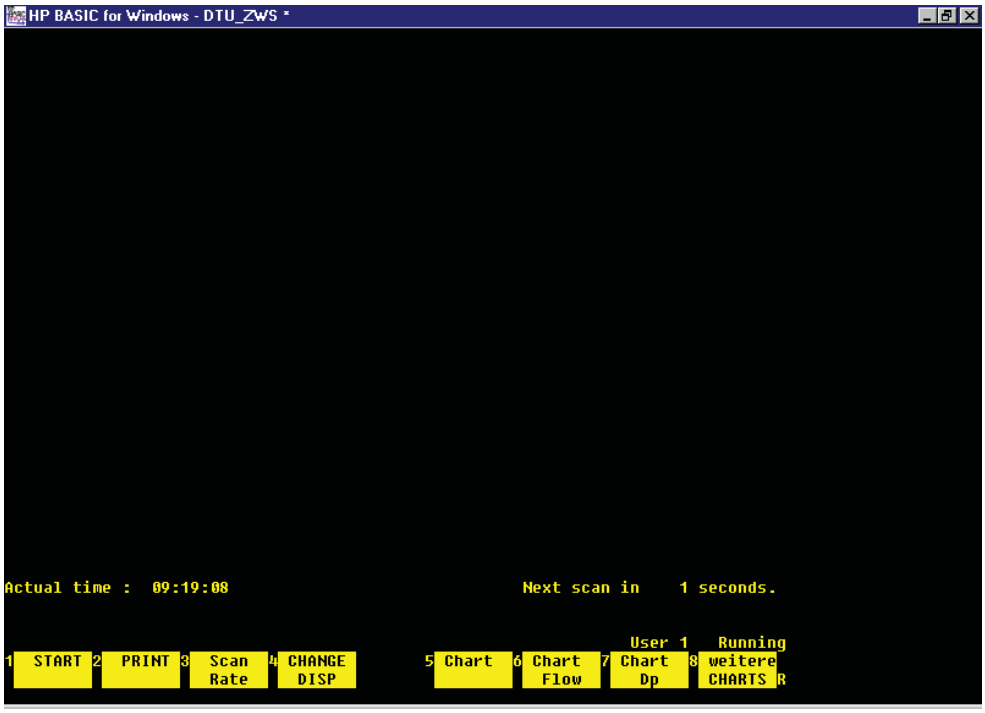


**Photo 3.1-6** screenshot on operation

When the measuring program is running, the remaining time to next scanning is displayed with current time. The Scan Rate is the interval to read data from IMPs and the default data scan rate is 10 seconds.

**START:**

It is used when the mean values in a certain time period are measured and saved. This is not used, as this is done by Lookout.

**PRINT:**

displays the measured (such as the measured voltage at the IMP from a sensor) and converted data values into a proper dimension.(**Photo 3.1-7**) After PRINT command, the specified matrix No. for the sensor to be displayed must be inputed.

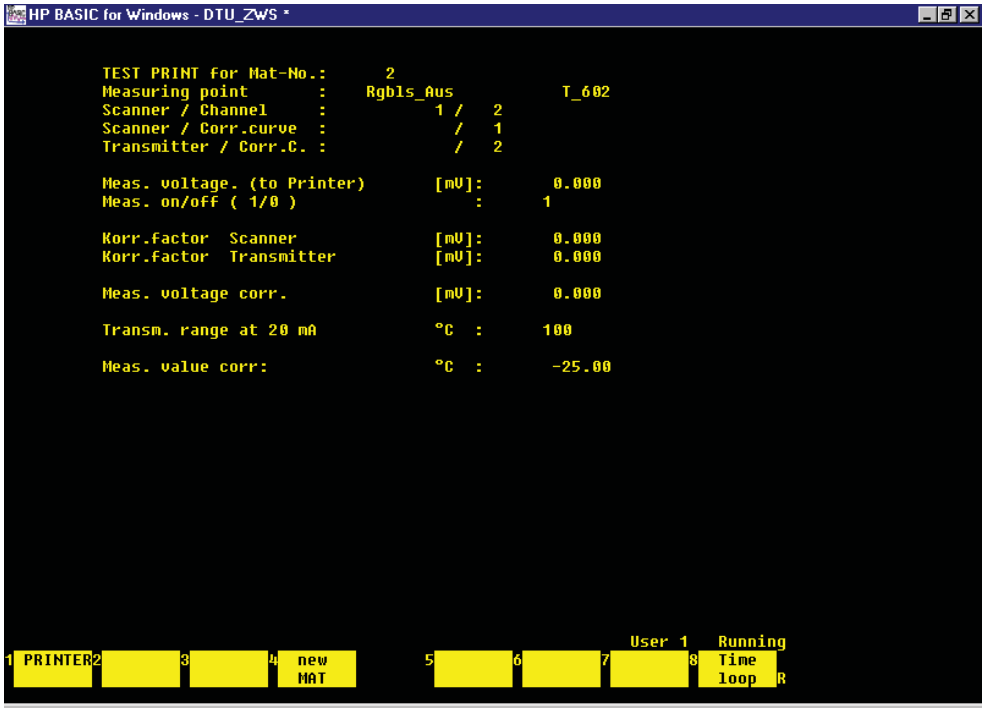


**Photo 3.1-7** Measured data from a specified sensor

**Scan rate:**

The scanning interval can be changed.

**Chart Flow:**

displays the graphs of volumetric flow rates.

**Chart Dp:**

displays the graph of the pressure difference for volumetric flow rates.

**Weitere Chatrs:**

More menus for temperature and pressure graphs.

In **Photo 3.1-8**,

**Chart P1:**

P101 – P110 graphs (Matrix No. 6 – 15)

**Chart P2:**

P201 – P 306 (Matrix No. 30 – 37), P501 and P 601 (Matrix No. 48 and 49)

**Chart P3:**

P401 – P410 (Matrix No. 38 – 47)

**Chart :**

Not used

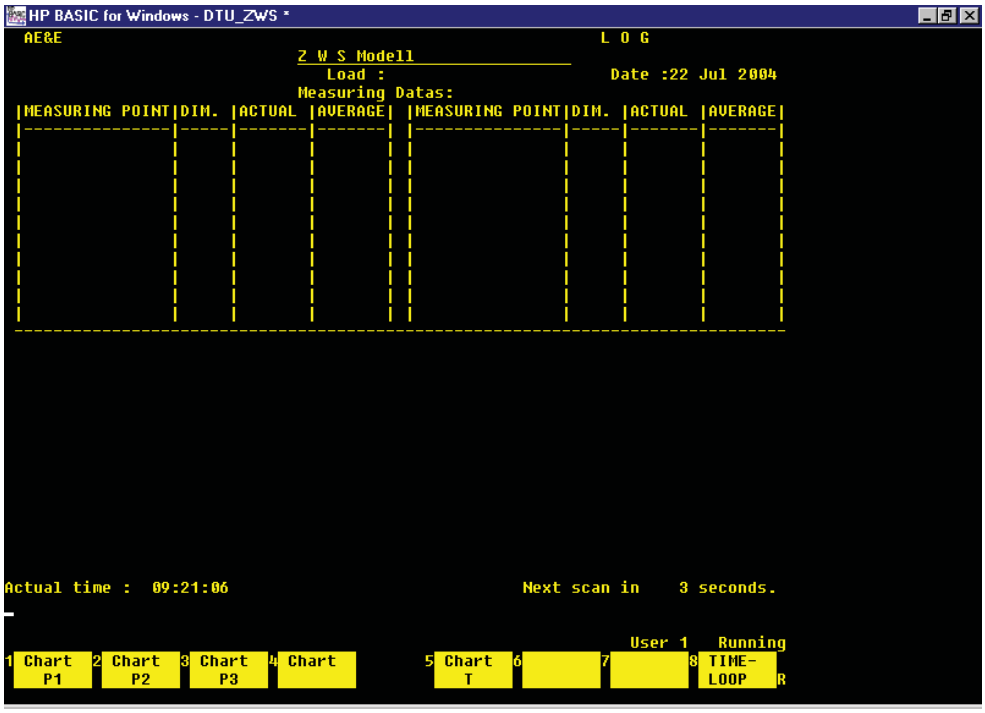


**Photo 3.1-8** Menus of more graphs

### 3.1.1.6. Some important lines in the source code

The un-compiled source code is used in Hp Basic for Windows and some configurations must be changed in the source code. Some important lines which may be changed as occasion demands are summarized in **Table 3.1-1**.

**Table 3.1-1** Some important lines and their use

| Lines | Usage |
|---|---|
| 10-12 | to save/restore the source code |
| 713-724 | configurations for orifice plates |
| 726-861 | configurations for in Photo 3.1-2 (program test/mili-volt save/..) |
| 3220 | to change the default interval for scanning |
| 7180-8081 | converting the measured signal into the proper dimension |
| 8112-8658 | variables for calculation of volumetric flow rate |
| 10350-10690 | volumetric flow rate calculation |
| 46340-47370 | program test data |
| 47540-47581 | correction curve |

## 3.1.2. Excel

The 'ZWS_DTU.xls' file reads the measured data from the temporary recorded text DB file, Exceldat, in the 'Daten' folder. The data is displayed on the 'Werte' worksheet. The Excel file is

located in the 'c:\Eigene Datei\' folder.

Excel can read an external text DB file every 1 min. This interval is too long to adjust our system. That's why a VBA program was needed and it was coded by Mark Read at VTIU. It mainly consists of two parts. One is for changing DB file format and saves as 'Exceldat2'. The other part of this program reads the 'Exceldat2' file and writes the data every 10 second on its own cell on 'Werte' worksheet in Excel. The interval can be changed on 'Do While interval' line on the VBA source code. To execute this script, click the 'Nur Daten lesen' button on the 'Werte' worksheet.

Although sensors are the same model from a same manufacture, the output signals can show deviations on each other under the same condition because of sensor their own error. The 'Null Punkt' button is used to initialize the initial data values (to make zero except temperature) and the initialized data values are displayed on the blue column (F); see **Photo 3.1-9**. Lookout reads these initialized values. The initializing must be executed before turning on the blowers or the roots pump.

See VBA source code.

| | A | B | C | D | F | G | H | K |
|---|---|---|---|---|---|---|---|---|
| 1 | ZWS - Kaltmodell | | | | | | Austrian Energy | |
| 2 | | | | | | | | |
| 3 | | | | | Nullpunkt | Daten lesen | Nur Daten lesen | |
| 4 | | | | | | | | |
| 5 | DATE / TIME (scan / load) | | 21- May 2004 | | 9:27:45 | 9:27:45 | 14:07:24 | |
| 6 | Measuring point | Dim | Mat. | symbol | Korrigierte | Actual | Average | |
| 7 | | | No. | AE | Werte | Value | Value | |
| 8 | Temperatures: | | | | | | | |
| 9 | BRENNKAMMER: Zylinder | °C | 1 | T_111 | 19 | 18.5 | | |
| 10 | ROOTSGEBLÄSE: Austritt | °C | 2 | T_602 | 18 | 18.3 | | |
| 11 | BOOSTERGEBLÄSE: Austritt | °C | 3 | T_701 | 19 | 18.8 | | |
| 12 | BETTMATERIALKÜHLER: Austritt | °C | 11 | T_411 | 18 | 18.1 | | |
| 13 | BETTMATERIALKÜHLER: Eintritt | °C | 12 | T_412 | 18 | 18.2 | | |
| 14 | Radialgebläse:Sekundär Luft | | | T_702 | 18 | 18.3 | | |
| 15 | Static pressures : | | | | | | | |
| 16 | BRENNKAMMER: Windbox | mb | 20 | P_101 | 0 | -0.1 | | |
| 17 | BRENNKAMMER: Konus Eintritt | mb | 21 | P_102 | 0 | -0.1 | | |
| 18 | BRENNKAMMER: Konus | mb | 22 | P_103 | 0 | -0.4 | | |
| 19 | BRENNKAMMER: Konus | mb | 23 | P_104 | 0 | -0.2 | | |
| 20 | BRENNKAMMER: Konus | mb | 24 | P_105 | 0 | -0.1 | | |
| 21 | BRENNKAMMER: Zylinder | mb | 25 | P_106 | 0 | -0.1 | | |
| 22 | BRENNKAMMER: Zylinder | mb | 26 | P_107 | 0 | 0.1 | | |
| 23 | BRENNKAMMER: Zylinder Austritt | mb | 27 | P_108 | 0 | -0.2 | | |
| 24 | Sek. Luft-Zufur Ebene 1 | mb | 28 | P_109 | 0 | -0.1 | | |
| | | mb | 29 | P_110 | | -0.2 | | |

**Photo 3.1-9** Worksheet in the excel file

### 3.1.3. Lookout

Lookout is a GUI(Graphic User Interface) application for automation and measurement from National Instruments. It's easy to set up measuring sensors and the measured data can be recognized intuitively.

Lookout has also functions to communicate with many communicating interfaces but cannot read GPIB/HPIB (General Purpose Interface Bus / Hewlett-Packard Interface Bus) data. The installed electrical devices for measuring are based on GPIB system and old types. This GPIB is needed for

a language interface application which must be programmed with a computer language such as C, C++, (Visual)Basic, etc.

The already installed Basic program can read the data from a GPIB modem and saves it to 'Exceldat' file temporary with text DB type. This data is read by Excel file which is by the name of 'ZWS_DTU.xls' located in 'c:\Eigene Datei\' folder. Lookout reads this measured data file with DDL (Dynamic Data Link) from Excel and displays it on a screen.

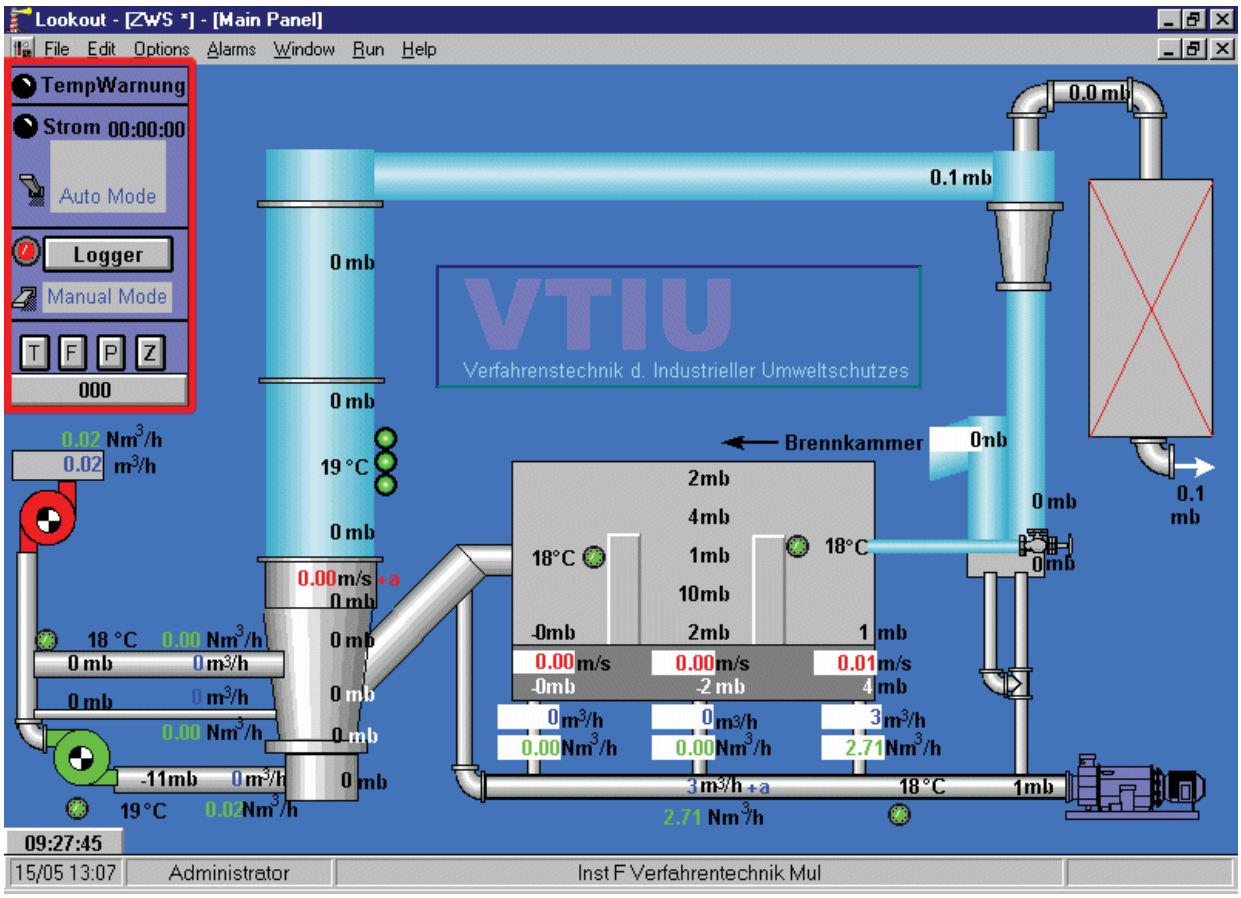


**Photo 3.1-10** Data acquisition with Lookout; main window

Almost all data which are measured from sensors on the system - pressure, normal/operating volumetric flow rate, calculated superficial velocity, temperature and their alarms (depending on temperature) are displayed. The alarm signs are displayed on this main window intuitionally (**Photo 3.1-10**) in a emergency.

Plexiglas is sky blue and white gradient parts.

### 3.1.3.1. Control box in main window

**TempWarnung :**

will be activated when one of the temperature measuring sensors in the system is too high or TempWarnung window is opened. See Alarms for details.

**Strom :**

is used to calculate the usage of electrical power. The gray box displays the operating blower such as blower or compressor. In case the blowers or the roots pump are turned off, they will still be displayed as active for ca. 10 min. for safety reasons.
The elapsed time is displayed on the right hand side of Strom. It can be switched between Auto Mode and Off by the switch located on the left side.

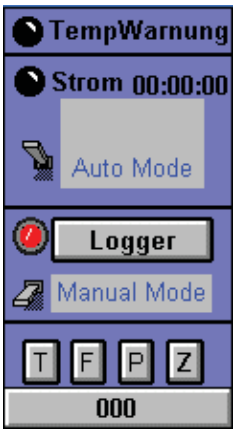


**Photo 3.1-11** Control Box

**Logger :**

This is used for saving the measured data.
It can be changed with the switch either to Manual Mode or to Auto Mode.

In Auto Mode, the data is recorded automatically every 10 seconds in the text file which is named on the Logger Control window, when the StromAktiv condition is true. The StromAktiv, logic variable, is true, if P100 (pressure of primary air) > 170 mbar or P110 (pressure of secondary air-2 , thick pipe) > 80 mbar or P109 (pressure of secondary air-1 , thin pipe) > 80 mbar or P601 (exit pressure from roots pump) > 30 mbar.
The push button (Logger) in Photo 3.1-12 is usually used for the Manual Mode. When the button is clicked, the Logger Control window is opened.

On the Logger Control window (Photo 3.1-12), the button, which is named as 'HFK1.txt' currently, is the file name to save. It can be changed by clicking the button and typing a new name.
The elapsed time since the beginning of saving is displayed under the file name button.
Comments can be also added on the save file with the third button which is named as 'BMK/HFK1/6, 05Hz/BB' currently.

The data is saved in 'c:\Lookout\2004\' as text based DB file. Each data is separated by comma and the measured data can be read in Excel by 'External Data'.

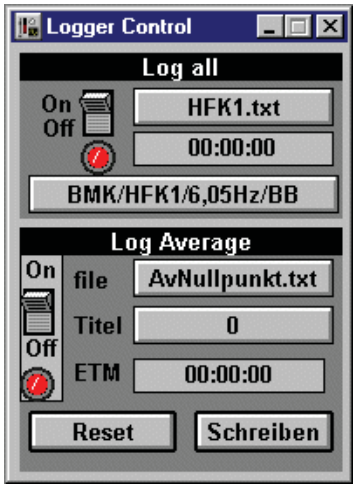


**Photo 3.1-12** Logger Control window

To record average values, the Log Average section is used. When the switch on the left hand side is turned on, Lookout calculates the average values from measured data with elapsed time and can be saved with 'Schreiben' button.

**The T, F, P, Z buttons:**

**T button** opens the Temperature Trends window, where all old and current temperature values in the system are displayed graphically and numerically. **F button** is for the gas volumetric flow rate window (including different pressure values, except normal volumetric flow rate). The **P button** opens the pressure window for blowers, combustion chamber and cylinder.

Finally the **Z button** opens the pressure trends window of filter exit, cyclone and pressure difference of P201 (pressure at cyclone entry) - P202 (pressure at cyclone exit) and P108 (pressure at cylinder exit which is located over the combustion chamber) - P202.

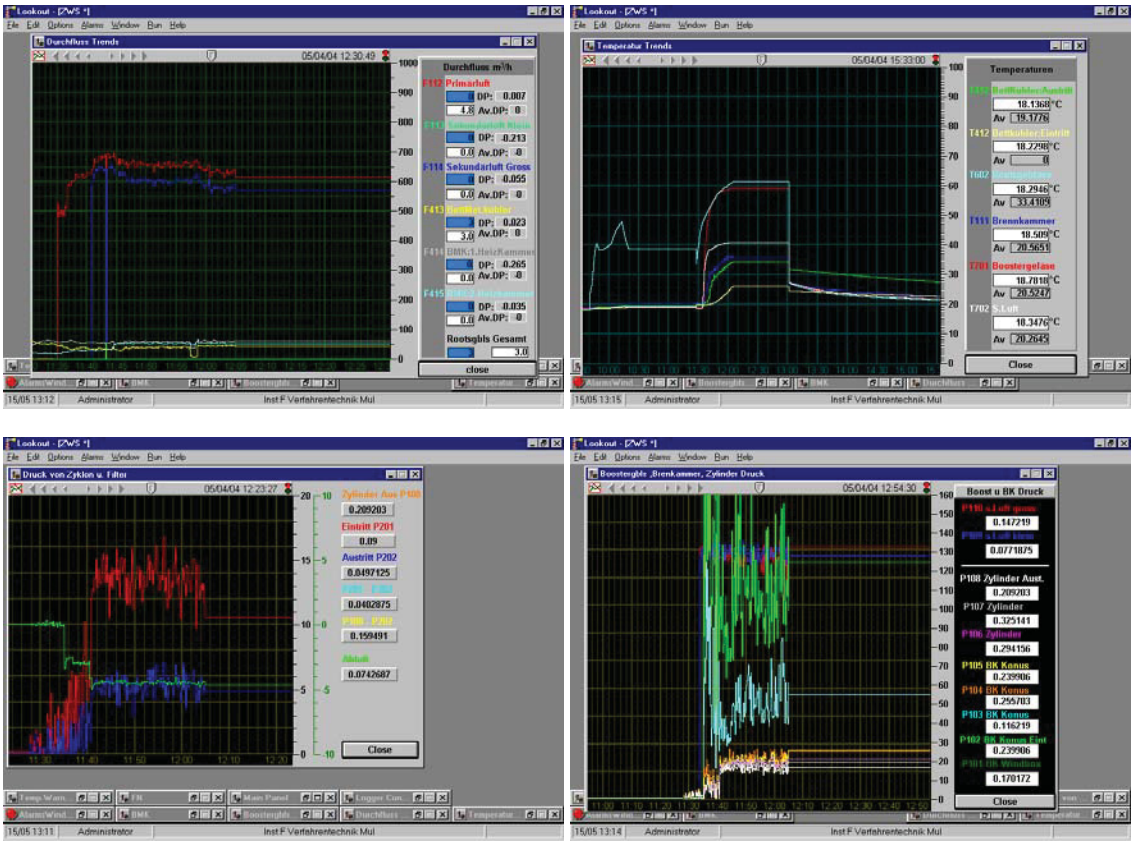

**Photo 3.1-13** Trend windows for Volumetric flow rates (left top), Temperature (right top), Pressure in the cylinder part (right bottom), other pressure readings(left bottom)

### 3.1.3.2. Alarms

The temperature of fluidizing air throughout the blowers and the roots pump is elevated by compressing, rubbing, friction etc. As Plexiglas is stable for operating temperature < 80 °C, the temperature of the air is very important for the safety of the construction.

If one of primary-, secondary air temperature (from the blowers) or compressed air temperature (from the roots pump) is too high, the overheated warning window is opened and the overheated part is indicated on the warning window.


**Photo 3.1-14** Overheated warning

The guide line for the upper temperature depends on the locations of temperature sensors. For example, the temperature of cylinder which is made of Plexiglas should be less than 75°C and the temperature of pipes from blowers to combustion chamber which is made of metal should be less than 80°C.

Whenever this overheated warning window is opened or any error such as reading data error exists on Lookout, the alarms are recorded on the alarms window and the number of alarms is displayed on the status bar which is located on the bottom of the main window. This alarms window can be opened by double clicking the alarms number on the status bar.

The alarms which are still active are indicated in red on the alarms window.


**Photo 3.1-15** Status bar on the main window

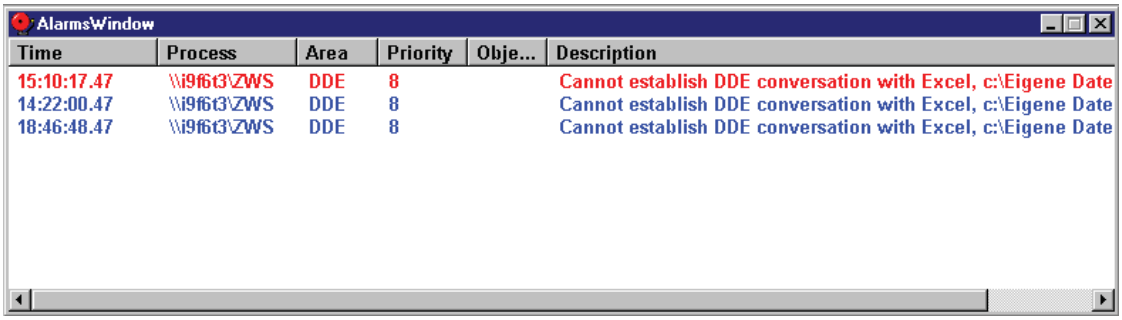


**Photo 3.1-16** Alarm window shows the alarms list

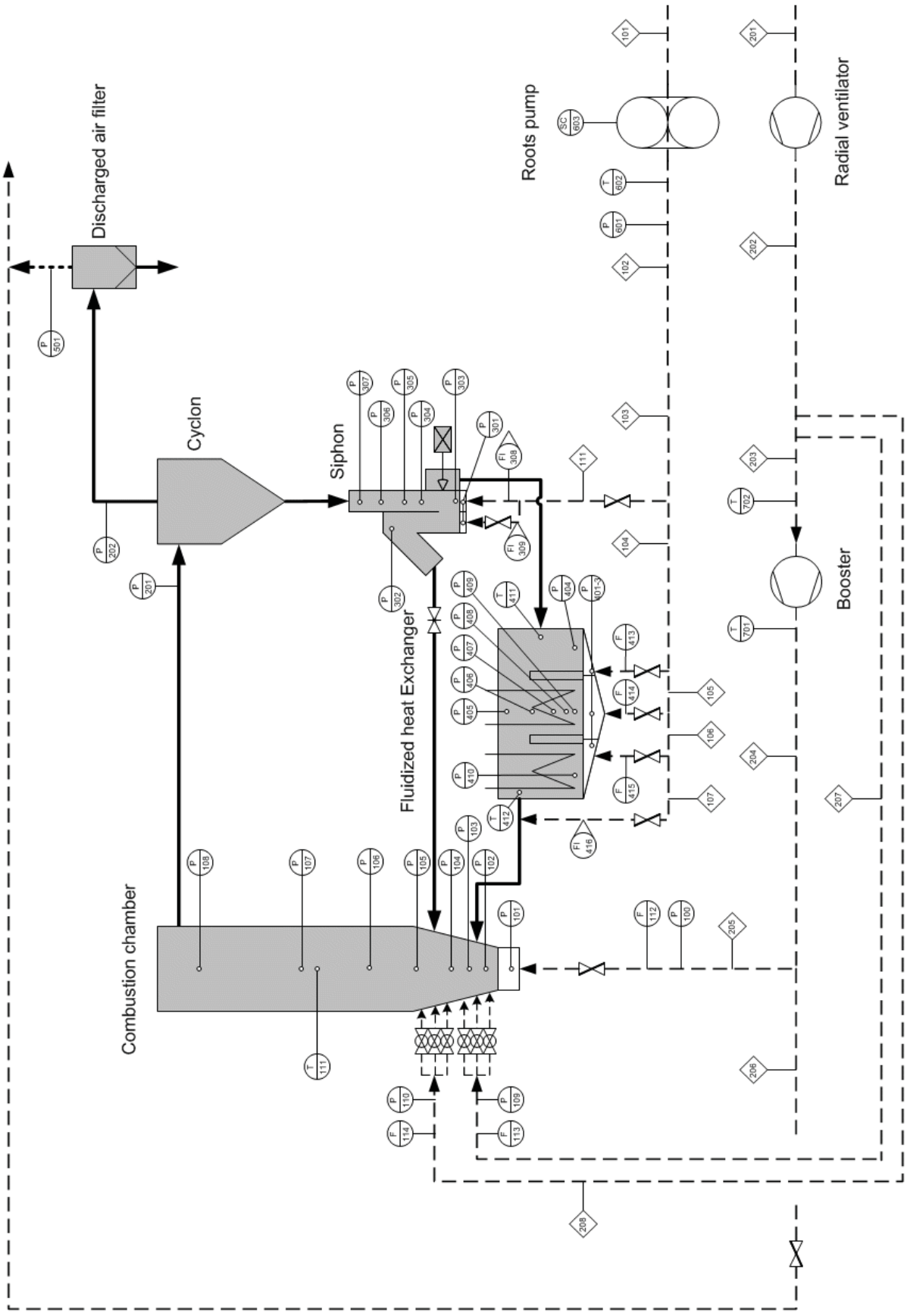


**Fig 3.1-3** Flow diagram and sensors' layout

## 3.2. Sensors

All sensors which are installed in the system use 4 – 20 mA as an output signal. This 4 – 20 mA signal cannot be recognized directly on a computer because it is an analog signal. Therefore, it must be converted to a 0/1 digital signal. This converting is done in a so called ADC (Analog to Digital Converter). For example, if an ADC has a 12 bit resolution power, the 4 – 20 mA analog signals is split up into $2^{12}$= 4096 digital signal steps. The converted digital signal is transmitted via a modem and a GPIB card into a computer. If the output analog signal from a pressure sensor with a range of 0 – 250 mbar is 12 mA (in fact mV is detected on the ADC according to Ohm's law with a shunt 100 Ω resistor), it denotes 125 mbar. In this way, the actual values of the operating variables, such as pressure, temperature, etc, can be measured and converted.

The 4 – 20 mA signal is used as an industrial standard, due to its advantages compared to the 0-20mA signal. Most of all, it is convenient to detect errors. For example, if the signal from a sensor indicates 0, it must have some error, such as a defect in the sensor or a short of circuit, etc.

### 3.2.1. Pressure sensors

The static pressure sensors which are installed in our cold model consist of mainly three types - high (0 - 1bar), middle (0 - 250 mbar) and low (0-50 mbar) pressure sensors in accordance with the amount of pressure drop in different parts of the system. The higher the range of the pressure sensor, the greater the fluctuation in the measured data. Therefore, average values should be taken over long enough time intervals.

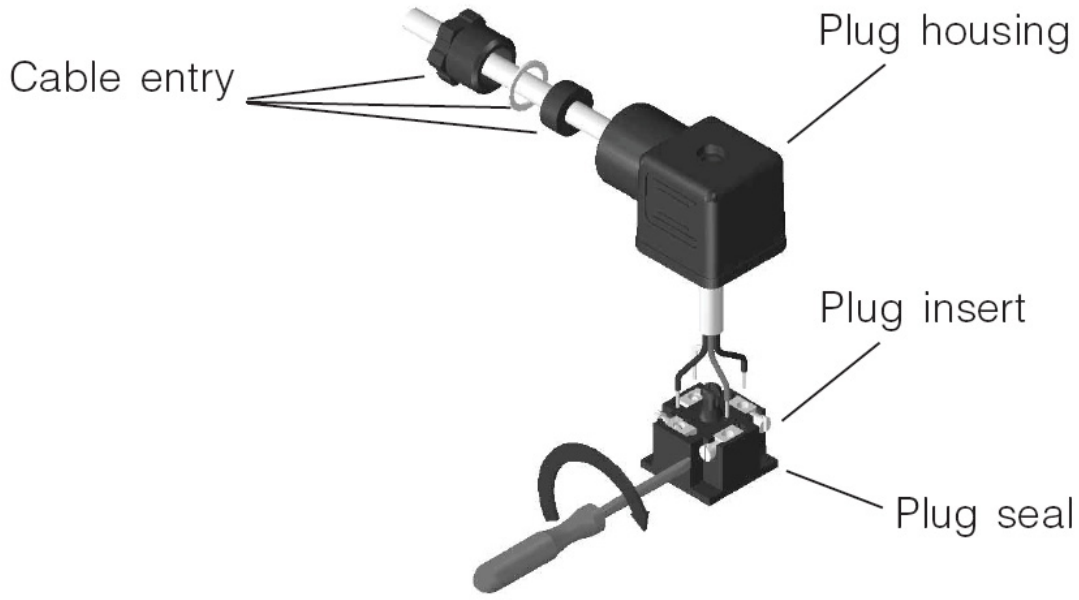


**Photo 3.2-1** Diagram for assembling a socket on a sensor and its fittings from a sensor manual

## High pressure sensors

These sensors are installed where Cu particles (or sand) cause relative high pressure, such as in the external **F**luidized bed **H**eat **E**xchanger (FHE) and the exit of the roots pump. The sensors can measure up to 1 bar and be overloaded up to 2 bar. Each sensor is connected with two wire. ( mostly + is brown )

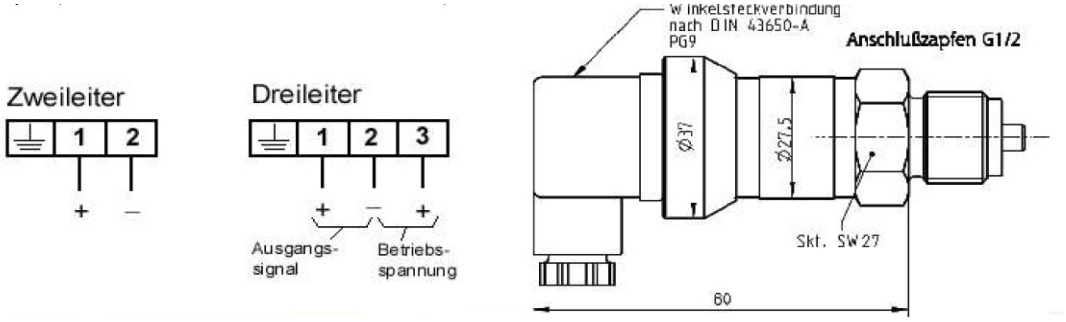


**Fig 3.2-1** Sensor dimensions and cable connections from manufacturer's data sheet

**Table 3.2-1** Specifications of the 1000mbar sensor from manufacturer's data sheet

| | |
|---|---|
| **Input pressure range** | |
| Nominal pressure gauge [mbar] | 1000 |
| Permissible overpressure [mbar] | 2000 |
| | |
| **Output signal / Power supply** | |
| Standard ( 2wire ) | 4 – 20 mA / 15 – 30 VDC |
| | |
| **Performance** | |
| Accuracy | < 1% FSO |
| Hysteresis | < 0.1% FSO |
| Permissible load ( V=24VDC ) | $R_{max}$ = 450Ω |
| | |
| **Thermal effect** | |
| Zero signal | 0.04% / K |
| Output signal | 0.01% / K |
| | |
| **Electrical protection** | |
| Protection type | IP65 after DIN EN 60529 |
| | |
| **Mechanical Stability** | |
| Vibration | 10g RMS (20 -2000 Hz) |
| Shock | 100g/11ms |
| | |
| **Permissible Temperature** | |
| Operating temperature | 0 – 80 °C |
| Storage | -40 – 100 °C |

For more information and questions : http://www.hy-line.de

### Middle pressure sensors

The sensors with a pressure range lower than 250 mbar are included in this type. They are installed at the combustion chamber and in the cylinder (P101 – P108), where pressure is relatively low, less than 250 mbar. Each sensor is connected with two wire cables between power supply and IMP. On the sensor socket (DIN 43650), part 1 is positive, mostly with the brown cable, and part 2 is negative.

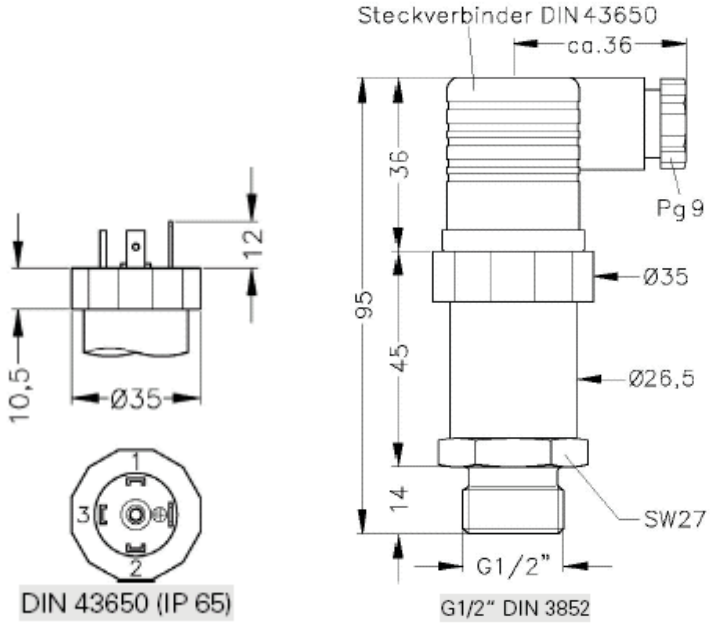


**Fig 3.2-2** Dimensions of the 250mbar sensor; from manufacturer guide lines

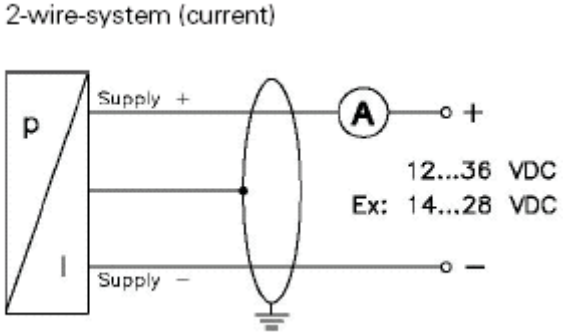


**Fig 3.2-3** Two cable connection; from manufacturer guide line

**Table 3.2-2** Specifications of the 250mbar sensor, acc. to the manufacturer data sheet

| **Input pressure range** | |
|---|---|
| Nominal pressure gauge [mbar] | 250 |
| Permissible overpressure [mbar] | 1000 |
| | |
| Output signal / Power supply | |
| Standard ( 2wire ) | 4 – 20 mA / 12 – 36 VDC |
| ===== Continued ==== | |

| ===== Continued ==== | |
|---|---|
| **Performance** | |
| Accuracy*1 | ≤ ± 0.35% FSO*2 |
| Permissible load | $R_{max} = [(Vs - V_{s\ min}) / 0.02]\Omega$ |
| Influence effects | Supply : 0.05% FSO / 10V |
| | Load 0.05% FSO / kΩ |
| | |
| **Thermal effect** | |
| Tolerance range for offset and span | ≤ ± 1 % FSO |
| In compensated range | 0-60 °C |
| | |
| **Electrical protection** | |
| Insulation resistance | >100 MΩ |
| Short-circuit protection | Permanent |
| Reverse polarity protection | No damage, but also no function |
| Electromagnetic compatibility | Emission and immunity according to EN 61326 |
| | |
| **Mechanical Stability** | |
| Vibration | 10g RMS (20 -2000 Hz) |
| Shock | 100g/11ms |
| | |
| **Permissible Temperature** | |
| Medium | -25 – 90 °C |
| Electronics / environment | -25 – 85 °C |
| Storage | -40 – 125 °C |

*1 : accuracy according to IEC 60770 – limit point adjustment (non-linearity, hysteresis, repeatability)
*2 : Full Scale Output
For more information and questions: http://www.bdsensors.de

## Low pressure sensors

The pressure at the cyclone inlet and discharged air filter outlet is considerably lower than 100 mbar and even shows a negative value at the filter. Therefore sensitive 100 mbar pressure sensors are installed. The two wire cable is connected like the other sensors. 1(+, brown) and 2 ( - ) are used at the connector ( IP65 ) for the sensor

**Table 3.2-3** Specifications of the sensor lower than 100 mbar; acc. to manufacturer's data sheet

| **Input pressure range** | |
|---|---|
| Nominal pressure gauge [mbar] | 100 |
| Permissible pressure [bar] | -0.2 / 15 |
| | |
| **Output variable / Power supply** | |
| Standard ( 2wire ) | 4 – 20 mA / 12 – 30 VDC |
| Range | 3-23 mA |
| Rise time ( 0 – 63% ) | 5 ms |
| === Continued === | |

| | |
|---|---|
| | === Continued === |
| **Performance** | |
| Accuracy *1 | < 0.5% FSO(inc. hysteresis and reproducibility) |
| Long-term drift of the zero signal | < 0.1% FSO / 2 years |
| Permissible load | $R_{max}$ = 37.5 ( V-12 )Ω |
| | |
| **Thermal effect** | |
| Zero signal | 0.015% / K |
| | |
| **Electrical protection** | |
| Protection type | IP65 after DIN EN 60529 |
| | |
| **Permissible Temperature** | |
| Operating temperature | -20 – 85 °C |
| Storage | -40 – 100 °C |

*1 : according to IEC770

For more information and questions : http://www.vega.com

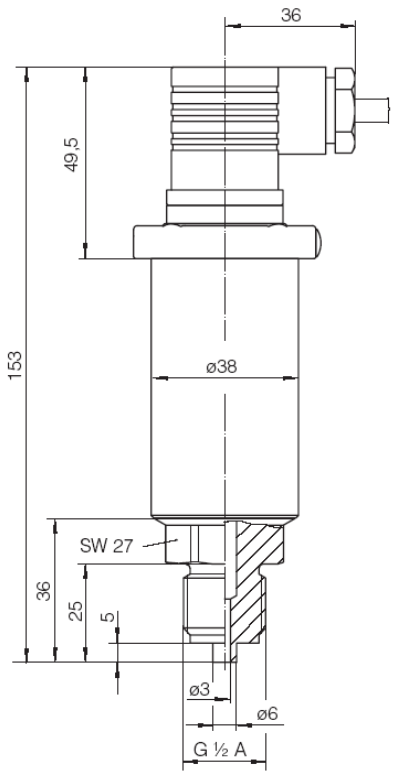


**Fig 3.2-4** Dimension of 50 mbar sensor; from manufacturer guide lines

### 3.2.2. Pressure difference sensors

The volumetric flow rate of the supply air is measured by the pressure difference between the upstream and the downstream side of an orifice plate. For this measurement the Siemens Sitrans P 7MF4422 ES is used. It contains a measuring cell filled with silicon oil.

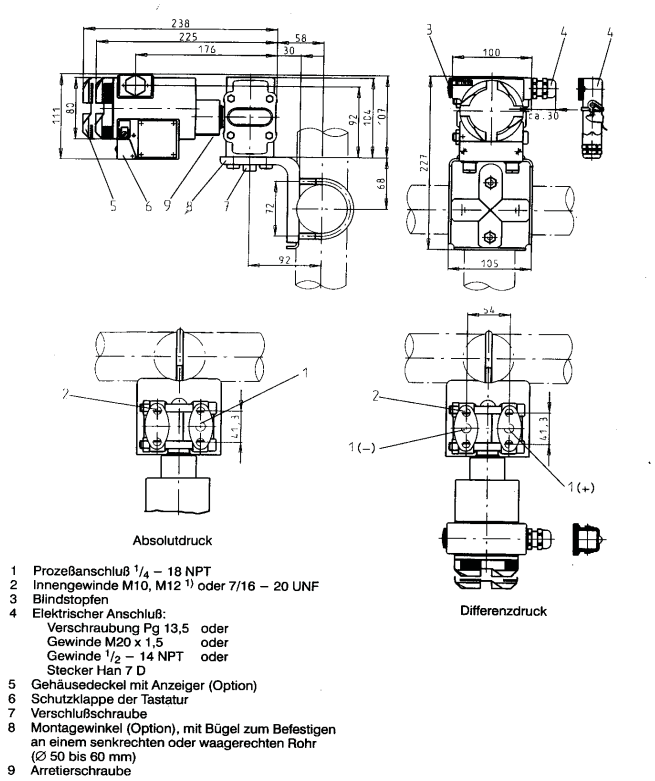


**Fig 3.2-5** Dimensions of pressure difference sensor Siemens Sitrans

**Table 3.2-4** General specifications for the pressure difference sensor Siemens Sitrans

| | | |
|---|---|---|
| | Nominal pressure | PN160 |
| Pressure | Measuring span | 1- +60 mbar |
| | Minimal static pressure in measure cell | 30 mbar |
| | Load limit (one side) | 30 mbar (absolute & nominal) |
| | Measure limit | -33 mbar - +90 mbar |
| Energy supply | Terminal voltage at sensor | DC11-45 |
| | Safety operation | DC 11- 30 |
| Output signal | | 4-20mA |
| | Under limt | 3.84 |
| | Over limit | 20.5 |
| | Residual ripple | ≤0.5% max. output signal |
| Permissible load | $R \le \frac{V_s - 11V}{0.023A}$ where, Vs is supplying voltage | |
| Temperature | | |
| | Permissible ambient temperature | -40 - +85 °C (in <5bar) |
| | Material to measure | -40 - +100 °C (in <5bar) |
| Limit error and others | | See manual |

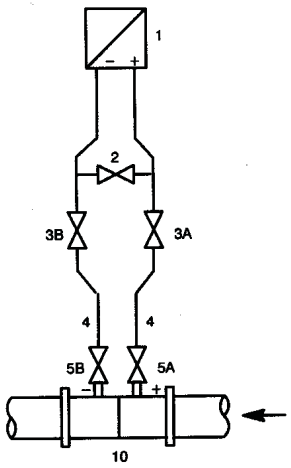


**Fig 3.2-6** Valve layout of the pressure difference sensor, 1. DP sensor, 2. balance valve, 3. operating valves, 4. pipes, 5. stop valves,10. pressure origin

**Zero compensation (all valves closed and not operating )**

1. open 5A&B (not installed in our case)
2. open '2' valve in **Fig 3.2-6**
3. open one of 3A or 3B
4. open the control panel cover with a screw driver
5. go mode 07 with m button
6. press both of up and down arrow for ca. 2 seconds (until 0.00 is displayed)
7. open the other valve of 3
8. measuring

See the sensor manual for more information.

### 3.2.3. Temperature sensors

Thermocouples work by producing a voltage proportional to the temperature differences between two junctions of dissimilar metals. By measuring this voltage, the temperature difference can be determined.

As the thermocouples produce a voltage, no external power supply is required to the test junction; however, for an accurate measurement, a reference junction is required. For a temperature monitoring system, reference junctions must be placed at each thermocouple or similar thermocouple wire.

On the other hand, Resistive Thermal Detectors (RTD) determine temperature by measuring the change in resistance of an element due to temperature. Platinum is generally utilized in RTDs

because it remains mechanically and electrically stable, resists contaminations, and can be highly refined. Since the temperature is determined by the resistance in the element, any type of electrical conductor can be utilized to connect the RTD to the indicator; however, an electrical current must be provided to the RTD.[35] The measuring range is -200 – 650 °C for class A and -200 – 850 °C for class B.[34]

According to NTB sensor data bank, the resistive values follow the next equations

$0°C < \vartheta < 850°C$ $\quad R_\vartheta = 100\Omega * (1 + 3.90802 * 10^{-3} * \frac{1}{°C} * \vartheta - 5.802 * 10^{-7} * \frac{1}{°C^2} * \vartheta^2)$

$-200°C < \vartheta < 0°C$ $\quad R_\vartheta = 100\Omega * (1 + 3.90802 * 10^{-3} * \frac{1}{°C} * \vartheta - 5.802 * 10^{-7} * \frac{1}{°C^2} * \vartheta^2 - 4.2735 * 10^{-12} * \frac{1}{°C^4} * (\vartheta - 100°C) * \vartheta^3)$

and the resistive value according to temperature in IEC 751 correlates according to the next table.

| Temperature [°C] | -100 | 0 | 50 | 100 | 200 | 300 | 500 | 850 |
|---|---|---|---|---|---|---|---|---|
| Resistive value [Ω] | 60.26 | 100 | 119.40 | 138.51 | 178.86 | 212.05 | 280.98 | 390.48 |

For our cold bed model, thermocouples have been selected due to economical reasons except at the **F**luidized bed **H**eat **E**xchanger (FHE). Problems were encountered due to sand which was electrically charged during operation by wall friction. The static electricity caused wrong thermal data readings.

Insulation and grounding were not effective. The only solution was the replacement with RTDs. Thereafter, the temperature data has showed no disturbance and the danger of a potential damage of the sensors and data acquisition system due to static electricity has been minimised.

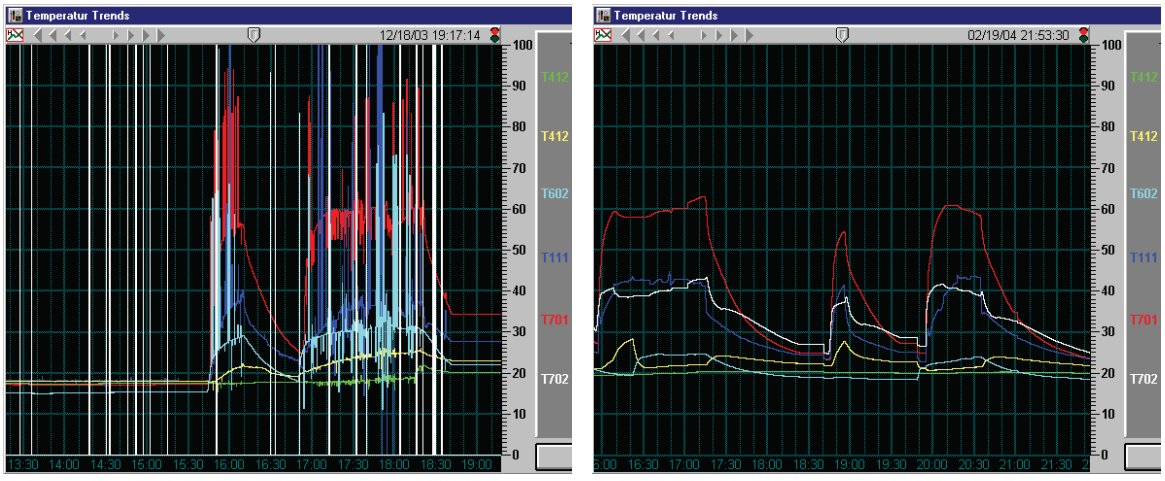


**Photo 3.2-2** Disturbed temperature values (thermocouples, left) and correct trend curves after replacing of the temperature sensors (RTD, right)

## Sitrans T

As noted before, a Pt100 returns a resistive value. However, the IMP detects measure data only as voltage. That's why a transformer between IMP and Pt100 is needed. This transforming is done by Siemens Sitrans T and changes resistance data from RTD into a 4 – 20 mA signal.

The following explanation about Sitrans T and its specifications is taken from the Sitrans T manual and reproduced here in edited form:

Beside RTD, the Sitrans T can be applied to the following sensor/signal sources with universal input circuit.

- Thermocouples
- DC voltage sources
- DC current sources

Resistance based sensor/potentionmeter

The green LED is used to indicate the operational status as follows:

| | |
|---|---|
| No power | LED not on |
| Normal operation | LED on |
| Fault condition | LED flashes (sensor breakage or transmitter error alarm) |

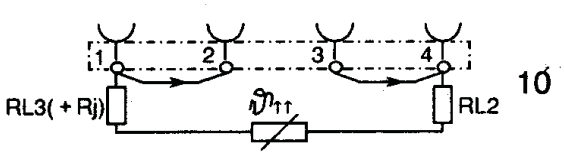


**Fig 3.2-7** Resistive thermometer connection with two wires

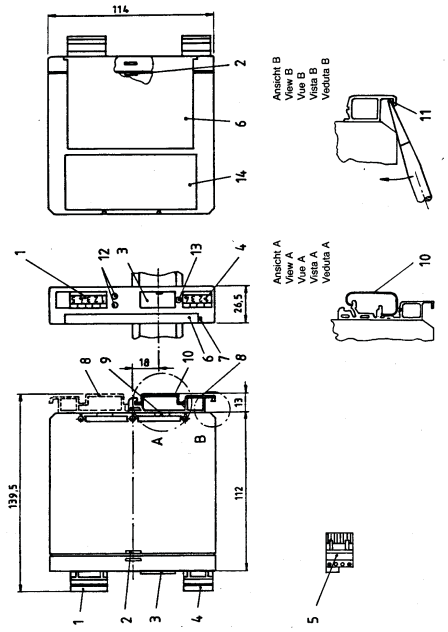

1. Plug-in screw terminal for ouput/power supply
2. Front panel latch
3. Parameterisation port and calibration push button
4. Plug-in screw terminal for input
5. Plug-in screw terminal as cold junction terminal for thermocouple
6. Rating plate and operation data
7. Cover latch
8. Mounting plate
9. Mounting plate latch
10. 35 mm DIN rail or 32 mm G rail
11. Test sockets for output signal
12. Test sockets for output signal
13. in operation indicator
14. Rating plate for explosion proof

**Fig 3.2-8** Dimensions of Sitrans

The calibration and parameterization can be done with the extra adapter, PC, 7NG3080 software package and printer for report.

**Line compensation**

Line compensation is only required if RTDs are being used in two wire circuits. Line compensation is performed using either the trimming resistor Rj (**Fig 3.2-7**) or the calibration push button, using the procedure described below.

- Short circuit the connections on the RTD.
- Press and hold the calibration pushbutton.
- The LED will flash in a 2 second cycle.
- After 3 flashes, the LED remains blank; release the button.
- The line resistances $R_{L2} + R_{L3}$ (**Fig 3.2-7**) are measured and stored.
- The LED remains off for about another second and then comes on and stays on.
- Remove the short circuit on the RTD

Technical data (concerned with RTD only)

**Table 3.2-5** Specifications for Sitrans T

| | |
|---|---|
| Sensor type | Pt100(IEC 751)<br>Pt100(JIS C1604)<br>Ni100(DIN 43760)<br>Cu100<br>Multiple or part of specified basic value (e.g. Pt500, Cu25) |
| Type of input connection | **Normal**, averaging or differential connection |
| Normal connection | One RTD in two, three or four wire circuit |
| Averaging/differential connection | See manual |
| Connection | **2**, 3, or 4 wire circuit |
| 2 wire circuit | Parameterized line resistance or line calibration using calibration pushbutton |
| 3, 4 and differential circuit | No calibration necessary |
| Line resistance | ≤ 100Ω |
| Measuring span<br>(2 and 3 wire circuit /<br>4 wire and differential circuit) | Min.: arbitrary; recommended 9Ω (9Ω corresponds about 25 °C)<br>Max.: 3230 / 500 Ω |
| Measuring range | Parameterisable |
| Characteristic | Resistance or temperature linear |
| | |
| Sensor breakage monitoring | Monitoring of all terminations for breakages<br>(functions can be disabled) |
| Response/drop threshold | 600 to 900 Ω line resistance |
| Temperature unit | °C, K, °F, °R parameterisable (°R (Rankine) = absolute °F) |
| Output | |
| Output signal | Load independent DC current |
| === continued === | |

| === continued === | |
|---|---|
| Rated current $I_{AN}$ | 20 mA |
| Rated range | 4 to 20 mA (= 0 to 100 %) |
| Resolution | 5888 steps (0 to 100 %) |
| Overrange | 3.8 to 20.8 mA (= -1.25 to 105 %) |
| Sensor breakage range | 3.6 to 21.2 mA ( -2.5 to 107.5 %) parameterisable |
| Load | $R_B/k\Omega = \frac{U_H / V - 12.0}{21.2}$ |
| Residual ripple | ≤ 1%, measured with a band width of 1MHz |
| Response time | |
| Sampling cycle | 100ms |
| Sensor breakage signaling | LED, relay output, NAMIR output or electronic power output |
| LED | Starts flashing |
| Others | See manual |
| Power supply | |
| Not explosion proof | DC 12 to 45 V |
| Explosion proof | DC 12 to 30 V |
| Error limits under nominal conditions [1)] | Input error limits [2)] |
| Pt100 (with/without calibration) | -200 to 280 °C ≤ ± 0.08 K / ≤ ± 0.03 K |
| Others | See manual |
| Environmental conditions | |
| Operating temperature | (permitted ambient temperature acc. To VDE/VDI 2912 |
| Installed in zone 1, T6 | - 10 to + 50 °C |
| Installed in zone 2, T5 | - 10 to + 65 °C |
| Installed outside hazardous area | - 10 to + 65 °C |
| Storage temperature | - 40 to + 85 °C |
| Relative humidity | |
| Nominal range | 5 to 95%, no condensation |
| Influencing effects, referred to $I_{AN}$ or $U_{AN}$ of ambient temperature | |
| During resistance measurement | |
| On start of scale | |
| On span | |
| Others(TC, voltage, ..) | See manual |
| Of power supply | ≤ 0.1 % with voltage changes between 12V and 40V |
| Of line resistance | ≤ 0.02% /10Ω |
| Long term effect on measuring | |
| Span and start of scale | ≤ 0.03 % / Month |

[1)] Nominal condition :

| | |
|---|---|
| Power supply | 15V ±1% |
| Load | 100Ω ±1% |
| Ambient temperature | 23°C ±1K |
| Interfering field | none |
| Warm-up period | ≥ 5 min |

[2)] incl. Characteristic linearization error of temperature sensor.

## 3.3. Orifice plates

A orifice plate has an square-edged or sharp-edged centered circular opening in it smaller than the internal diameter of the pipeline. This changed cross-section of the flow causes pressure difference between upstream and downstream flow like a venturi tube.
For a centered circular orifice in a pipe, the pressure differential is customarily measured between one of the following pressure-tap pairs. Except in the case of flange taps, all measurements of distance from the orifice are made from the upstream face of the plate; [36].

***Corner taps***. Static holes drilled one in the upstream and one in the downstream flange, with the openings as close as possible to the orifice plate.
***Radius taps.*** Static holes located one pipe diameter upstream and one-half pipe diameter downstream from the plate.
***Pipe taps***. Static holes located 2a pipe diameters upstream and eight pipe diameters downstream from the plate.
***Flange taps***. Static holes located 25.4 mm (1 in.) upstream and 25.4 mm (1 in.) downstream from the plate.
***Vena-contracta taps***. The upstream static hole is one-half to two pipe diameters from the plate. The downstream tap is located at the position of minimum pressure


**Photo 3.3-1** Types of orifice plates

The following derived equations are taken from [28].
Assuming that there is no loss of energy, no changing of internal energy and applying Bernoulli's equations,

$$\frac{p_1}{\gamma}+\frac{V_1^2}{2g}=\frac{p_2}{\gamma}+\frac{V_2^2}{2g} \qquad (3.3\text{-}1),$$

where γ is the specific weight. The relation with density is $\gamma = \rho g$. V = volumetric flow rate, p = static pressure and g = gravitational acceleration.
The compression coefficient is derived as $C_c=A_2/A$.
For incompressible flow, continuity holds in the form $A_1V_1=AV_2$,

$$\frac{\pi d_1^2}{4} V_1 = \frac{\pi d^2}{4} C_c V_2 \qquad (3.3\text{-}2)$$

Substituting ( 3.3-2 ) in the Bernoulli's equation (3.3-1)

$$V_2 = \sqrt{\frac{2g(p_1 - p_2)/\gamma}{1 - C_c^2 (A/A_1)^2}} \qquad (3.3\text{-}3)$$

The $V_2$ is the theoretical value which will be slightly greater than the actual value.

To apply this formula for real fluid, some energy loss must be considered.

Therefore a coefficient of velocity, $C_v$, is introduced and the flow rate $Q_2$ becomes:

$$Q_2 = C_v A_2 V_2 = C_v C_c A \sqrt{\frac{2g(p_1 - p_2)/\gamma}{1 - C_c^2 (A/A_1)^2}} \qquad (3.3\text{-}4)$$

Substituting $\gamma = \rho g$ in this equation, the equation can be now written:

$$\boxed{Q = C\sqrt{\frac{\Delta p}{\rho_g}}} \qquad (3.3\text{-}5)$$

where $\Delta p$ = pressure difference, $p_1$-$p_2$, $\rho_g$ denotes the density of the fluid at the actual temperature.

The coefficient C is

$$C = C_v C_c \sqrt{\frac{2}{1 - C_c^2 (A/A_1)^2}} \qquad (3.3\text{-}6)$$

Table 3-1 and 3-2 specify numerical values for the constant C of the installed orifice plates in the system. After replacing an orifice plate, the Basic source code must be changed according to case 1 or 2.

See also Basic source code in order to change orifice plates or C values.

**Table 3.3-1** Installed C values in Basic program; case 1 denotes smaller opening in orifice plate than case 2

| | | | | |
|---|---|---|---|---|
| combustion chamber | primary air | C112 | case 1 | 138.19 |
| | | | case 2 | 246.12 |
| | secondary air-1 | C113 | case 1 | 24.84 |
| | | | case 2 | 57.09 |
| | secondary air-2 | C114 | case 1 | 104.42 |
| | | | case 2 | 247.88 |
| | | | | |
| FHE | empty chamber | C413 | | 28.22 |
| | 1st heating chamber | C414 | case 1 | 19.8 |
| | | | case 2 | 52.06 |
| | 2nd heating chamber | C415 | | 52.06 |
| | =current installed plate | | | |

**Table 3.3-2** Pipe diameter (Di), orifice opening (d), orifice plate diameter (D), thickness of orifice plate (E), thickness of square-edged part (e)

| Pos. Nr. | measuring point | class | Di mm | d mm | D mm | E mm | e mm |
|---|---|---|---|---|---|---|---|
| 112 | primary air | case 1 | 125 | 73.04 | | 3 | 1.5 |
| | | case 2 | 125 | 91.7 | | 3 | 1.5 |
| 113 | secondary air | case 1 | 82.5 | 33.64 | | 3 | 1.5 |
| | | case 2 | 82.5 | 46.83 | | 3 | 1.5 |
| 114 | secondary Air | case 1 | 125 | 64.27 | | 3 | 1.5 |
| | | case 2 | 125 | 91.7 | | 3 | 1.5 |
| 413 | FHE empty chamber | | 54.5 | 32.47 | | 3 | 1.5 |
| 414 | FHE 1st heating chamber | case 1 | 54.5 | 28 | | | |
| | | case 2 | 54.5 | 41.26 | | 3 | 1.5 |
| 415 | FHE 2nd heating chamber | | 54.5 | 41.26 | | 3 | 1.5 |

*) Pitch circle diameter

**Table 3.3-3** The maximal measurable volumetric flow rates of the installed orifice plates, which is verified with a turbine- and a hot wire anemometer

| | $Q_{max}$[Nm$^3$/h] |
|---|---|
| Primary air | 880 |
| Secondary air -1 | 350 |
| Secondary air -2 | 1500 |
| Empty chamber | 180 |
| 1st heating chamber | 350 |
| 2nd heating chamber | 350 |

# 3.4. Electrical devices

This section includes electrical devices between sensors and computer as well as electrical layouts.

## 3.4.1. Electrical layouts

The circuit diagram from power supply box 4 with all temperature sensors, some static pressure sensors and pressure difference sensors connected, is shown in **Fig 3.4-1**. See also Tables in the appendix.

The power no. are the power supply box numbers and channels where the sensor are connected. For example, power no. 4/2 denotes that the sensor is connected to power supply box 4, channel 2 on

the box.

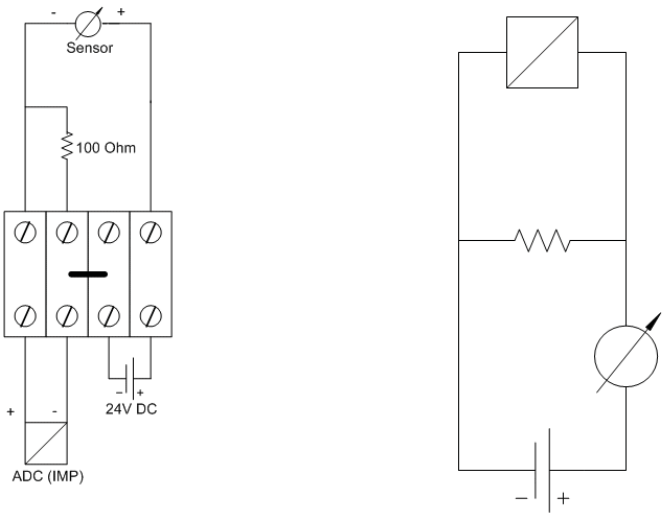


**Fig 3.4-1** Connection layout in power box 4

Current transformers from AC to DC supplies 24V DC. Resistors and ADC( IMP ) are connected as a parallel circuit. Output signal is mA. According to Ohm's law, V = IR, voltage can be measured at ADC with a shunt 100 Ω resistor. This voltage depends on the output signal from the sensor and the operation variables of the process.

There was a lack of 100 Ω resistors on installing the system and T602, T111, T701 are shunted with 169 Ω resistors. Correction of measured values is done in the Basic program; ( line 8050 – 8081 ).

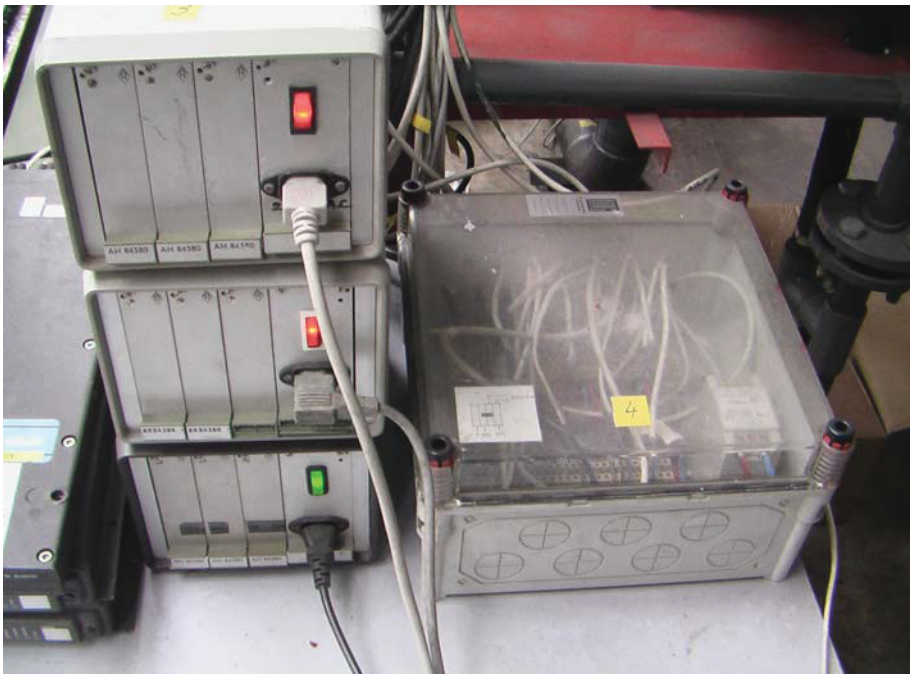

**Photo 3.4-1** Power supply boxes

### 3.4.2. ADC(IMP)


**Photo 3.4-2** IMPs

IMP (**I**solated **M**easurement **P**od) is a data acquisition module containing: signal conditioning, 16bit ADC, communications to host computer, built-in sensor energisation and a detachable connector block, housed in a NEMA 4 / IP55 environmentally protected case and built to ISO 9001 standards. IMPs can make measurements of DC voltage, current, temperature (direct from thermocouples or PRTs), resistance, 4-20mA signals, pressure, frequency, and so on, under the control of the internal processor, as directed by commands from the host computer.

Each IMP consists of a sealed case containing a measurement module and a separate connector block that slides into the main IMP housing and is screwed securely in place.
The Universal IMPs 3595 1H which is installed in our system can be used with SCADA, C & I and DAS environments.

General Specifications from the manufacturer are as follows:

Environment

| | |
|---|---|
| Storage temperature : | -25° to 75°C (-13° to 167°F) |
| Operating temperature: | -20° to 70°C (-4° to 158°F) |
| Humidity, at 40°C (non-condensing): | 95% |
| Vibration, operating for 2 hours: | 5g, 11Hz to 500Hz |

Otherwise, to Def. Std 66/31, Issue 01, Cat. IV.

**Table 3.4-1** General specification of IMP acc. to manufacturer's data sheet

| **Features** | |
|---|---|
| Number of Channels | 18 |
| Switching | reed relay, 3 or 6 pole |
| Reed relay life | $>10^8$ |
| Maximum signal measured : | ±12V |
| Maximum input voltage : | ±14V |
| Overload protection, continuous : | 50V |
| Max voltage between any two inputs | 200V |
| Common mode, between IMPs | 500V |
| Mean Time Between Failures : | 64,000 |

| **Measurement** | |
|---|---|
| Voltage dc ( Standard connector ) : | ±12V |
| Current dc (with 100ohm shunt) | ±20mA |
| Thermocouple type : | B,E,J,K,N,T,R,S |
| Thermocouple Cold Junction : | External or Automatic |

## Limits of errors

**All limits of error shown in the following specifications are for 1 year at 20°±3°C (68°±5°F)**

**DC Voltage**

Temperature coefficient of ADC:
<(0.0015%rdg+0.2µV) per °C
3595 3D High Voltage Connector introduces 0.04% + 100µV rdg additional error.

*20ms/16.67ms Integration time:*

| Range | Full Scale | Sensitivity | Limits of Error |
|---|---|---|---|
| 20mV | 22.000 | 1µV | ±[0.02%rdg + 5µV] |
| 200mV | 220.00 | 10µV | ±[0.02%rdg + 0.01%fs] |
| 2V | 2.2000 | 100µV | ±[0.01%rdg + 0.01%fs] |
| 12V | 12.000 | 1mV | ±[0.05%rdg + 0.01%fs] |

*5ms/4.17ms Integration time:*

| Range | Full Scale | Sensitivity | Limits of Error |
|---|---|---|---|
| 20mV | 22.000 | 2µV | ±[0.02%rdg + 20µV] |
| 200mV | 220.00 | 20µV | ±[0.02%rdg + 0.04%fs] |
| 2V | 2.2000 | 200µV | ±[0.01%rdg + 0.04%fs] |
| 12V | 12.000 | 2.5mV | ±[0.05%rdg + 0.04%fs] |

*1.25ms/1.04ms Integration time:*

| Range | Full Scale | Sensitivity | Limits of Error |
|---|---|---|---|
| 20mV | 22.000 | 8µV | ±[0.02%rdg + 80µV] |
| 200mV | 220.00 | 80µV | ±[0.02%rdg + 0.16%fs] |
| 2V | 2.2000 | 800µV | ±[0.01%rdg + 0.16%fs] |
| 12V | 12.000 | 8mV | ±[0.05%rdg + 0.16%fs] |

**DC Current**

Sensitivity, (using 100Ω shunt): 10nA
Error as for DC Voltage + error of shunt resistor + leakage currents

**Thermocouples**

The following figures are based on 20ms/16.67ms integration times.
All specified in degrees Celsius.
Error quoted is conformity to IEC584 (BS4937).
(IMC 3595 51A, 51C and 51E must be in draught-free enclosure: no forced cooling)

| Type | Mid Range | Error | Full Range | Error |
|---|---|---|---|---|
| B (Pt-30% Rh/Pt-6%Rh) | 400 to 1820 | <0.3 | 80 to 1820 | <2.0 |
| E (Ni-Cr/Cu-Ni) | -100 to 250 | <0.3 | -210 to 1000 | <0.5 |
| J (Fe/Cu-Ni) | -100 to 350 | <0.3 | -210 to 1200 | <0.7 |
| K (Ni-Cr/Ni-Al) | -100 to 450 | <0.3 | -200 to 1370 | <1.0 |
| N (Nicrosil/Nisil) | -180 to 1280 | <0.3 | -250 to 1300 | <0.8 |
| T (Cu/Cu-Ni) | -100 to 400 | <0.3 | -200 to 400 | <0.5 |
| R (Pt-13% Rh/Pt) | 0 to 1600 | <1.0 | -50 to 1760 | <2.0 |
| S (Pt-10% Rh/Pt) | 0 to 1760 | <1.0 | -50 to 1760 | <1.5 |

Sensitivity, Types B,E,J,K,N,T: 0.1°C (0.18°F)
Sensitivity, Types R,S: 0.2°C (0.36°F)
Total thermocouple error equals Conformity plus voltage errors
Additional error when using automatic Cold Junction Compensation:
Range: -15° to 60°C (5° to 140°F): <0.4°C (0.72°F)
-20° to 70°C (-4° to 158°F): <0.6°C (1.08°F)
External Cold Junction range: -30°C to +80°C (-22° to 176°F)
Open circuit detection threshold: 1.9kΩ ± 0.1kΩ

### 3.4.3. Controller

**Main switch**

The main switches which controls electricity to the ventilators as well as to the roots pump is shown in **Photo 3.4-3**. to operate ventilators, turn on the radial ventilator (middle switch) at first and then the booster (right switch) about 30 seconds thereafter in order to prevent an overload.


**Photo 3.4-3** Main switch

**Roots pump controller**

One needs to establish the proper frequency of electricity which is supplied to the roots pump, in order to control the proper volumetric flow rate and pressure. This can be done in the converter which is shown in **Photo 3.4-4**. After turning on the main switch in **Photo 3.4-3**, press the green button to activate the converter, the green lamp "Bereit" will turn on. Now manipulate the left arrow key to change A1 mode (i.e. Home, press just one) and the frequency of electricity can be set with the up and down arrows to the target value. An example of the proper frequency is about 14 Hz for 109Nm$^3$/h fluidizing air for the FHE.

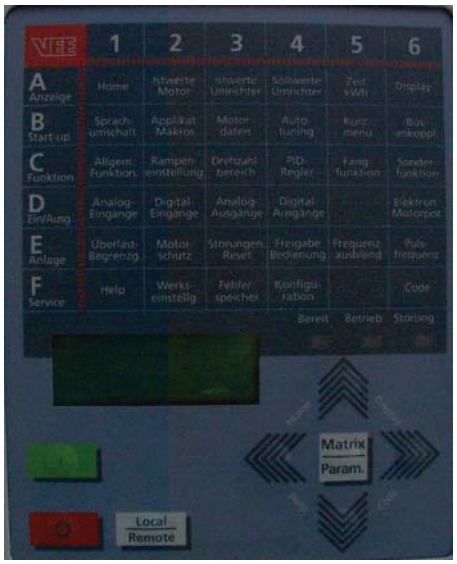


**Photo 3.4-4** Control panel of the frequency converter for the roots pump flow control

**Discharging ventilator controller**

The discharged air from the cyclone enters a filter and a pressure drop occurs due to the increased volume in the filter house. Therefore, to discharge the air in the filter properly, the air discharging pipe after the filter is connected with a gas discharging system, which has a ventilator and is shared with the $SO_2$ scrubber system in the lab. The speed of this ventilator can be controlled via the control panel in **Photo 3.4-5**.

To start the discharging ventilator, first turn the middle switch (black and white) counter clockwise, then press the green button (named 'Gebläse') at the bottom to activate the ventilator.

The speed of the ventilator can be controlled with the controller at the bottom and the proper speed must be established according to the supply amount of fluidizing air. Otherwise, the dust collecting bag or the connecting part which is connected with the discharging system could be damaged.

Note that the two valves for the discharging system must be reset properly because the discharging system is used together with the $SO_2$ scrubber in the lab.


**Photo 3.4-5** Controller for the ventilator in the air discharging system

Starting the system (full operation)

1. check air discharging system valves
2. start the data acquisition programs
3. turn on the roots pump main switch
4. establish a proper frequency for the converter for the roots pump and adjust the FHE valves
5. turn on the radial ventilator
6. wait for about 30 sec.
7. turn on the booster
8. establish the primary- secondary air valves and the discharging ventilator simultaneously
9. measuring

# Chapter 4.

# Tests and result

The experiment of investigation was divided into two parts – a preliminary experiment and a main experiment. The preliminary experiment includes the determination of the pressure losses of the gas distributing plates according to the various superficial velocities, determination of cyclone pressure drops with the siphon valves closed, the lapse until overheating, the effect of the ratio of primary air to fluidizing air on the pressure profile and the superficial velocity.
The main experiment covered the following tests

### 1st. Stage

- ✓ Observation of the behavior of bed material in the new- and old (Lenzing) siphon
- ✓ Mass flow rate in the CFB and into FHE with respect to various fluidization air flows, bed material loads and FHE valves conditions
- ✓ Observation of the two-phase flow in the FHE; flowing boundary between stagnant and moving bed material, dead zone, behavior of bubbling, effect of weir with respect to the fluidizing air and flux of bed material into the FHE.

### 2nd. stage

- ✓ Change of flowing boundary position according to modification of the weir geometry and various fluidizing air conditions
- ✓ Influence of the gas outlet depth in the cyclone on the separation efficiency

### 3rd. stage

- ✓ Measurement of cyclone pressure drop as function of bed material loading
- ✓ Observation of tangential and radial particle velocity in the cyclone; correlation of particle movement with Δp.
- ✓ Installation of heat exchanging bundles in the FHE

The gray colored tests are either still in planning, canceled or not discussed in this paper.

Most of tests in the CFB were performed according to a volumetric flow rates table which was constructed from recalculated fluidizing air conditions from Lenzing according to the conditions in the cold model; see data table in the Appendix.

The numbers with splitter "/" at the title column on the volumetric flow rate table (e.g. **Table 4.1-3** , **Table 4.2-1**, **Table 4.2-2** , etc) for experiments indicate the fluidizing air conditions and the charged amount of bed material in the combustion chamber. For example, 40/50/109/50 denotes the ratio of 40 % primary air in the total fluidizing air for the riser / 50 % load factor / 109 $Nm^3/h$ FHE fluidizing air / 50 kg bed material charged in the combustion chamber. The load factor here is the average power divided by the peak power which is generated over a period of time.

# 4.1. Tests without load of bed material

## 4.1.1. Pressure profile in the riser

**Fig 4.1-1** shows the pressure profile from wind-box P101 to cyclone outlet P202 in the combustion chamber, the riser and the cyclone without any bed material charged and it shows typical pressure profile shape, i.e. the supplied fluidizing air from the blowers into the wind box looses its pressure at the gas distributing plate and the pressure curves show large pressure drops between P101 and P102. Thereafter the pressure is preserved up to cyclone inlet, with no noticable pressure drop.
The contraction of the area at the cyclone inlet, the geometrical structure of inlet and the cyclone itself cause the pressure change once more. The pressure in P201 and P202 decreases but the P201 sensor may indicate wrong values, as the measuring point of P201 is in front of the cyclone inlet where the contraction of the cross sectional area causes acceleration of the gas. Moreover, these low pressure sensors - especially P201 – had produced some errors due to electrostatic energy under particle loaded tests and were replaced with VEGA sensors thereafter.

**Table 4.1-1** Average volumetric flow rates from DB file for fluidizing air in combustion chamber.

| | primary air | secondary air | |
|---|---|---|---|
| | F112 | F113($2^{nd}$ air1) | F114($2^{nd}$ air2) |
| | [$Bm^3/h$] | [$Bm^3/h$] | [$Bm^3/h$] |
| line 1 | 391.55 | 368.60 | 268.05 |
| line 2 | 515.95 | 344.00 | 533.83 |
| line 3 | 795.46 | 316.33 | 894.76 |

**Table 4.1-2** Recalculated values from **Table 4.1-1**

| | primary air | secondary air | |
|---|---|---|---|
| | F112 | F113($2^{nd}$ air1) | F114($2^{nd}$ air2) |
| | [$Bm^3/h$] | [$Bm^3/h$] | [$Bm^3/h$] |
| line 1 | 360.40 | 706.86 | 118.49 |
| line 2 | 467.66 | 658.56 | 235.16 |
| line 3 | 691.72 | 601.27 | 391.53 |

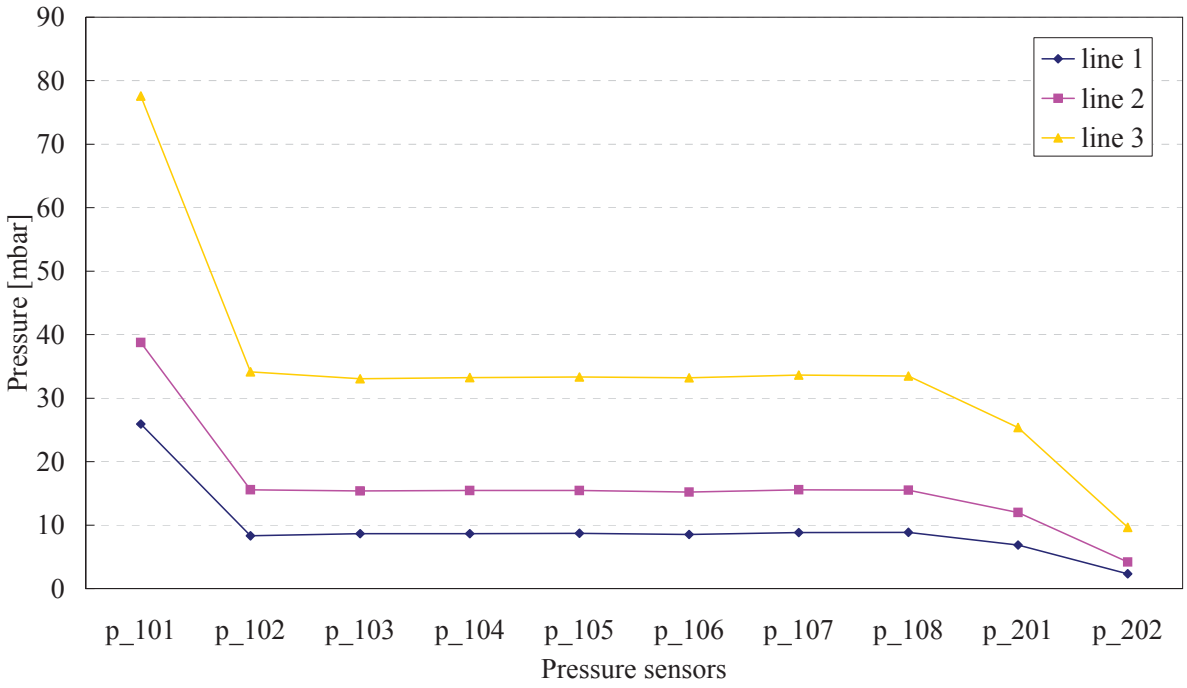


**Fig 4.1-1** Pressure profiles in the CFB, gas-only operation (single-phase flow); see **Table 4.1-1** and **Table 4.1-2** for legend explanation

**Table 4.1-1** and **Table 4.1-2** present the recorded vol. flow rates for **Fig 4.1-1** from DB and re-calculated values with the correct flow rate equations due to coding mistake in the Rob's basic program. Furthermore, the temperature sensors (thermocouples) were disturbed by the flow even in the one-phase (gas only) tests. The temperature measurement errors (about 490°C) cause big differences between the values from DB which was calculated with a wrong equation in the source code and recalculated ones in secondary air. On the other hand, the temperature of the primary air showed typical values without any interference from static electricity (about 60 °C).

### 4.1.2. The influence of the equation error in the data acquisition program

After the coding mistake in the equation to calculate the volumetric flow rate had been corrected, the unloaded test was conducted again according to the normal volumetric flow rate table. See also target values in the Appendix.

The former test (before equation correction) had been conducted with operating volumetric flow rate of fluidizing air. However, the new ones (after equation correction) was done with normal volumetric flow rate. As the volumetric flow rates with the same fluidizing air condition were not so different from each other, the influence of fluidizing air adjustment according to normal- or operating volumetric flow rates is slight.

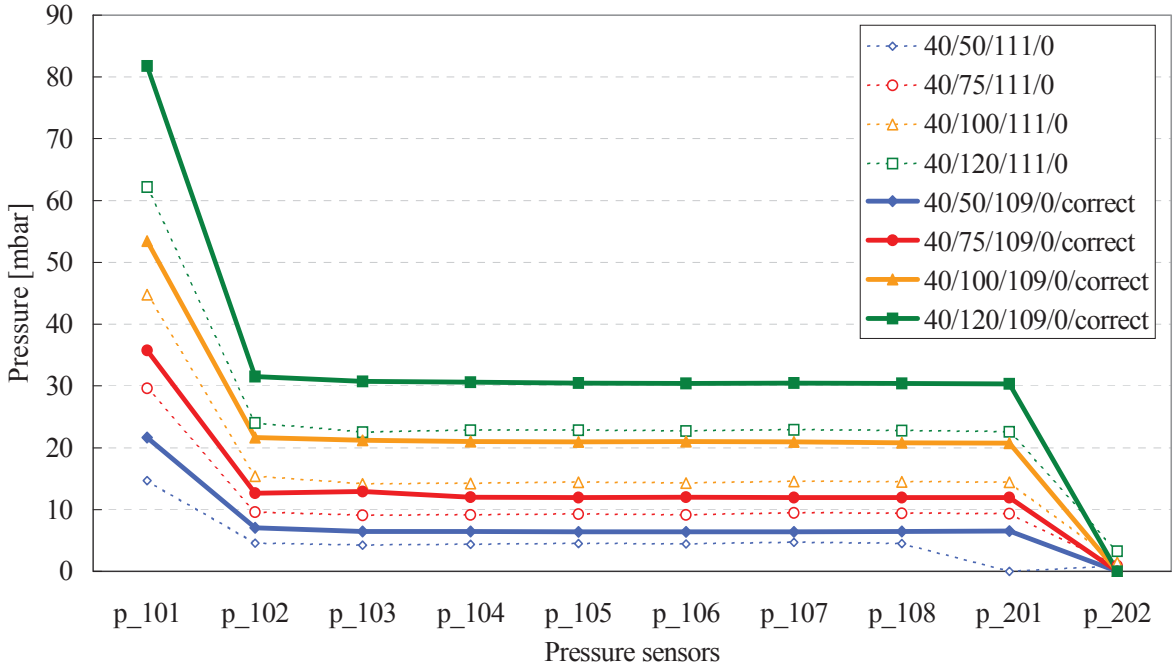


**Fig 4.1-2** Pressure profile in the CFB part after equation correction; single-phase (gas only) operation, the dotted lines are based on the data from before equation correction (The low pressure sensors at cyclone inlet/outlet and thermocouples had been replaced before the equation was corrected. The former test values – dotted – reflect also the replaced sensors' values.)

In **Fig 4.1-2**, the values for volumetric flow rate after and before the correction of the equation are compared for the same fluidizing air conditions. The thicker curves are based on the later data which are measured and saved on a computer after correction of the equation for volumetric flow rate in the Basic source code. The pressure profiles show differences, as can be seen in **Fig 4.1-2**.
The values in **Table 4.1-3** are the volumetric flow rates for **Fig 4.1-2** with their percentage.
"% 1" is the ratio between old and re-calculated values and "% 2" is the ratio between new tested and recalculated data from old values. The former test values are based on the DB before eq. correction and new test values are from the new experiment after equation correction.

The primary air was supplied on average 18.16% less than the target value, secondary air about 16.89% and FHE fluidizing air 20.25%. As a result, the total fluidizing air was supplied 17.74% less than target values in the former test (%1) and this caused the remarkable differences in the pressure profile.
The total average pressure increases by 37.8% from former tested pressure. When the re-calculated values from former test are compared with the new tested values, it was found that the supplied air in the former test was just 85.40% of new tested values with corrected equation on an average (%2).

**Table 4.1-3** Volumetric flow rate of fluidizing air for **Fig 4.1-2**

| | | Old | Recalculated | %1 (-) | New | % 2 |
|---|---|---|---|---|---|---|
| Primary air | 40/50/111/0 | 309.82 | 249.00 | 19.63 | 311.19 | 80.02 |
| | 40/75/111/0 | 459.09 | 372.93 | 18.77 | 465.25 | 80.16 |
| | 40/100/111/0 | 616.73 | 499.31 | 19.04 | 591.78 | 84.37 |
| | 40/120/111/0 | 711.30 | 603.17 | 15.20 | 797.01 | 75.68 |
| | AV | | | 18.16 | | 80.06 |
| Sum of secondary air streams | 40/50/111/0 | 303.05 | 251.91 | 16.88 | 294.40 | 85.57 |
| | 40/75/111/0 | 543.62 | 451.48 | 16.95 | 494.40 | 91.32 |
| | 40/100/111/0 | 773.67 | 640.73 | 17.18 | 734.01 | 87.29 |
| | 40/120/111/0 | 963.38 | 803.94 | 16.55 | 819.80 | 98.07 |
| | AV | | | 16.89 | | 90.56 |
| Sum of FHE fluidizing air streams | 40/50/111/0 | 111.93 | 89.75 | 19.81 | 107.70 | 83.34 |
| | 40/75/111/0 | 115.81 | 92.82 | 19.85 | 106.34 | 87.29 |
| | 40/100/111/0 | 114.15 | 91.05 | 20.24 | 104.40 | 87.21 |
| | 40/120/111/0 | 104.76 | 82.67 | 21.09 | 102.06 | 81.00 |
| | AV | | | 20.25 | | 84.71 |
| Total | 40/50/111/0 | 724.79 | 590.66 | 18.51 | 713.29 | 82.81 |
| | 40/75/111/0 | 1118.52 | 917.23 | 18.00 | 1065.99 | 86.05 |
| | 40/100/111/0 | 1504.55 | 1231.09 | 18.18 | 1430.19 | 86.08 |
| | 40/120/111/0 | 1779.44 | 1489.78 | 16.28 | 1718.87 | 86.67 |
| | AV | | | 17.74 | | 85.40 |

## 4.2. Tests with quartz sand as bed material

The test results with sand particles have still the same problems as the unloaded tests such as low pressure sensor errors, thermocouple errors by electrostatic energy from inter-particles and particles/Plexiglas and the wrong equation for volumetric flow rate calculations, because the problems were not known on that time. Experiments with Cu particles are currently in progress. The data for the sand bed material are documented in this report in their recalculated form.

Note that the test results with sand cannot be applied directly to the commercial scale CFBs with the same kind of bed material; [2].

Therefore, the test is focused on the following questions:

Are there problems with the construction, exemplary due to sealing, welding, assembling or material (especially concerning the parts made from Plexiglas or safety glass)?

Does the measurement system work properly?

Does the volumetric flow rate in the test plant corresponds to the calculated theoretical values from the industrial plant (Lenzing)?

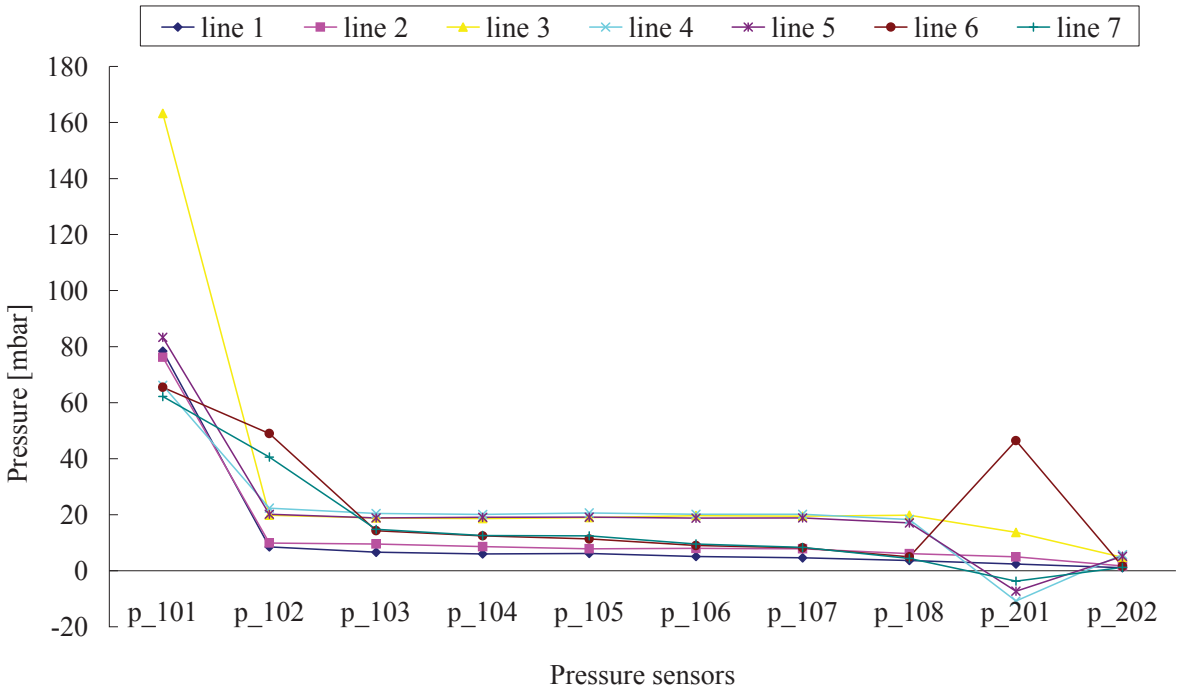


**Fig 4.2-1** Pressure profiles in the CFB for two phase operation with sand as bed material; see **Table 4.2-1** and **Table 4.2-2** for the data of lines(1-7)

**Table 4.2-1** Re-calculated volumetric flow rates [$Bm^3/h$] for **Fig 4.2-1**

| line | | Fluidization air for CFB | | | Fluidization air for FHE | | | Sum |
|---|---|---|---|---|---|---|---|---|
| | | FB112 cal. | FB113 cal. | FB114 cal. | FB413 | FB414 | FB415 | |
| 1 | 22kg sand | 650.5 | 0.0 | 0.0 | 3.7 | 42.1 | 0.0 | 696.3 |
| 2 | 22kg sand | 667.4 | 0.0 | 404.2 | 74.2 | 119.6 | 0.0 | 1265.4 |
| 3 | 22kg sand | 891.0 | 0.0 | 804.7 | 67.0 | 107.6 | 0.0 | 1870.3 |
| 4 | 30/100/223/100 | 469.2 | 171.9 | 896.1 | 8.2 | 35.1 | 144.3 | 1724.8 |
| 5 | 40/100/223/100 | 588.9 | 145.3 | 735.7 | 8.2 | 34.6 | 145.5 | 1658.3 |
| 6 | 30/50/ | 224.6 | 99.5 | 376.7 | 9.1 | 35.6 | 174.8 | 920.3 |
| 7 | 40/50 | 288.2 | 61.0 | 321.5 | 9.1 | 36.5 | 173.9 | 890.1 |

**Table 4.2-2** Re-calculated volumetric flow rate for tests (after the correction of temperature errors)

| line | | Fluidization air for CFB | | | Fluidization air for FHE | | | Sum |
|---|---|---|---|---|---|---|---|---|
| | | FB112 cal. | FB113 cal. | FB114 cal. | FB413 | FB414 | FB415 | |
| 1 | 22kg sand | 650.5 | 0.0 | 0.0 | 3.7 | 42.1 | 0.0 | 696.3 |
| 2 | 22kg sand | 667.4 | 0.0 | 594.2 | 74.2 | 119.6 | 0.0 | 1455.4 |
| 3 | 22kg sand | 891.0 | 0.0 | 1204.5 | 67.0 | 107.6 | 0.0 | 2270.1 |
| 4 | 30/100/223/100 | 469.2 | 156.7 | 816.5 | 8.2 | 35.1 | 144.3 | 1629.9 |
| 5 | 40/100/223/100 | 588.9 | 132.4 | 670.2 | 8.2 | 34.6 | 145.5 | 1579.8 |
| 6 | 30/50/ | 224.6 | 130.0 | 492.0 | 9.1 | 35.6 | 174.8 | 1066.1 |

| | | | | | | | | |
|---|---|---|---|---|---|---|---|---|
| 7 | 40/50 | 288.2 | 55.4 | 292.2 | 9.1 | 36.5 | 173.9 | 855.2 |

### 4.2.1. Pressure profile in the CFB

**Fig 4.2-1** shows some of tested results with sand as bed material and the supplied volumetric flow rate of fluidizing air for the curves are in **Table 4.2-1**. The values are re-calculated from the DB file but the volumetric flow rates of the secondary air have still errors due to the temperature sensor which shows fluctuations between 0-490°C. Therefore, the re-calculated values with the temperature sensor for primary air which have normal values are given in **Table 4.2-2**.

The pressure drops, P101-P102, of the curves 1-5 show a different tendency from that of 6 and 7 in **Fig 4.2-1**. For the cases 1-5, following the pressure decreased between P101 and P102, the values become almost constant up to P108. This is caused by the fact that a gas distributing plate with more holes has been installed in the combustion chamber, as the pressure loss at the gas distributor had been too high and the change of fluidizing air conditions hadn't caused enough variation of the pressure profile in the riser. Most of pressure drop occurred at the steel screen on the drilled plate.

P201 sensor shows fluctuations, as mentioned before.

### 4.2.2. Minimal bubbling point of the sand particles

This test was conducted in the second heating chamber. The injected fluidizing air in the chamber was controlled by the electricity on the roots pump. The volumetric flow rate for fluidization air in the FHE was also re-calculated due to the equation error in the Basic source code The actually injected volumetric flow rate for this test is about 80% of the recorded values on an average. This result agrees with that of the unloaded test re-calculations; See chapter 4.1.2.

The relationship between the pressure differences from P402 (the pressure at wind box) or P409 (the pressure over the gas distributing plate) to P405 (the pressure over the bed material level) vs. the superficial velocities which is based on the re-calculated volumetric flow rate per cross sectional area of the second heating chamber is illustrated in **Fig 4.2-3**. The **Fig 4.2-2** shows the static pressure for the same condition according to electrical load on the roots pump. The pressure difference is maximal, when the superficial velocity is 0.0089 m/s. i.e. the minimal fluidization velocity ($u_{mf}$) is 0.0089 m/s.

The calculated dimensionless numbers for a (simplified-)Reh-diagram and the necessary data for the calculation are in **Table 4.2-3**, where $\Delta\rho=\rho_p-\rho_f$, $\rho_p$=density of bed material, $\rho_f$ =density of air at 300K, $d_p$= mean particle diameter, g=gravity acceleration, $\mu_f$ =dynamic viscosity of air at 300K, $\nu_f$ =kinematic viscosity of air at 300K, $u_{mf}$ =minimum fluidizing velocity, $Re_p=u_f\ d_p\ /\nu_f$ , $u_f$ =superficial velocity of fluidizing air, $Fr^*=u_f^2\ \rho_f\ /gd_p\Delta\rho$, $Ar=g\ d_p^3\Delta\rho/\nu_f^2\rho_f$, $dp^*=Ar^{1/3}$, $u^*=u[\rho 2/\Delta\rho g\mu_f]^{1/3}$

The minimal fluidization condition for CFB with our sand bed material requires u*≥2.8 according to the simplified Reh-sketch(**Fig 4.2-4**), where the minimal theoretical superficial velocity for CFB ($u_{fmin}$) is about 2.0 m/s.

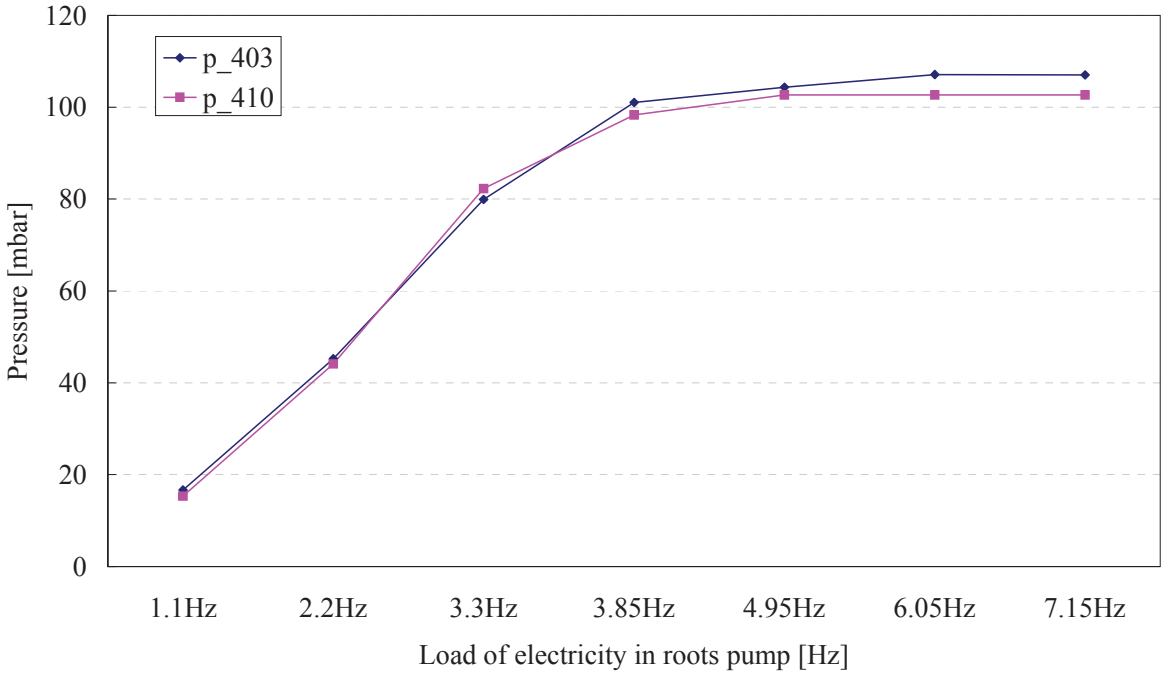


**Fig 4.2-2** Pressure trends vs. electrical load on the roots pump; tested in the first heating chamber without heat exchanging bundle with sand bed material

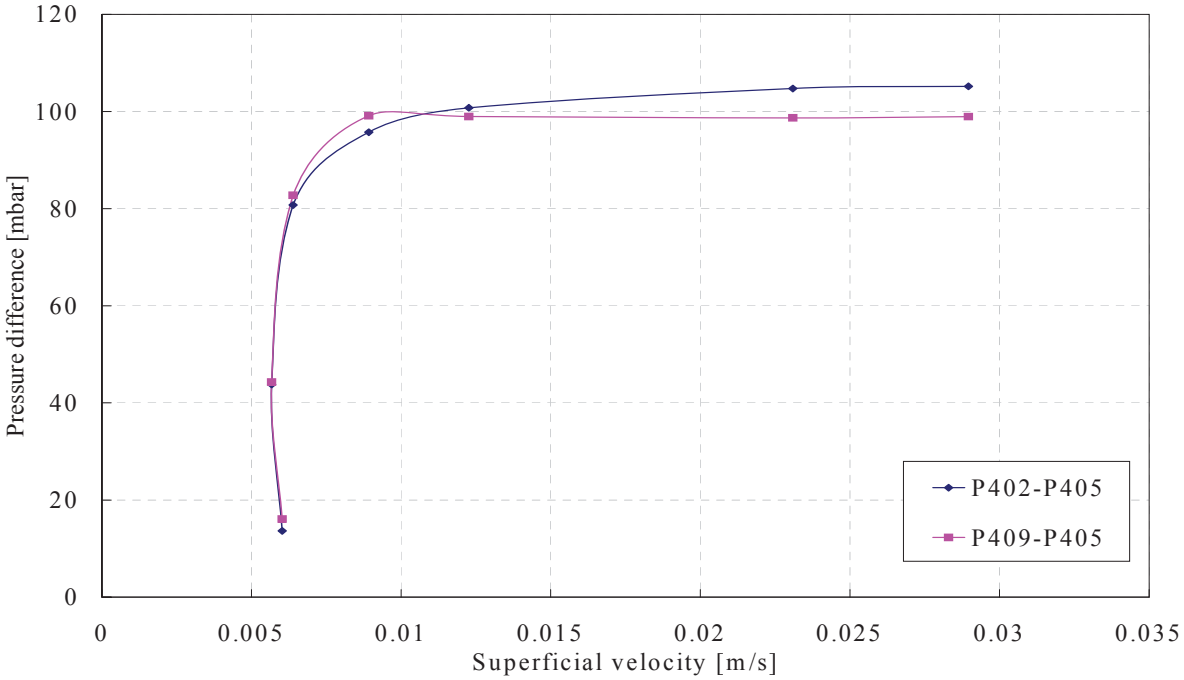


**Fig 4.2-3** Minimal fluidization velocity; tested in the first heating chamber without heat

exchanging bundle with sand bed material

**Table 4.2-3** Input data and dimensionless characteristic number for determining the operating point of the cold model (with sand as bed material) in the Reh-diagram

| | | |
|---|---|---|
| $\Delta\rho$ | [kg/m$^3$] | 2648.8 |
| $\rho_f$ (T=300K) | [kg/m$^3$] | 1.177 |
| $\rho_{f0}$ | [kg/m$^3$] | 1.293 |
| $\rho_p$ | [kg/m$^3$] | 2650 |
| $d_p$ | [m] | 0.0001 |
| g | [m/s$^2$] | 9.81 |
| $\mu$ (T=300K) | [kg/ms] | 1.85E-05 |
| $\nu$ | [m$^2$/s] | 1.57E-05 |
| $u_{mf}$ | [m/s] | 0.009 |

| | |
|---|---|
| $Re_p$ | 0.057 |
| $3/4Fr_p$ | 2.75E-05 |
| Ar | 89.3 |
| M | 2.1E-06 |
| (See **Fig 1.4-2** for M) | |
| dp* | 4.47 |
| U* | 0.013 |
| $u_{f\ min}$ [m/s] | 1.967 |
| | |

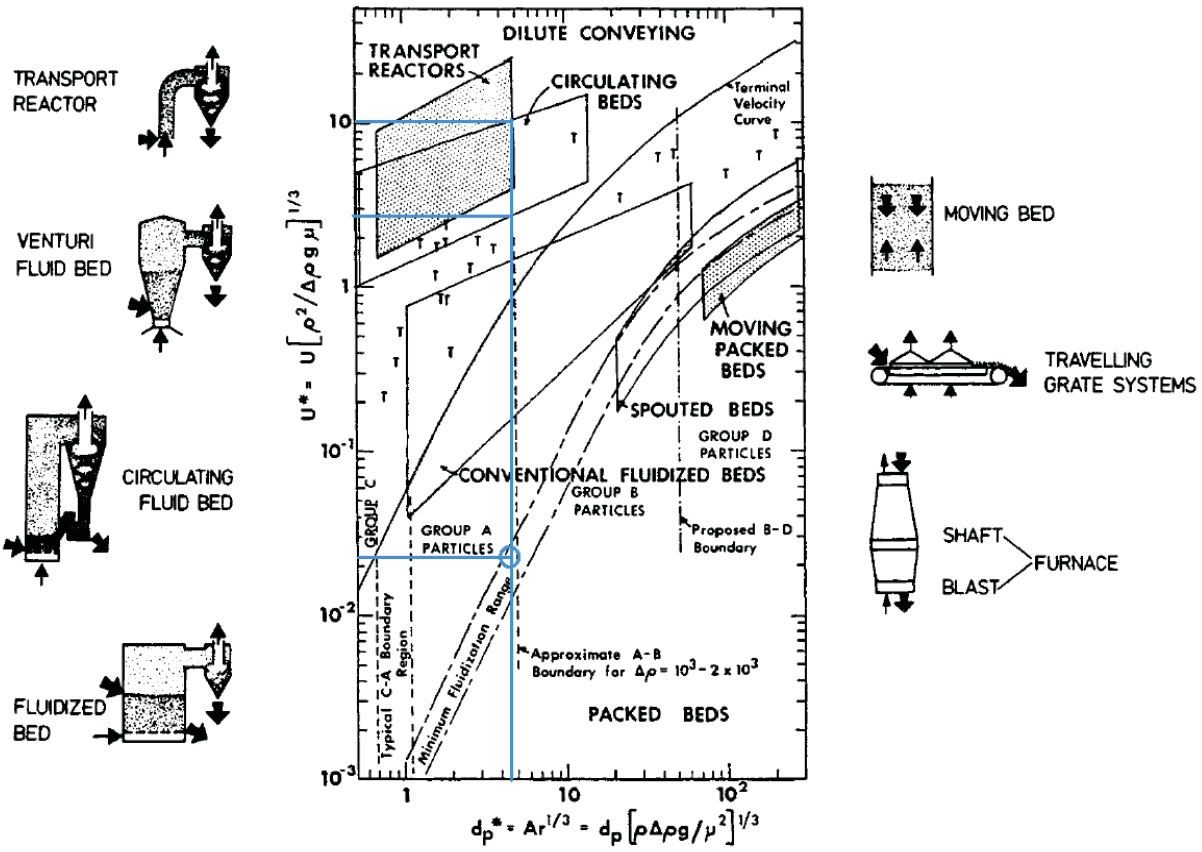


**Fig 4.2-4** Simplified Reh-diagram from [4]

## 4.2.3. Observation of the siphon

A new designed siphon is installed in the cold model, as the old type siphon which is now installed

in Lenzing has been blocked occasionally, when the fluidized air is highly loaded with bed material. The newly designed siphon which is installed in the cold model is illustrated in **Fig 4.2-5**. It works without any problem (no blockage) throughout the experimental range (30/50 – 50/120) of volumetric flow rates of fluidizing air not only with sand but also with Cu bed material, excepting that the level in the downcomer under the cyclone is somewhat higher, as the superficial velocity (volumetric flow rate) or the charged amount of combustion chamber is increased. Therefore, the new designed siphon can replace the old type one and the known problems will be solved therewith. The fluidizing air is supplied from the roots pump into separated wind boxes to fluidize re-circulated bed material in the siphon. The fluidizing air for the siphon is split into two sections (See **Fig 4.2-5**) Air supplied for the downcomer section is about 5 $m^3$/h and for the delivering chamber section 10$m^3$/h.

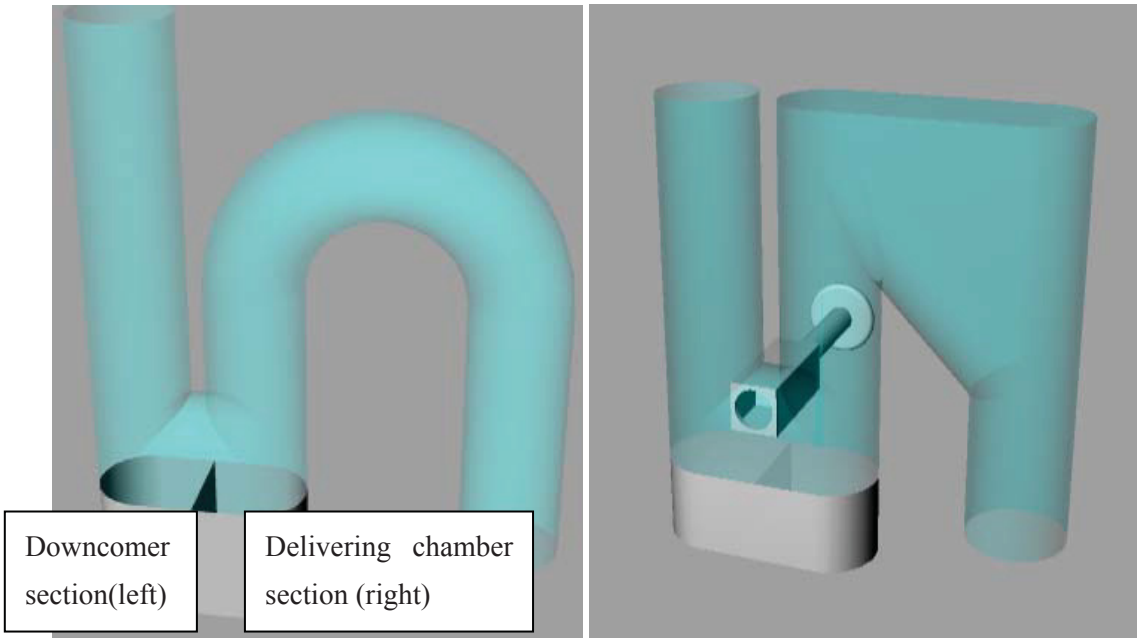


**Fig 4.2-5** Old type siphon as installed in Lenzing (left) and a new designed one for the cold model (right)

## 4.2.4. Observation of bed material behaviour in the FHE

Some photos which were taken every 7 ms from a video clip are shown in **Photo 4.2-1**. As soon as a bubble is collapsed on the surface of the bed material, another one begins to build. The interval is about 70 ms on average.

According to the superficial velocities of the FHE fluidizing air, the behavior of the fluidizing regime reaches from bubbling regime to turbulent regime. Most of our experiments are carried out with about 111 $Nm^3$/h of total FHE fluidizing air. It shows a slugging flow regime.

When the bubbles rise upward in a chamber, they tend to rise in the center of the chamber because of wall friction. Therefore, bed material in a chamber is fluidized upward in the center and flows downward near the wall.

Furthermore, some dead zones are formed, where the bed material doesn't move or flows only slightly. First, near edges and corners at the bottom of the chamber, the bed material is stagnant. Second, the inclined surface at the upper part of a weir obstructs flowing of bed material and a small dead zone is formed. However, there is no dead zone on the left inclined weir surface, as bed material flows macroscopically from the empty chamber through the second heating chamber to the combustion chamber and the angle of the leeward inclined weir surface as seen in the photo is greater than the repose angle of sand or Cu-particles.

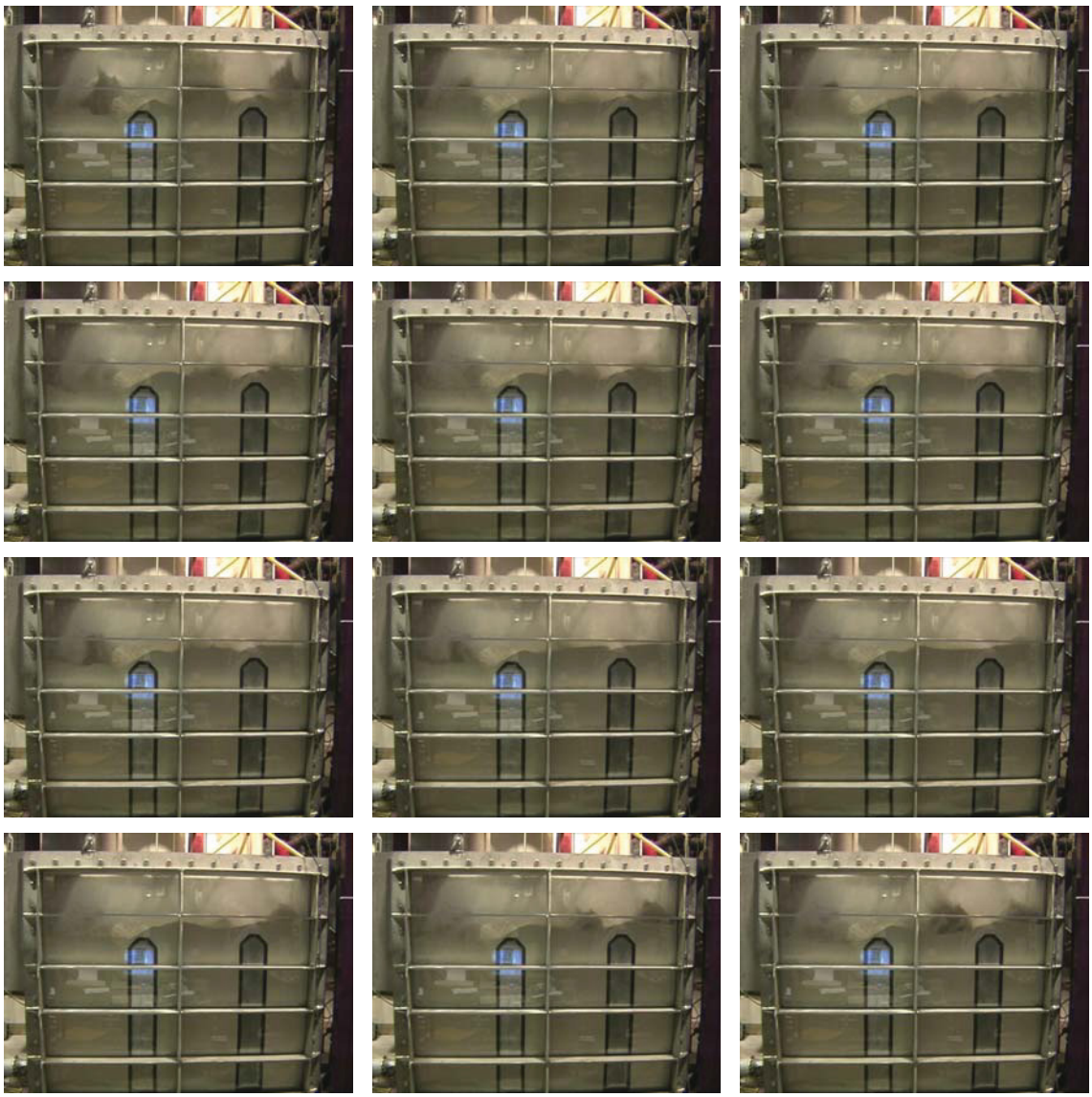

**Photo 4.2-1** Behavior of the bed material (**sand**) in the FHE from "Dimplomarbeit.wmv" file on the enclosed CD

# 4.3. Tests with Cu as bed material

The commercial bed is operated at elevated temperature (about 850 °C) and at atmospheric pressure. Therefore, the fluid density and viscosity will be significantly different between these two gas conditions, e.g. the gas density of the cold bed is 3.5 times as large as the density of the hot bed. Then, to maintain a constant ratio of particle-to-fluid density, the density of solid particles in the cold bed must be 3.5 as large as the density in the hot bed; [26].

The density of Cu is 8850 kg/m$^3$ and that of quartz sand 2650 kg/m$^3$. The Cu density is about 3.38 as large as that of sand. Therefore, most of tests are conducted with Cu-bed material and the experimental results with Cu-bed material can be applied for commercial hot beds.

The following vol. flow rate of fluidizing air for Cu-bed material is adjusted according to normal volumetric flow rates.

## 4.3.1. Pressure profile in the riser

The pressure profile will be different according to various conditions, e.g. according to various fluid conditions, variously charged amounts in the combustion chamber or the amount of re-circulated bed material.

### 4.3.1.1. Influence of various fluidizing air ratios

**Fig 4.3-1** shows the pressure profiles in accordance with various conditions of fluidizing air with constant bed material in the combustion chamber-100 kg Cu bed material. When the charged bed material is constant in the combustion chamber and the flow pattern is in the aggregative fluidization range (see **Fig 1.4-1**), the pressure difference (or the gradient from P102 to P108) will be almost constant, although the volumetric flow rates of fluidizing air is changed. This can be proven theoretically by the equation for pressure drop in a fluidized bed.

The theoretical pressure drop (Δp) can be calculated from the following equation.

$$\Delta p = \Delta\rho g \cdot (1-\varepsilon) \cdot H \ ,$$

where Δρ is the density difference between fluid and bed material, g is gravity acceleration, ε is porosity and H is the height of the fluidized layer.

However, the pressure difference in the real fluidized bed grows proportional the fluid velocity, as inter-particle forces and friction with wall must be considered; [33]. Moreover in our case, the secondary air whose inlets are installed between P102 and P103 for secondary air-1 and between P103 and P104 for secondary air-2 must be considered, too. See **Fig 4.3-3**. This slight changing of pressure drop in the real bed operation agrees with the results from our cold model - the pressure drop is in the range of 90-135 mbar for the flow conditions 40/50-120/109/100.

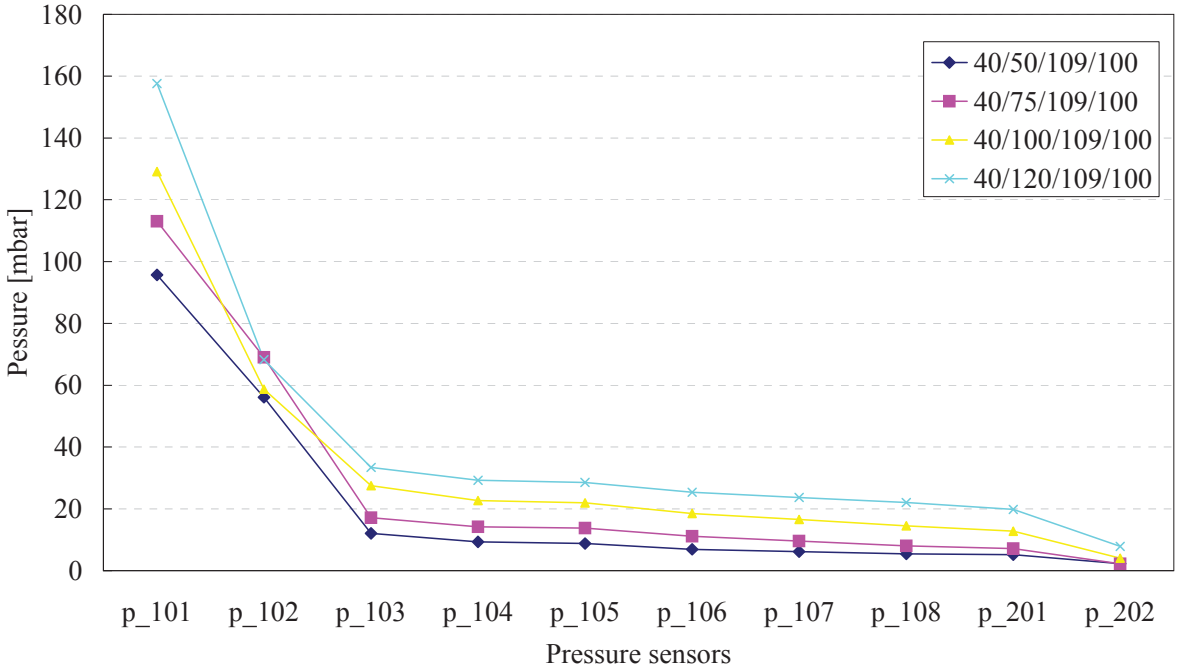


**Fig 4.3-1** The pressure profile with 100 kg charged Cu bed material in the riser and the cyclone according to various loads of fluidizing air

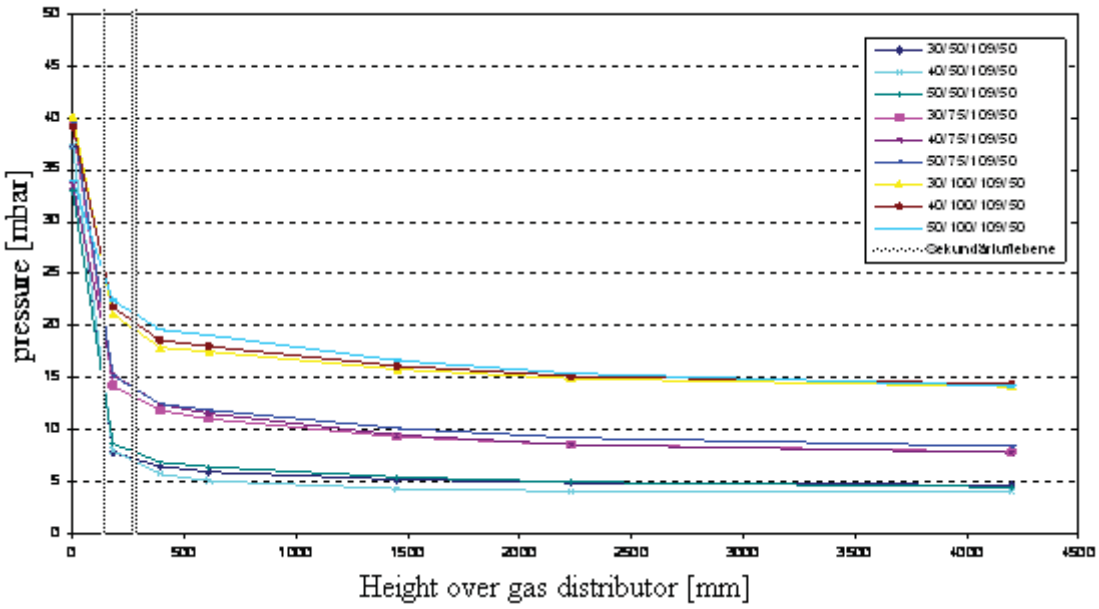


**Fig 4.3-2** The pressure profile with 50 kg charged Cu bed material in the riser according to the height of the installed sensors, the dotted lines are the height of secondary air inflow; from the AEE report.

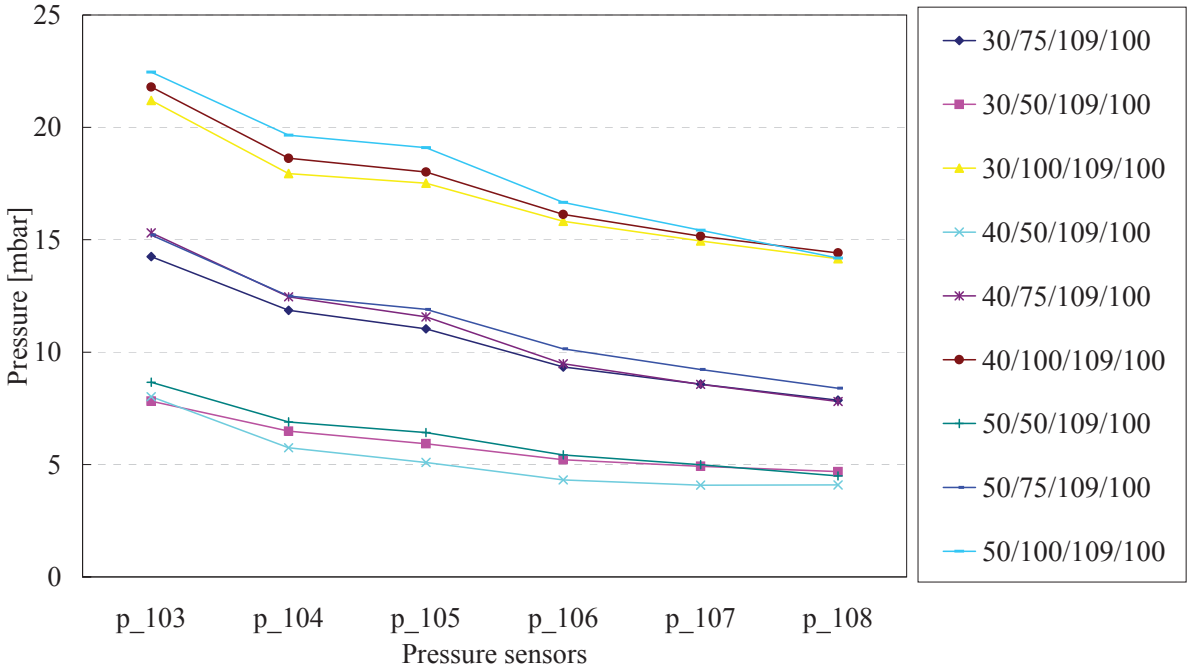


**Fig 4.3-3** Pressure curves between P103 and P108 with 100 kg charged Cu bed material in the riser

### Influence of the primary air ratio on the pressure profile

**Fig 4.3-3** shows the pressure profiles between P103 and P108 according to various fluidizing air conditions. Although the three curves which have the same load factor of fluidizing air - same amount of total fluidizing air for riser, i.e. same superficial velocity - but different primary air ratio, for example 30/50, 40/50 and 50/50, show slightly increasing pressure according to the increase of the primary air ratio at the given pressure sensor. Contrary, the pressure sensor P102 which is installed over the gas distributor under the secondary air-1 outlet shows almost the same values (See **Fig 4.3-2**). The reasons are:

The pressure at P102 between gas distributor and secondary air outlets is constant, as the total amount of fluidizing air is constant.

The total amount of fluidizing air is constant. However, primary air is supplied vertically upward and the secondary air about 45 degrees downward. The higher primary air flux, the smaller are disturbances in the direction of fluid movement from secondary air. Therefore, pressure over the secondary air outlets (e.g. P103) shows deviations according to different primary air ratios under the conditions of the same amount of fluidization air.

The pressures differences cannot be distinguished at P108 and the effect of primary air ratio fades away.

Nevertheless, to change the ratio of primary air may be effective in the hot commercial plant such as in Lenzing, as it affects not only the turbulent condition in the combustion chamber but changes also the burning condition. (Note that RV-Lenzing uses the waste gas from viscose fibre production

factory as secondary air).

#### 4.3.1.2. Influence of various charging of bed material in the combustion chamber

Using constant fluidizing air in **Fig 4.3-4** shows the pressure profile from P101, which is the pressure sensor for the wind box, to P202, which is installed at the cyclone outlet, according to various chargings of bed material in the combustion chamber.

The more charged bed material causes more resistance, i.e. pressure drop by the increased weight and flow resistance. This pressure drop can be recognized in the **Fig 4.3-4**. The curve, 40/100/109/0 (40% primary air / 100% load factor / 109 $Nm^3/h$ FHE air / 0 kg charged bed material), illustrates the pressure profile without charging (gas only) and shows an almost vertical trend between P103, which is installed in the middle of conical combustion chamber under secondary air-2 inlets, and P201, which is the sensor at the cyclone inlet. However, the 100 kg charged graph, 40/100/109/100, shows the pressure drop clearly in the same region.

The increased bed material which is charged in the combustion chamber shifts the intercepting points, where the pressure profile curves for the charged bed material intercept the gas only curve, to right, because fluidizing air is compressed by the increased weight of the bed material.

Our pressure profile curves are not so ideal like the model which is compared with a molecular system [13], especially due to the influence from the inflow of the secondary air. However, it can be estimated that the boundary between dilute/dense phase may exist in the near of these measured heights where the pressure starts to be lower than the unloaded pressure. As a result, the height of the dense phase increases with the increased bed material in the combustion chamber.

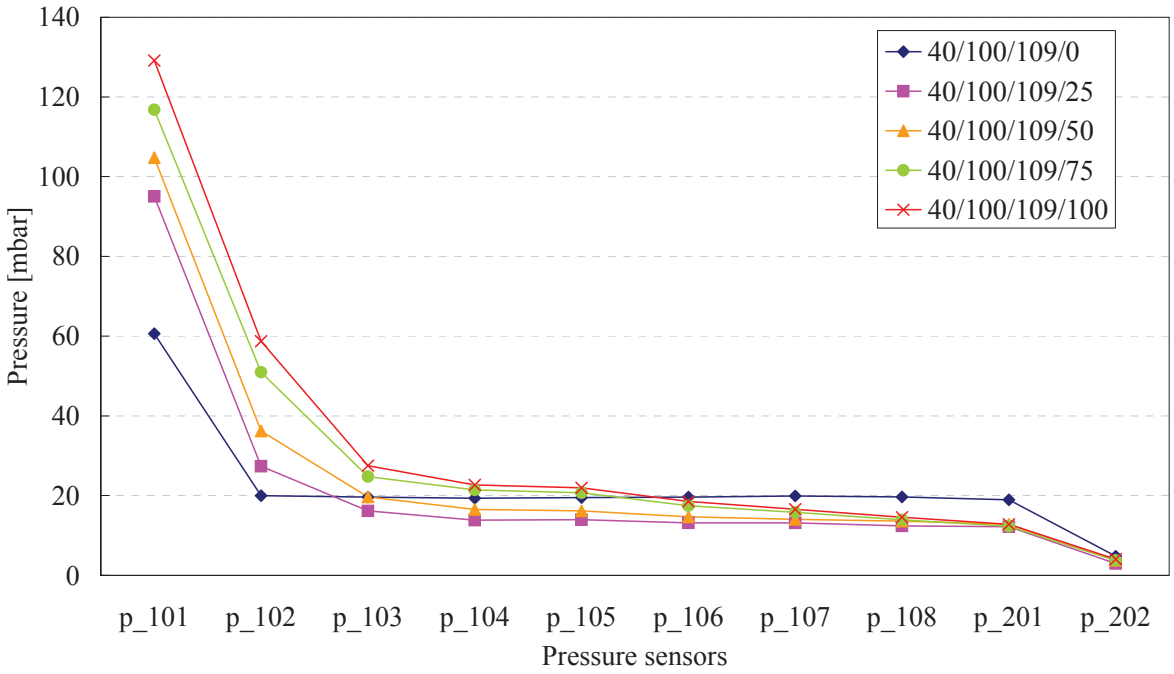


**Fig 4.3-4** The pressure profile in the riser according to various charged amount of Cu bed material in the riser

#### 4.3.1.3. Relationships between charged amount and gradient of the pressure profile

According to the pressure profiles to be discussed in paragraph 4.3.1.2, a gradient of the pressure trend curve can be considered with the amount of charged bed material. The pressure curves from P105 to P108 in the relation of the height of the system with various charged amount of bed material are illustrated in **Fig 4.3-5**, where the condition of fluidizing air is fixed to 40/50/109 – 40% primary air / 50% load factor / 109 $Nm^3/h$ FHE fluidizing air. In other words, the superficial velocity remains constant but the charged amount of bed material varies.

The P105 pressure sensor is installed at the lower end of the cylinder on the combustion chamber and the P108 sensor is almost at the upper end of the cylinder. Between these two sensors, the pressure of the system will be influenced by the amount of bed material, inter-particle forces and gravity in the case of constant fluidizing air condition.

As the height increases, so the pressure for the case of 0 kg bed material (gas only) increases. Both of the gradient of the 0 kg bed material curve and that of a trend line – dotted line – in **Fig 4.3-5** show a slightly increase. This can be considered in relation to the geometry of the riser. i.e. the fluidizing air is slightly compressed at the riser outlet because the cross-sectional area of the riser outlet is smaller than that of the cylinder (Exit effect).

The other gradients of the pressure drop trend curves have negative values as the height increases. i.e. the pressure decreases over height due to the bed material. However, note that the gradients are different according to the amount of bed material. As more bed material is charged in the combustion chamber, the absolute value of the gradient increases. Therefore, the charged amount of bed material has a definite relationship with the gradient of the trend line from the pressure profile. Moreover, the flow rate of bed material will be estimated in **Fig 4.3-6** with the same quantity of fluidizing air.

**Fig 4.3-6** is based on the gradient of the trend line in **Fig 4.3-5**. It illustrates the gradient curve according to the amount of bed material in case of 40/50/109. This shows that the higher charged amount of bed material in the combustion chamber causes the more pressure drop over height.

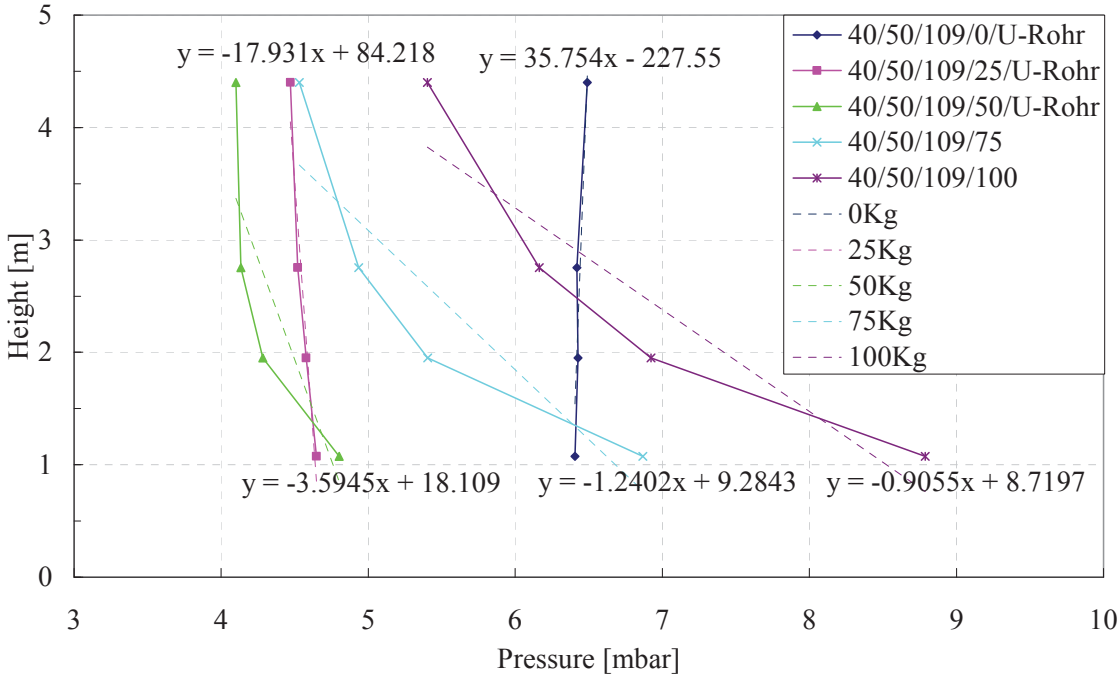


**Fig 4.3-5** Pressure profiles from P105 to P108 with various charged amounts of Cu bed material according to the height of sensors in the riser and their trend lines (dotted)

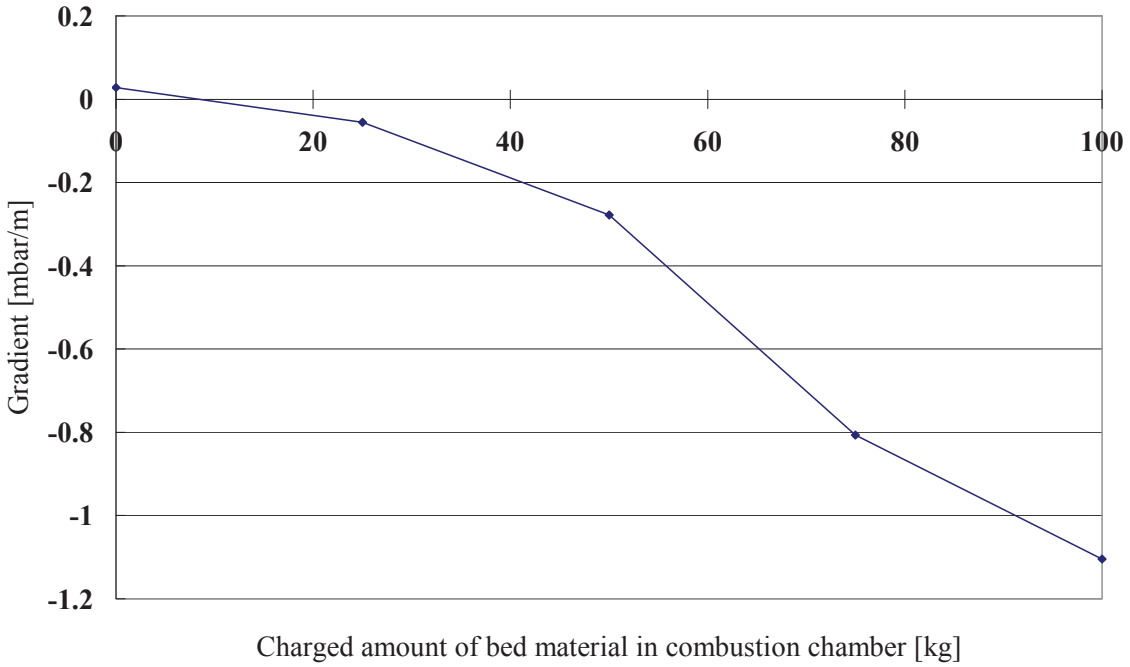


**Fig 4.3-6** Gradient of the pressure profile according to the charged amount of bed material (data from **Fig 4.3-5**)

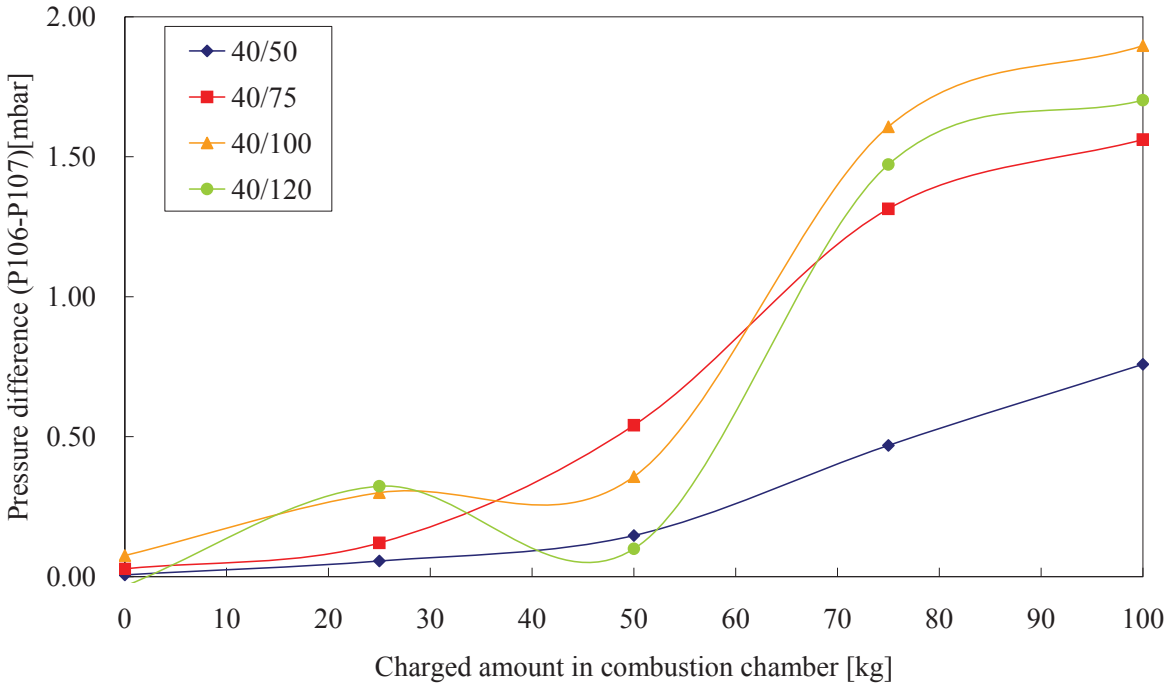


**Fig 4.3-7** Comparing the pressure difference between P106 and P107 according to various fluidizing air conditions

As the P108 is installed before the cyclone inlet and P105 is after the conical part on the combustion chamber, the pressure from these two P108 and P105 can be influenced by the flow geometry. On the contrary, the pressure sensors P106 and P107 are installed in the middle of the cylinder and the pressure influence from geometry might be much less than the case of P105 or P108. Moreover, to calculate the gradient of four pressure sensors according to fluidizing air or charged amount of bed material conditions is quite difficult with a trend line.

In **Fig 4.3-7**, the pressure difference from just two sensors (P106 and P107) is compared according to various fluidizing air conditions. When the pressure difference curve between P106 and P107 is determined for a given fluidizing air condition, the amount of charged bed material in the combustion chamber can be estimated from this graph.

Interestingly the pressure drops with 40/100 (40% primary air in fluidization air and 100% load factor) are larger than the ones with 40/120 (40% primary air in fluidization air and 120% load factor), compared for the same charged bed material amount except the 25 kg charged case. Even at 50 kg, the pressure drop with 40/75 is larger than the ones discussed before. See also chapter 4.3.2

However, the pressure difference is very small and errors must be expected from sensor fluctuations.

### 4.3.2. Flow rate of bed material

In the following, the particle loading is defined as the bed material mass flow rate per the total volumetric flow rate (a sum of primary-, secondary- and FHE fluidizing air) of fluidizing air at the time.

$$\text{Particle loading (P)}\,[\text{kg/m}^3] = \frac{\text{mass flow rate of solid } (\dot{m}_s)\,[\text{kg/s}]}{\text{total volumetric flow rate of gas } (\dot{V}_g)\,[\text{m}^3/\text{s}]} \qquad (4.3\text{-}1)$$

To measure a mass flow rate of bed material during operation according to various fluidization air conditions and various charged amount of bed material in the combustion chamber, the rising level of bed material at the downcomer which feeds the separated bed material from the cyclone into the siphon was measured every 10 sec, after fluidizing air for the siphon has been turned off. **Fig 4.3-8** shows the measured data and the calculated bed material particle loading [kg/m$^3$] according to various conditions.

The data which is measured every 10 sec. cannot represent the actual flowing mass flow rate and the actual mass flow rate of bed material is estimated by various methods in **Fig 4.3-9**, where **10 sec**. data denote the first 10 seconds values to be measured, **exponential** data are from the coefficient (y intercept value) of the exponential trend curve which is illustrated from 6 values for 1 minute, **quadratic** data are from quadratic functional trend curves, **average** data are averaged values from 10sec., exponential and quadratic values, and **Mattihas** data are the y intercept values which are obtained from the quadratic functional trend curves for just 50 seconds in a minute except the first 10 second values.

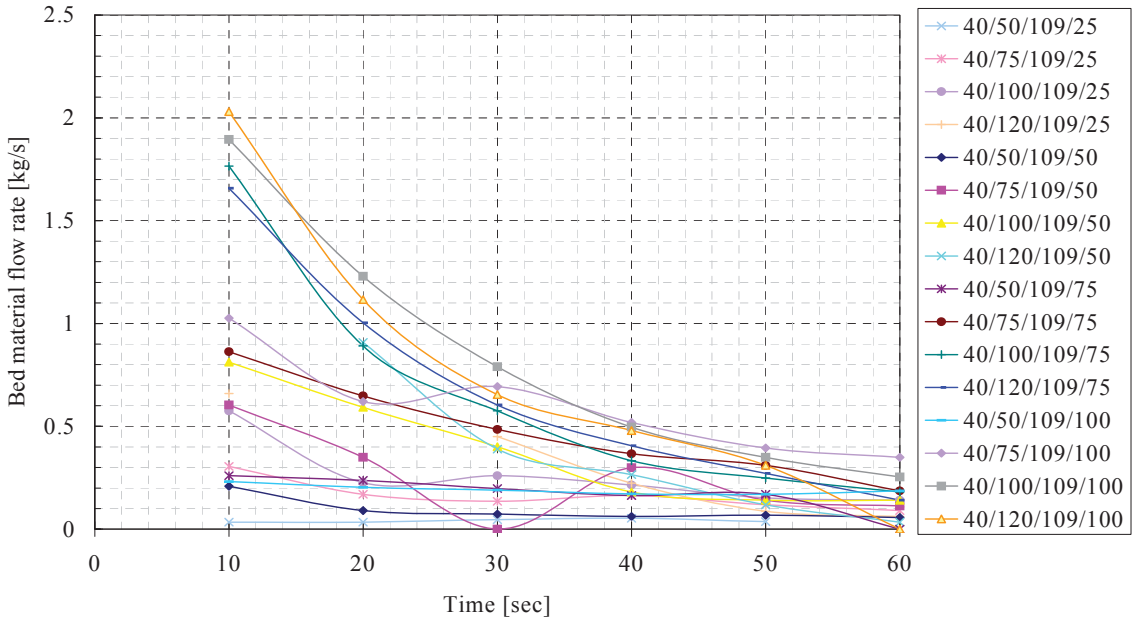


**Fig 4.3-8** Mass flow rate [kg/s] of bed material in the downcomer according to various fluidization conditions with various charged amounts of Cu bed material

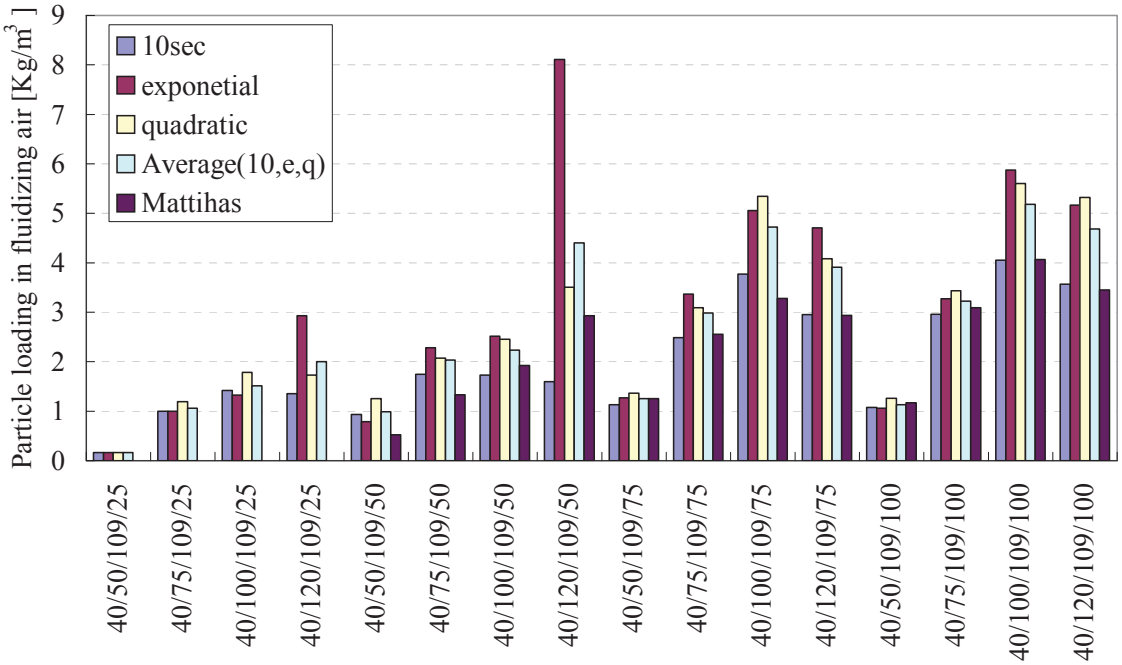


**Fig 4.3-9** Circulating Cu particle loadings according to the various fluidization conditions as estimated by different methods; the estimating methods are classified in the legend.

The cause of these various estimations is the measuring errors from manual measurement. However, the deviations among the estimating methods are relative large and the first 10sec. values are used in this investigation. To measure the accurate values, a new method for measuring the flow rate of bed material would be needed.

In **Fig 4.3-10**, the mass flow rates of bed material from the 10 sec. values are illustrated with actual supplied amounts of fluidization air. The circulating mass flow rate in **Fig 4.3-10** increases according to the increased volumetric flow rate (superficial velocity) of fluidization air but it doesn't increase lineally over the whole volumetric flow range. This result agrees with the experiment of Hirama et al [32].

Their experiment is without re-circulation and with alumina particles which have a smaller density than our Cu particles. The bed material (alumina particles) was fed with a constant amount into a riser by a forced feeding system. When $\varepsilon_{pd}$ (particle volume fraction in dense region) is 0.013 and 0.018, i.e. with relative small amounts of particle feeding in their experiment, the mass flow rate curves show one or two transition(s) in the range of their superficial velocities for the fluidized bed. (See **Fig 4.3-11**)

The cause of this gradient transition may be that the more fluidized particles over a critical superficial velocity hinder the particles' movement which moves upward. i.e. according to Glicksmann's theory [2], the viscosity term is increased by denser particles over a critical velocity and the inertial term is decreased, as the superficial velocity is increased.

If the superficial velocity exceeded our test range, the transition in the curve's slope can occur again, because the much higher superficial velocity would overcome the adhesive forces between the fluidized particles in the riser and moreover the regime would be diluter.

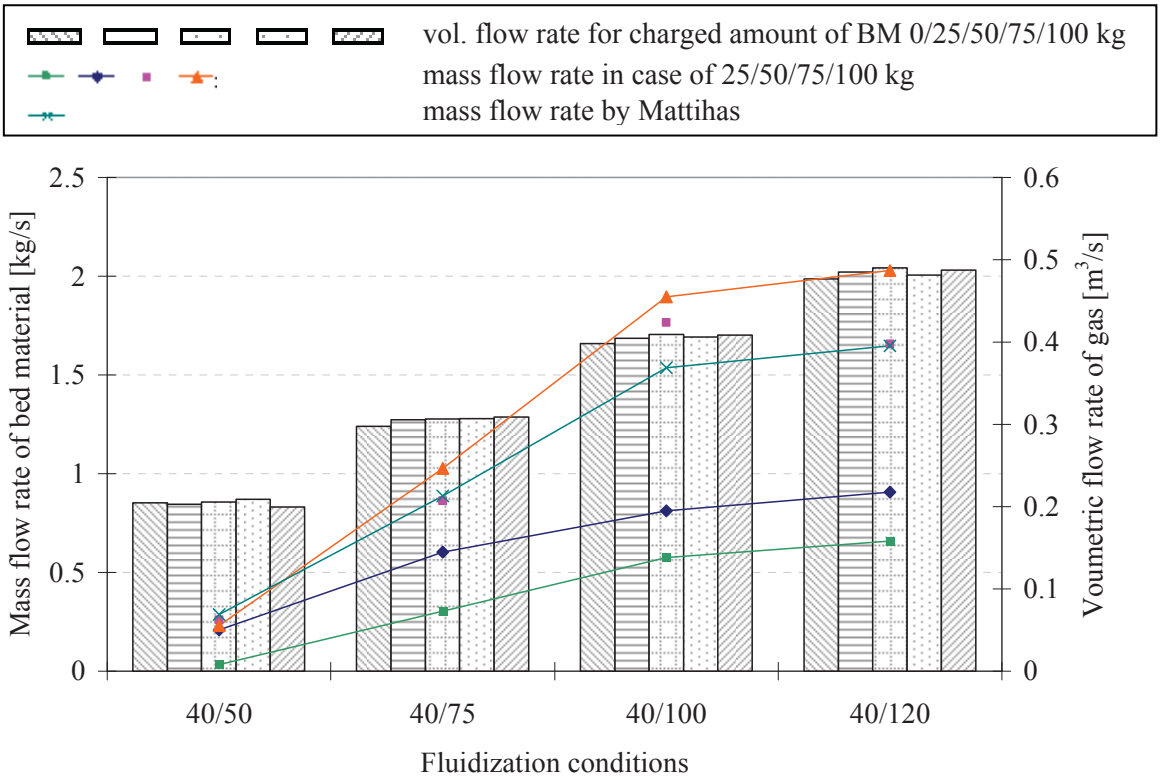


**Fig 4.3-10** Mass flow rates of bed material (BM) acc. to various charged amounts of bed material and actually supplied amount of fluidizing air

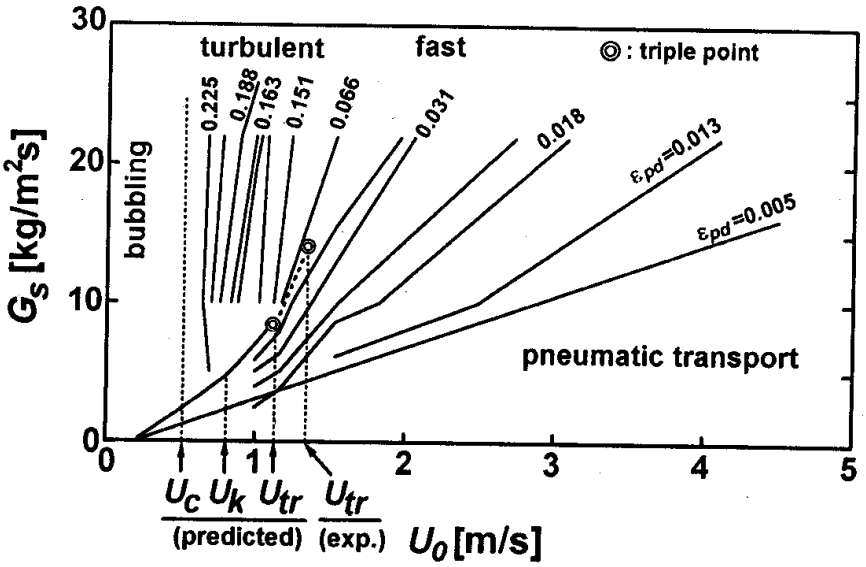


**Fig 4.3-11** Bed material's mass flow rate transition from the experiment from Hirama et al [32] (superficial gas velocity on the x-axis)

Just for the case of the 75 kg curve in **Fig 4.3-10**, although the fluidization air increases from 40/100 to 40/120, the mass flow rate decreases. This may be due to a measurement error for the 40/100 condition. The remaining three values on the 75 kg curve are coincident with Mattihas'. Therefore, the curve with 75 kg is selected from Mattihas'. Note also that the values of 25 kg charged BM can have some errors, as the data was measured under the condition that the FHE is fully filled with bed material and some amount of particles could flow into the CFB parts, i.e. into the combustion chamber, although fluidizing air for FHE is injected just into the empty chamber.

### The influence of the superficial velocity in the riser on the particle loading

The relation between the particle loading and the superficial velocity which is calculated in the cylinder is illustrated in **Fig 4.3-12**. The curves -except the 50 kg one- show a tendency that the particle loading decreases around 2.3 m/s (40/100). As shown in **Fig 4.3-10**, the mass flow rate has a critical point at 40/100 (the mass flow rate increases relative lineally up to 40/100) except the 50 kg curve. Therefore, the particle loading which is calculated from the mass flow rate of particles and the volumetric flow rate of gas has also a critical point at 2.3 m/s.

As a result, it is not helpful just to increase superficial velocity (also the volumetric flow rate of gas) in order to increase the particle loading (or the circulating mass flow rate of particles in gas) above a critical point; e.g. above 1.7 m/s in the case of 50 kg bed material in the combustion chamber, when the charged amount of bed material in the combustion chamber is constant.

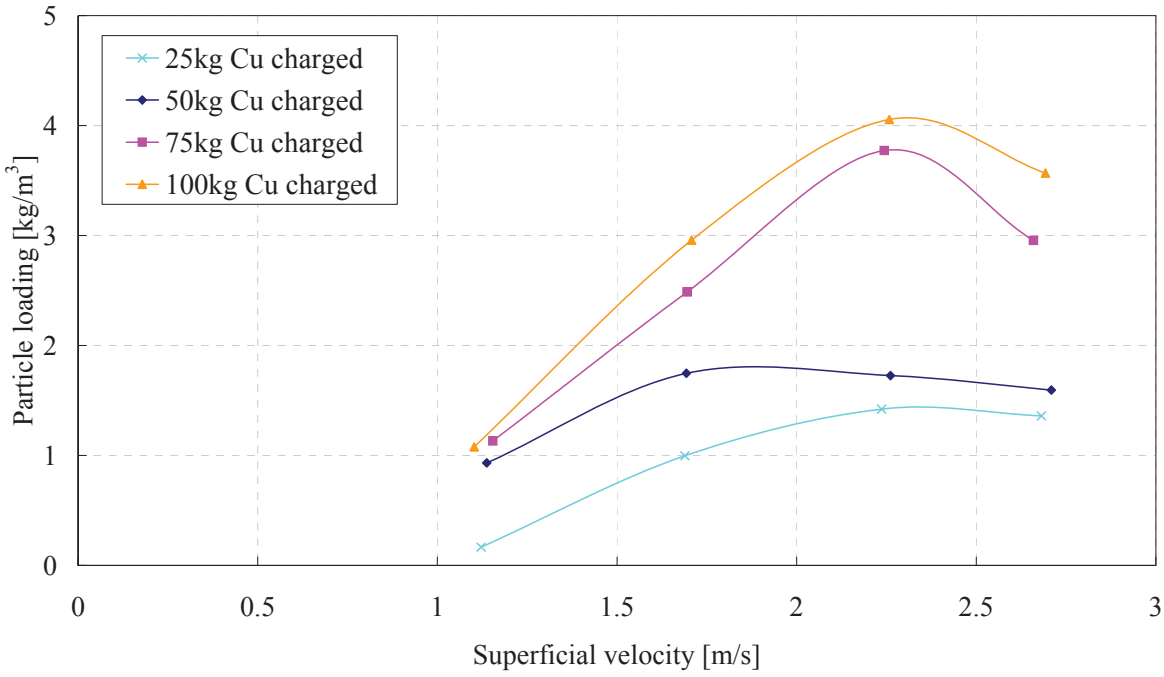


**Fig 4.3-12** Particle loading vs. actual superficial velocity according to various charged amounts of bed material

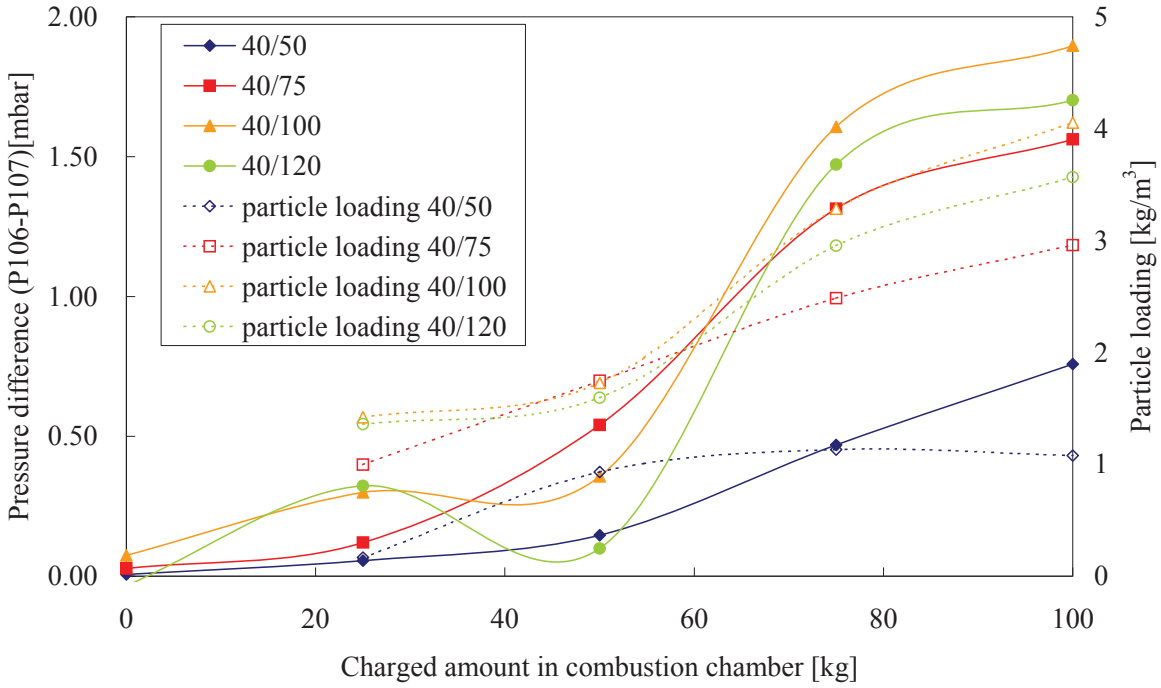


**Fig 4.3-13** Comparison of pressure difference (P106-P107) profiles and particle loading curves versus charged amount of bed material in the combustion chamber

## Correlation of static pressure profiles in the riser with particle loading

**Fig 4.3-13** shows the particle loading curves and the pressure difference of the sensors P106 and P107 for the different fluidization conditions. A clear correlation is visible between the two curve families. Besides some deviation for the condition 40/50 and 40/120 at the 50 kg data point, in most cases the trends of the particle loading are coincident with the pressure drop curves in the cylinder. This result tells that the particle loading in the gas is related with the pressure drop in the riser or in other words, causes a considerable fraction of the total pressure drop. Therefore, the estimation of the particle loading or the mass flow rate of circulating bed material from the pressure drop in the riser is possible.

The solid mass flow rates according to the amount of bed material in the combustion chamber are illustrated in **Fig 4.3-14**. The more bed material is charged in the combustion chamber, generally the higher solid mass flow rates are obtained at a certain gas flow rate. With the same amount of bed material in the combustion chamber, the increased volumetric gas flow rate (superficial velocity) causes higher solid mass flow rates; see also **Fig 4.3-10**. The gradient of solid mass flow curve decreases above 40/100 condition. However, the volumetric flow rate of fluidizing air increases almost proportionally according to the load factors. Therefore, when the solid mass rate is divided by the total gas flow rate in order to calculate the particle loading, the particle loading of 40/100 (40% primary air in the total gas / 100% load factor, i.e. about 0.46$m^3$/s of volumetric flow rate of gas) becomes larger than that of 40/120 (about 0.57$m^3$/s) in **Fig 4.3-13**.

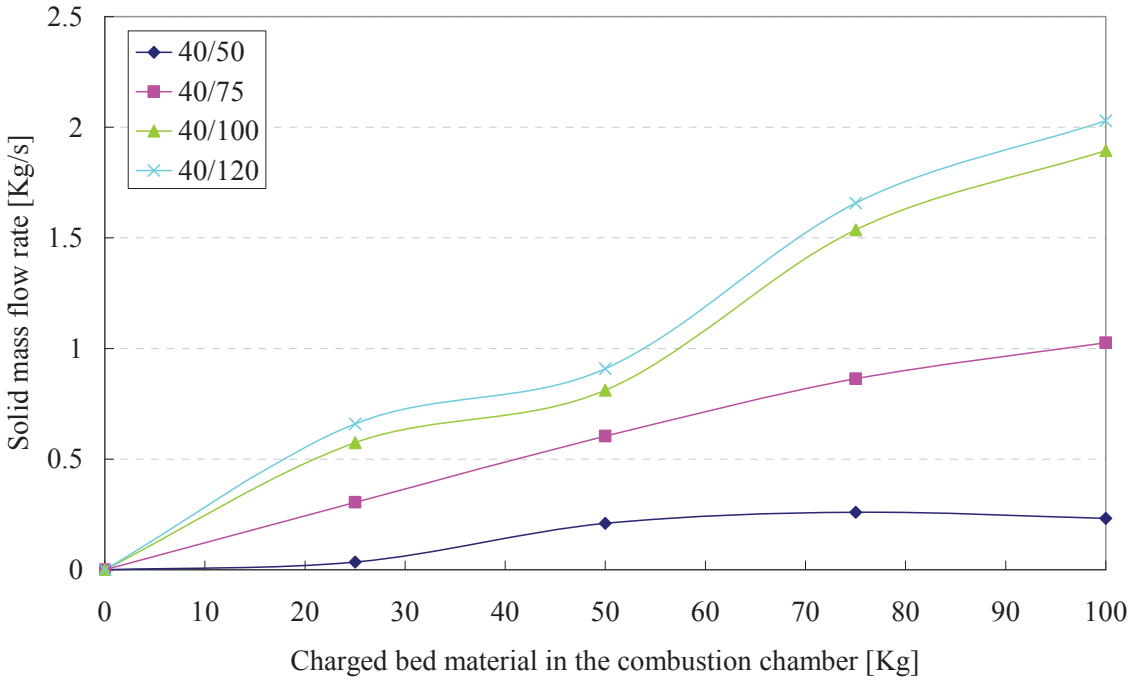


**Fig 4.3-14** Mass flow rate according to charged amount of bed material in combustion chamber

### 4.3.3. Minimal bubbling point in Cu particles

When gas is passed upward through a non-moving bed of particles, friction between gas and particles causes a pressure drop. As the gas velocity is increased, the pressure drop increases until it equals the weight of the bed divided by the cross-sectional area. This velocity is called minimum fluidization velocity, $u_{mf}$. When this point is reached, the bed material of group A will expand uniformly until, at some higher velocity, gas bubbles will form (minimum bubbling velocity, $v_{mb}$). For group B and D particles $u_{mf}$ and $u_{mb}$ are essentially equal; [4].

**Table 4.3-1** Supplied fluidizing air and pressure

| | F_415 [Bm³/h] | FN_415 [Nm³/h] | v [m/s] | p_405 [mbar] | p_403 [mbar] | p_410 [mbar] |
|---|---|---|---|---|---|---|
| 2.75Hz | 19.4 | 18.6 | 0.036 | 2.0 | 78.3 | 76.1 |
| 4.95Hz | 18.5 | 19.3 | 0.035 | 2.8 | 172.4 | 168.8 |
| 6.05Hz | 21.7 | 24.0 | 0.041 | 2.7 | 247.8 | 241.6 |
| 6.6Hz | 25.2 | 28.0 | 0.047 | 2.8 | 266.1 | 259.0 |
| 7.15Hz | 33.2 | 36.3 | 0.062 | 2.2 | 267.4 | 259.4 |
| 8.25Hz | 49.9 | 53.8 | 0.093 | 2.4 | 269.8 | 255.2 |
| 9.35Hz | 66.6 | 71.3 | 0.125 | 2.0 | 268.8 | 245.2 |

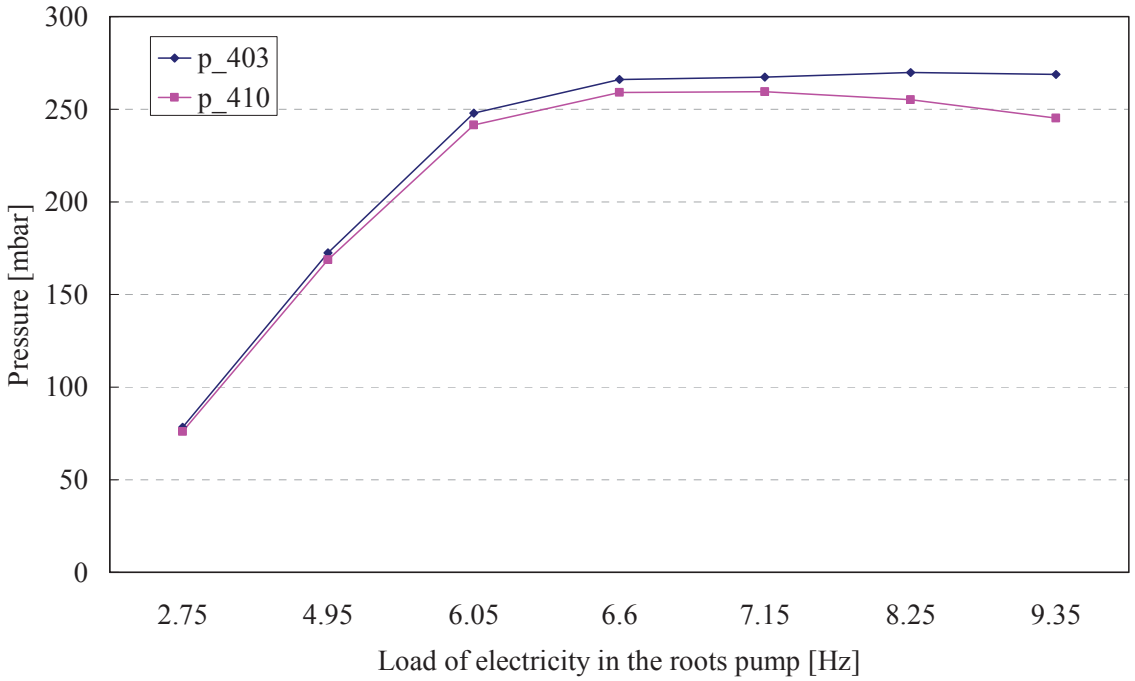


**Fig 4.3-15** Pressure profiles of the sensors P403 and P410 as a function of the fluidization air flow as provided by the roots pump with different settings of the frequency transducer

The pressure profiles which are tested in the second heating chamber are illustrated in **Fig 4.3-15** and the supplied fluidizing air at that time and pressure at each concerned sensor is in **Table 4.3-1**. The values of the x-axis in **Fig 4.3-15** is the supplied electrical frequency at the roots pump.

The superficial velocity versus pressure difference graph which is based on the data from the test can be seen in **Fig 4.3-16**. For superficial velocities in the second heating chamber higher than 0.04 m/s, the pressure difference between P410/405 and P403/P405 becomes nearly constant, where P405 is located at the wind box, P410 is just over the gas distributor and P405 is over the particle level.

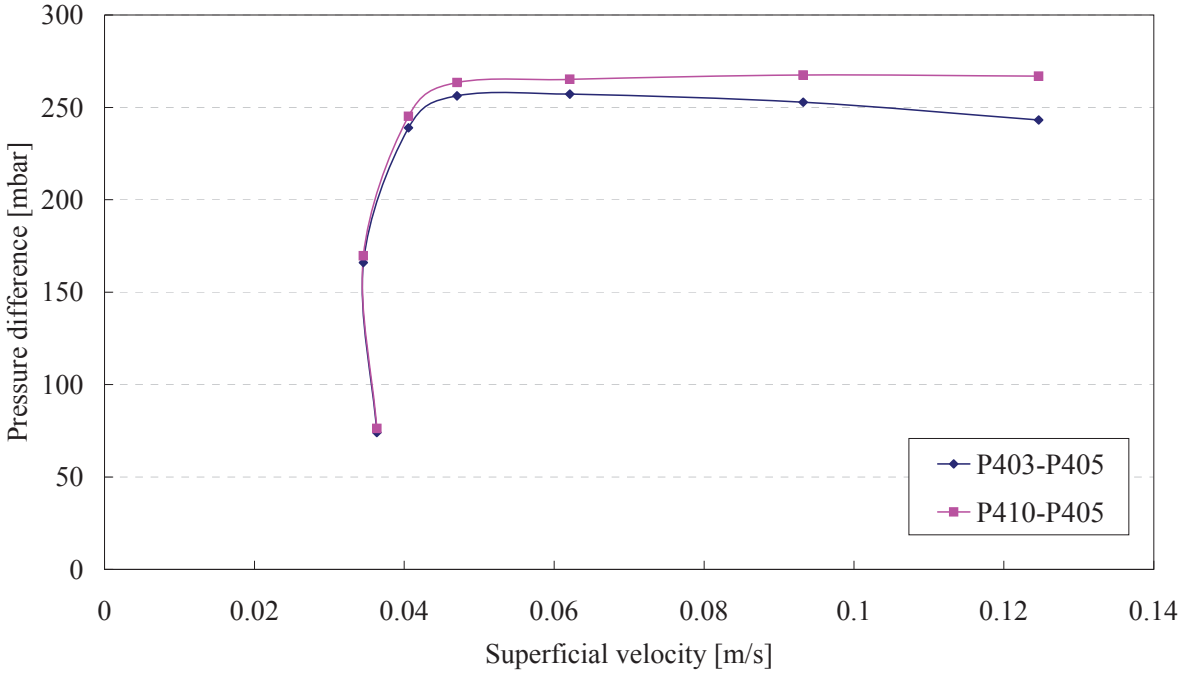


**Fig 4.3-16** Superficial velocity vs. pressure difference; tested with Cu particles in the second heating chamber

**Table 4.3-2** Data for the operating point of the cold model in the Reh-diagram

| | | |
|---|---|---|
| $\Delta\rho$ | [kg/m$^3$] | 8948.8 |
| $\rho_f$ at T=300K | [kg/m$^3$] | 1.177 |
| $\rho_{f\,0}$ at T=273K | [kg/m$^3$] | 1.293 |
| $\rho_p$ | [kg/m$^3$] | 8950 |
| $d_p$ | [m] | 6.30E-05 |
| g | [m/s$^2$] | 9.81 |
| $\eta_f$(T=300K) | [kg/ms] | 1.85E-05 |
| $\nu_f$ | [m$^2$/s] | 1.57E-05 |
| $u_{mf}$ | [m/s] | 0.044 |
| $Re_p$ | [ ] | 0.176 |
| $3/4Fr^*_p$ | [ ] | 3.066E-04 |
| Ar | [ ] | 75.4 |
| $d_p^*$ | [ ] | 4.225 |
| u* | [ ] | 0.042 |

According to the Reh-diagram, at a minimal fluidizing velocity ($u_{mf}$) of 0.044, the voidage ($\varepsilon$) is about 0.5; see **Fig 1.4-2**. The numbers required for the Reh-diagram and simplified Reh-diagram from Grace are calculated in **Table 4.3-2**, where $\Delta\rho=\rho_p-\rho_f$, $\rho_p$=density of bed material, $\rho_f$ =density of air at 300K, $d_p$= mean particle diameter, g=gravity acceleration, $\mu_f$ =viscosity of air at 300K, $\nu_f$ =kinematic viscosity of air at 300K, $u_{mf}$ =minimum fluidizing velocity, $Re_p=u_f\ d_p\ /\nu_f$ , $u_f$ =superficial velocity of fluidizing air, $Fr^*=u_f^2\ \rho_f\ /gd_p\Delta\rho$, $Ar=g\ d_p^3\Delta\rho/\nu_f^2\rho_f$, $dp^*=Ar^{1/3}$, $u^*=u[\rho 2/\Delta\rho g\mu_f]^{1/3}$.

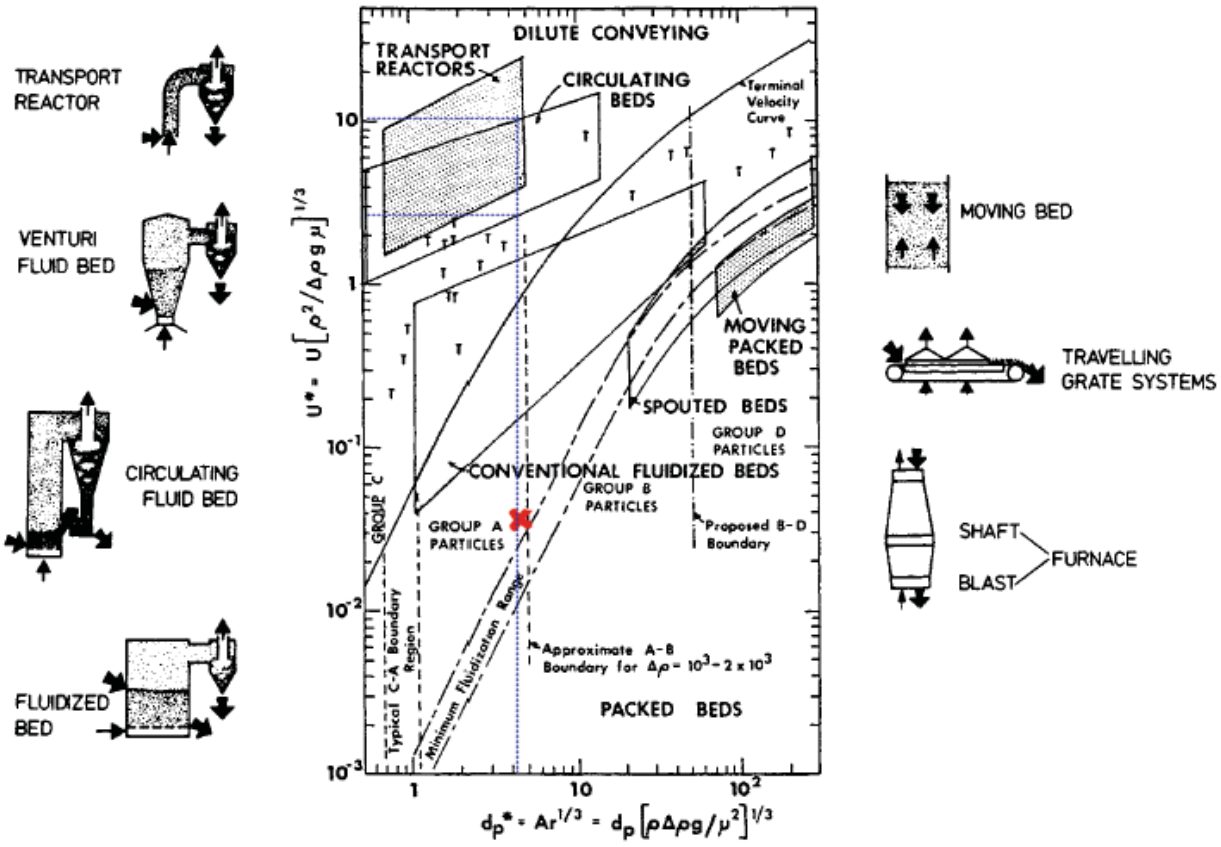


**Fig 4.3-17** Simplified Reh-diagram from Grace (1997)

The simplified Reh-diagram from Grace is illustrated in **Fig 4.3-17**, where the point from $u_{mf}$ for our case is marked as a red X. To satisfy the conditions for a circulating fluidized bed in the diagram, the u* value must be located in the range from 2.7 to 10.5 m/s in case of our $d_p$* from Cu particles. As a result, the calculated range for $u_f$ from u* is between 2.85 m/s and 7.50 m/s for our Cu bed material.

When the $d_p^*$ value is compared with the one for sand particles, although the density of Copper is 3 times as large as that of sand, the two $d_p^*$ values, which are a function of Ar number, are almost the same, because the Ar number is proportional to $d_p^3$ and the mean diameter of sand particles is about 40% larger than that of Cu particles.

The actual superficial velocity range from our experiment is about 1.1 m/s at 50 % load factor to about 2.7 m/s at 120% load factor. (Note that the theoretical range recalculated from the RV-Lenzing plant is within 1.3 m/s to 3.0 m/s). Actually, to classify between CFB and FB is difficult. When the calculated point for Reh-diagram is located between CFB and FB, the graphical calculation may not be precise enough. For these reasons, although the actual superficial velocity values measured are out of range from the CFB-field in the diagram, they can be roughly accepted.

### 4.3.4. Pressure drop in the cyclone

Pressure drop is determined by summing five flow losses associated with the cyclone.

- ✓ Inlet contraction
- ✓ Particle acceleration
- ✓ Barrel friction
- ✓ Gas flow reversal
- ✓ Exit contraction

The total pressure drop is the sum of the 5 individual pressure drops. However, the actual pressure drop observed turns out to be a function of the solids loading. The pressure drop is high when the gas is free of solids and then it decreases as the solids loading increases up to about 3 kg/m$^3$. The cyclone Δp then begins to increase with loading. The initial decline is caused by the presence of solids decreasing the tangential velocity of the gas; [29].

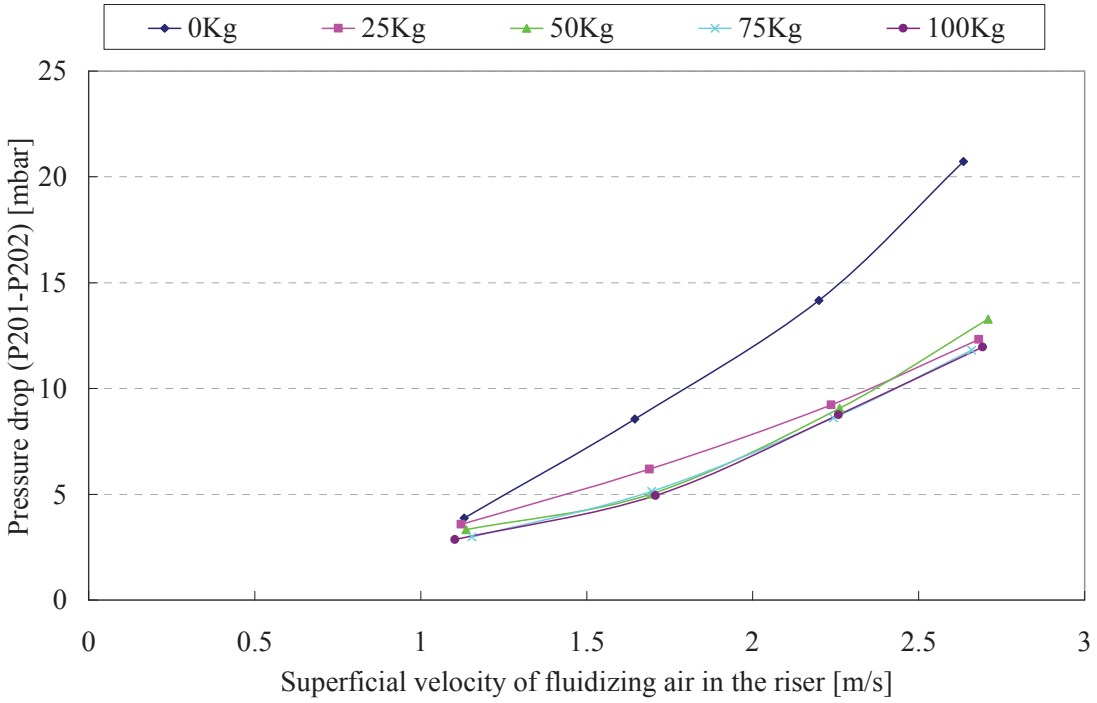


**Fig 4.3-18** Pressure drop in the cyclone according to the various amounts of Cu bed material

**Fig 4.3-18** illustrates the measured pressure drop in the cyclone according to various amounts of bed material. At the same amount of charged bed material in the combustion chamber (along a curve), the pressure drop between inlet and outlet in the cyclone increases, as the superficial velocity (in the riser) increases. However, the pressure drop decreases roughly according to the increase of bed material amount in the combustion chamber (as a result of the increased particle loading in the cyclone inflow) at a constant superficial velocity. These findings in accordance with [33] may lead to the conclusion that the particle loading doesn't exceed 3kg/m$^3$ in our tests. As can be seen from the pressure drop and the particle loadings in **Fig 4.3-19** and **Fig 4.3-20**, the pressure drop is almost constant even for particle loading slightly exceeding 3 kg/m$^3$.

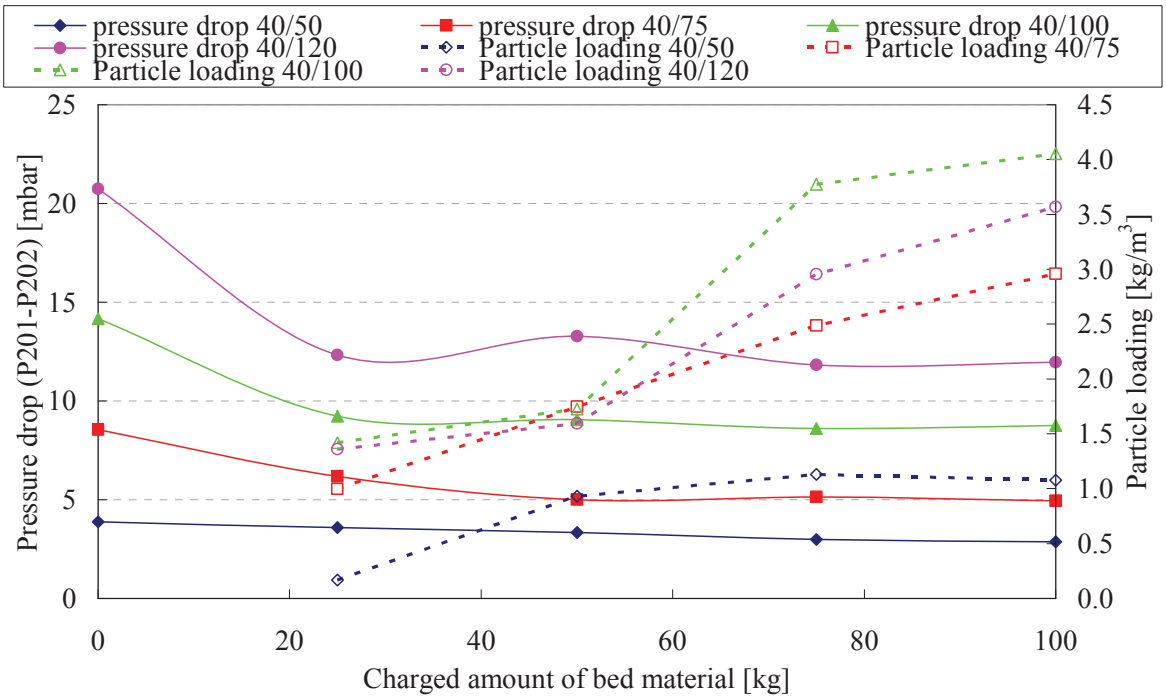


**Fig 4.3-19** Particle loading and pressure drop in the cyclone according to the charged amount of Cu bed material

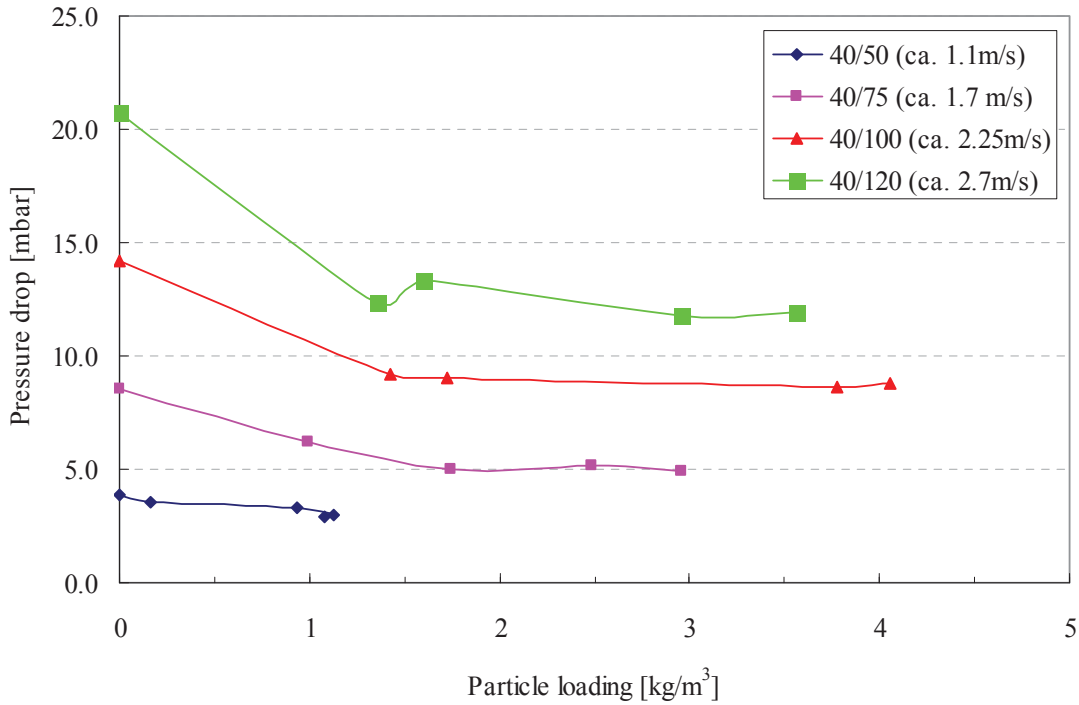


**Fig 4.3-20** The effect of the particle loading on the pressure drop at the constant superficial velocity

It is well explained from Yuu's experiment in [30] that the pressure drop between cyclone inlet and outlet decreases with increasing particle loading in the dilute regime. However, the phenomenon that the pressure drop stays constant after the first decrease cannot be found in any reference.

First of all, the possibility of any measurement error is checked by calculating the pressure drop. However, the values from the calculation (see **Appendix**) are almost coincident with our measured data by an average of 95 %. See **Table 4.3-3**. Note that the P202 sensor is installed not at the gas outlet in the cyclone but after the 180 degree bend. Therefore, the pressure at the gas outlet is calculated under the assumption of unloaded air. Moreover, the calculated pressure drop values show relatively large differences from measured values in cases of 25 kg charged bed material, especially at 40/120/109/25. This may be due to the inflow of bed material from the fully filled FHE.

The reason for this constant pressure drop can be found in the calculation. The increased particle loading or mass flow rate which flows into the cyclone increases wall friction, the tangential velocity ($u_i$) decreases. Therefore, the total pressure drop becomes almost constant, although the particle loading in the inflow is changed. As a result, the change of the charged amount (over 50 kg) in the combustion chamber under a constant superficial velocity doesn't affect the pressure drop in the cyclone of our cold model. In other words, the changed superficial velocity in the riser affects the pressure drop.

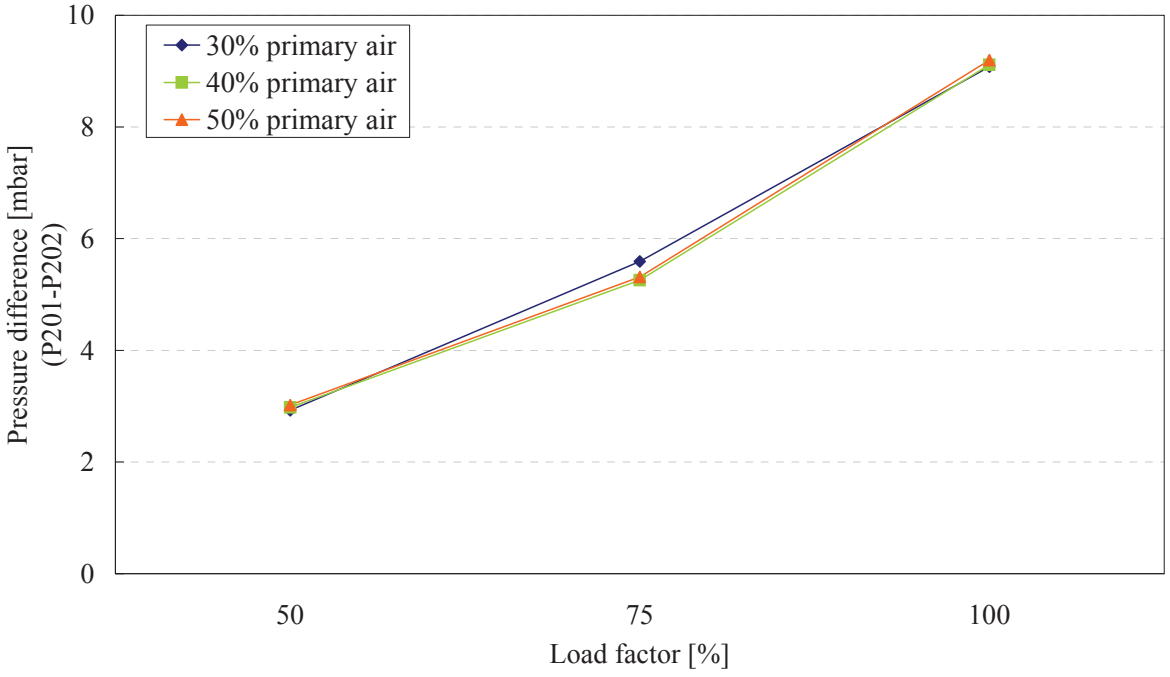


**Fig 4.3-21** The influence of primary- / secondary air ratio on the pressure drop in the cyclone.

**Table 4.3-3** Comparison of measured pressure drop in the cyclone with calculated one.

| | Δp. calc. | p201-p202 | p201-p outlet | Deviation (%*)) |
|---|---|---|---|---|
| 40/50/109/0 | 3.6 | 3.9 | 3.7 | 102.3 |
| 40/75/109/0 | 7.7 | 8.6 | 8.2 | 107.0 |
| 40/100/109/0 | 13.7 | 14.2 | 13.5 | 98.8 |
| 40/120/109/0 | 19.7 | 20.7 | 19.8 | 100.9 |
| 40/50/109/25 | 3.4 | 3.6 | 3.4 | 100.6 |
| 40/75/109/25 | 6.6 | 6.2 | 5.8 | 88.2 |
| 40/100/109/25 | 11.5 | 9.2 | 8.6 | 74.3 |
| 40/120/109/25 | 16.7 | 12.3 | 11.4 | 68.4 |
| 40/50/109/50 | 3.0 | 3.3 | 3.2 | 106.0 |
| 40/75/109/50 | 5.3 | 5.0 | 4.6 | 87.8 |
| 40/100/109/50 | 9.4 | 9.1 | 8.4 | 89.3 |
| 40/125/109/50 | 13.7 | 13.3 | 12.3 | 89.9 |
| 40/50/109/75 | 2.7 | 3.0 | 2.8 | 103.1 |
| 40/75/109/75 | 4.9 | 5.1 | 4.8 | 97.2 |
| 40/100/109/75 | 8.1 | 8.6 | 8.0 | 98.5 |
| 40/120/109/75 | 11.6 | 11.8 | 10.9 | 94.2 |
| 40/50/109/100 | 2.7 | 2.9 | 2.7 | 99.2 |
| 40/75/109/100 | 4.8 | 4.9 | 4.6 | 94.9 |
| 40/100/109/100 | 7.9 | 8.8 | 8.1 | 103.2 |
| 40/120/109/100 | 11.4 | 12.0 | 11.0 | 96.6 |

*) Δp. calc. / (p201-p outlet) *100

The influence of the ratio of primary air to fluidizing air is also negligible for the cyclone's pressure drop. **Fig 4.3-21** shows the pressure drop curves in the cyclone according to the various primary air ratios. The curve with 30 % primary air at 75 kg bed material shows a difference but it is still in the range of sensor fluctuation.

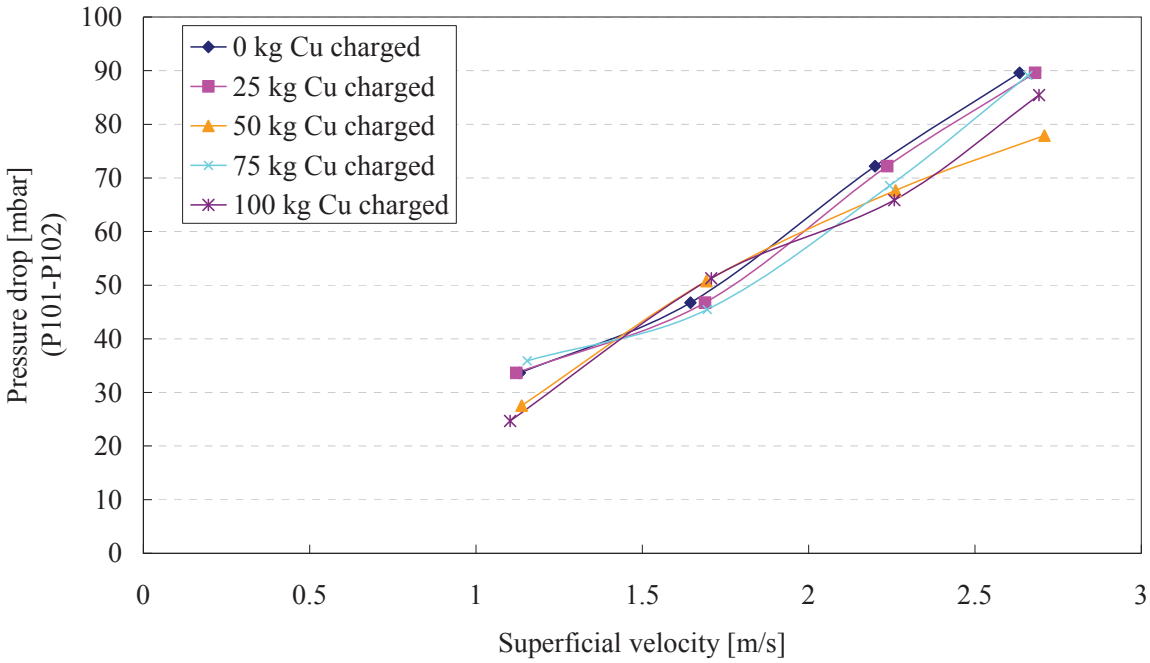


**Fig 4.3-22** Pressure drop at the gas distributing plate in the combustion chamber

### 4.3.5. Pressure drop at gas distributor

At the design stage of the cold model, the pressure loss of the steel screen for a gas distributing plate is not given by the manufacture. As noted before, this resulted in further holes being drilled in the gas distributing plates in the combustion chamber. The pressure drop from the new installed plate in the combustion chamber is illustrated according to various charging conditions in the combustion chamber in **Fig 4.3-22**. The more bed material is charged in the combustion chamber, the higher pressure loses occur at the plate. Near the 40/75 condition (about 1.7 m/s superficial velocity), it is difficult to find out any relationship between pressure drop and superficial velocity or charged amount of bed material. This may be due to the irregular frequency of bed material movement relative to the gas.

The pressure drop of the first heating chamber in the FHE is illustrated according to superficial velocities in **Fig 4.3-23**. The steepness of the trend curve increases with the superficial velocity. Moreover, it shows a steep slope around a superficial velocity of 0.25m/s.

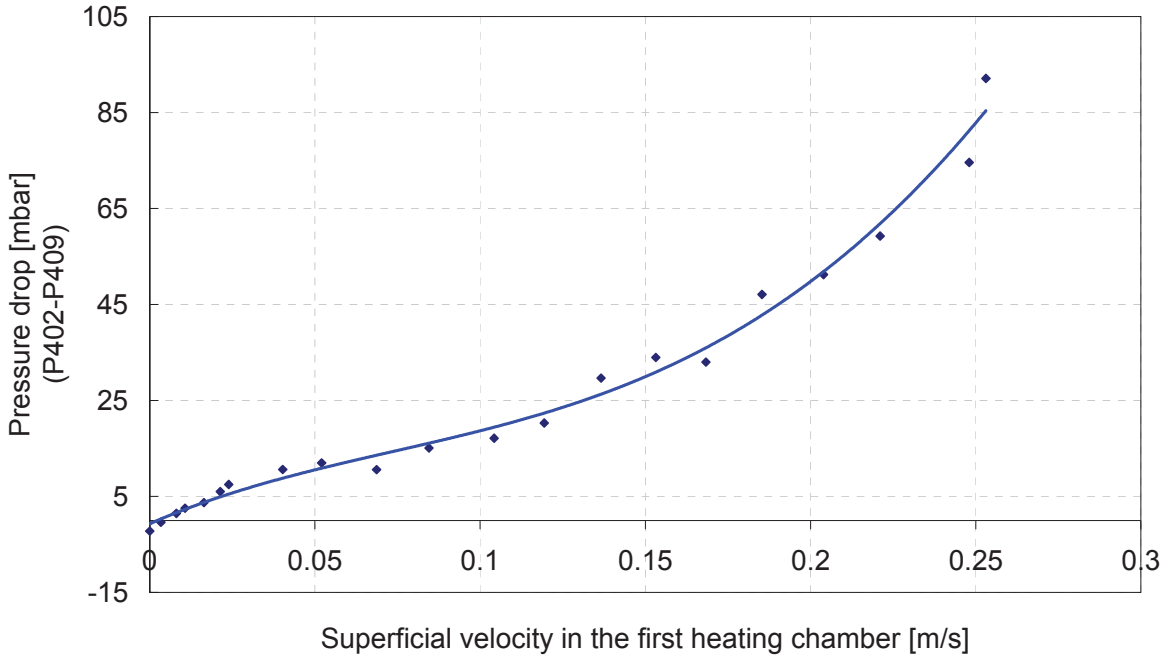


**Fig 4.3-23** Pressure loss at the gas distributing plate in the charged FHE; tested in the first heating chamber with heat exchanging bundle

## 4.3.6. The influence of heat exchanging bundles in the FHE

To observe and measure the influence of heat exchanging bundles in the FHE, a down-sized bundle is installed in the second heating chamber (**Photo 4.3-1**).

The bubbles are dispersed throughout the chamber and the bed material is uniformly mixed. In case of the tests without bundles, the mixing action induced by the bubbles is lower, while the bubbles tend to be merged with one another and rise preferentially through the center of the chamber, where the friction is lower relative to the wall near region. Hence, the bubbles cannot be observed during the test without bundles but they can be observed through the glass window after bundle installation.

The level of packed bed material rises, until the bubbling point is reached according to the minimal fluidization tests without bundles, but due to the disturbance of the rising bubble's movement and pressure loss at the bundles, the level doesn't show remarkable change in this test. Photos taken every 7 ms from a video clip are shown in **Photo 4.3-2**.

The changed fluidizing condition changes also $u_{mf}$, the maximal pressure difference is 304.7 mbar at 0.085 m/s after the bundle installation; (**Fig 4.3-24**).

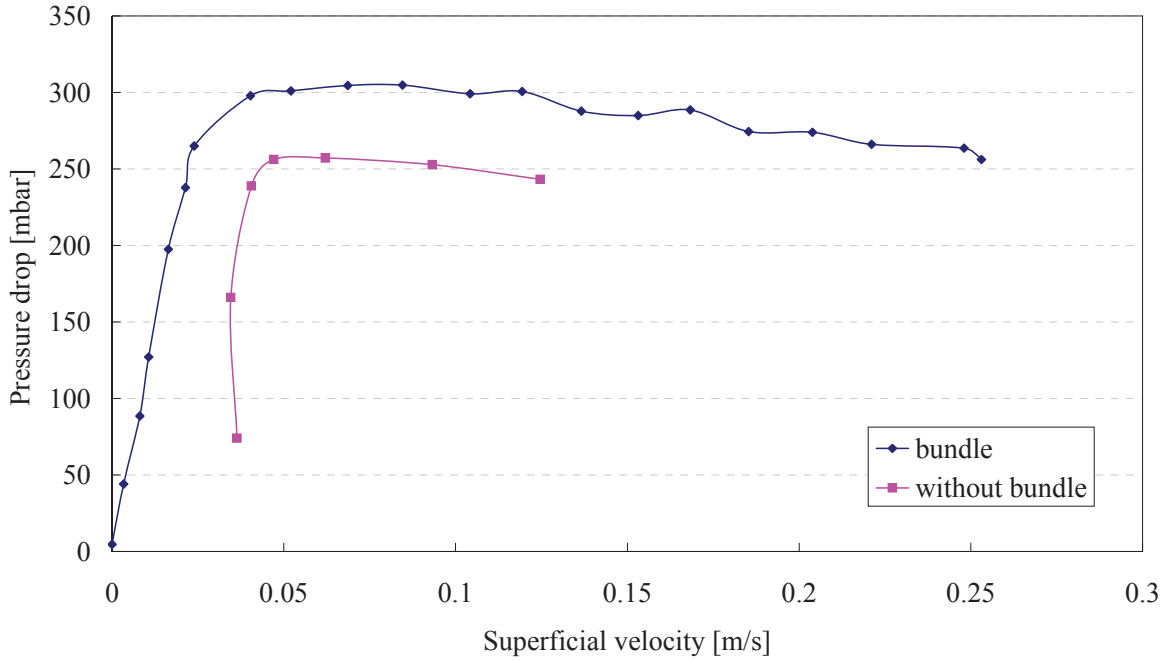


**Fig 4.3-24** The influence of heat exchanging bundles as installed in the second heating chamber on the minimal fluidization velocity, $u_{mf}$

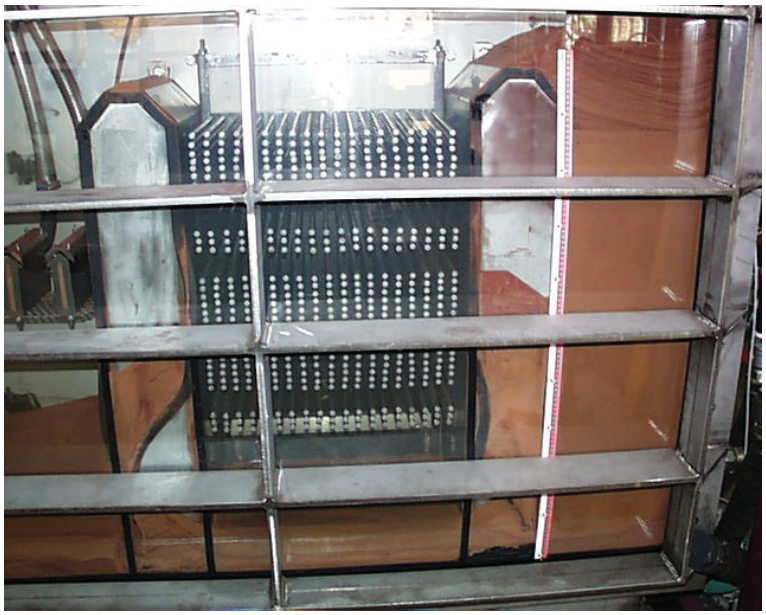

**Photo 4.3-1** Installation of a heat exchanging bundle in the second heating chamber of the cold model's FHE

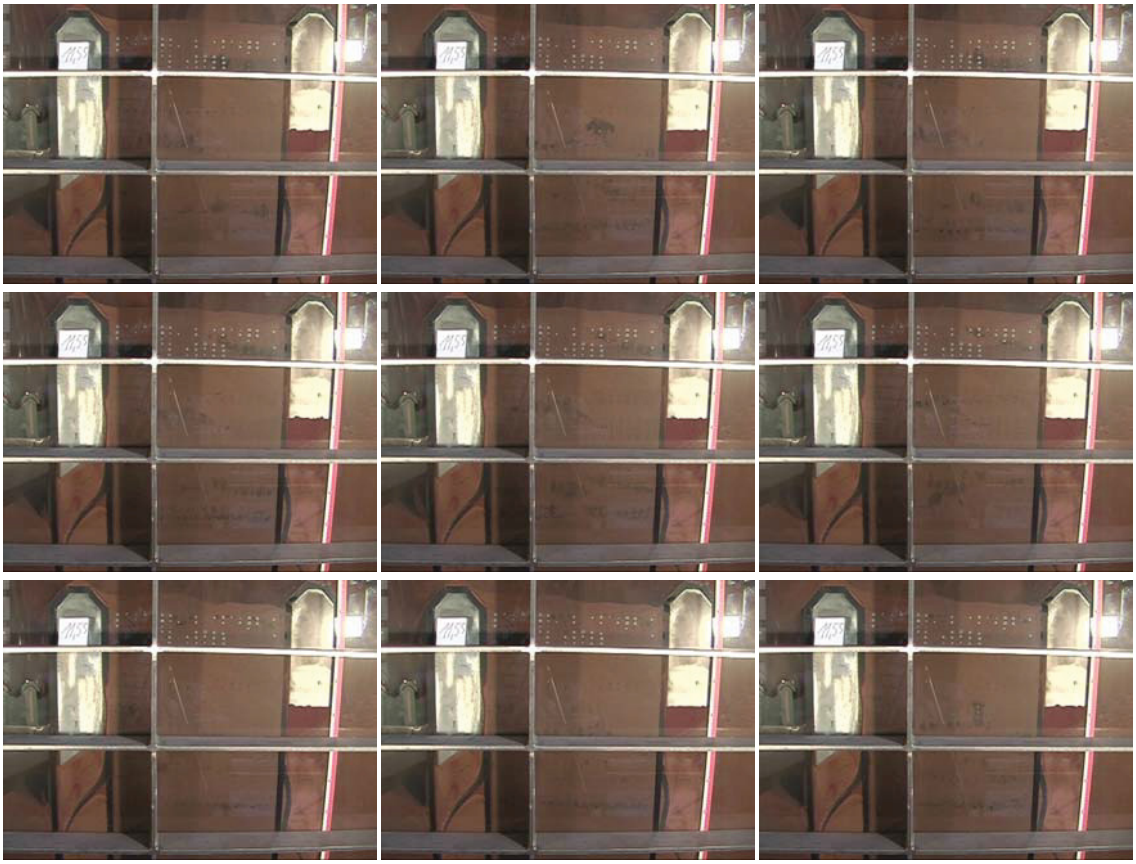

**Photo 4.3-2** The behavior of bed material in the second heating chamber after bundle installation from bundles.wmv file on the enclosed CD

## 4.4. Problems and solutions

Problems which occured in building the system are very important to be documented, as the same issues can occur either in a pilot plant or in a commercial plant. Many of them cannot be predicted during the stage of planning. The problems which we encountered during installation and start-up are good examples of issues which can be prevented in building a similar system.

### 4.4.1. Static electricity

The electrostatic energy due to friction either from inter-particles or particles / Plexiglas interaction causes significant problems. Not only does it affect the function of sensors, it can even damage some of them. Moreover, according to the Glicksman's experiment[26], the electrostatic forces can reduce the minimum fluidization velocity by 33%.

In Fig 4.4 1, the captured sparks can be seen, which are recorded from a test video clip with sand bed material , at P201 sensor. The sparks were not observed any more with Cu bed material.

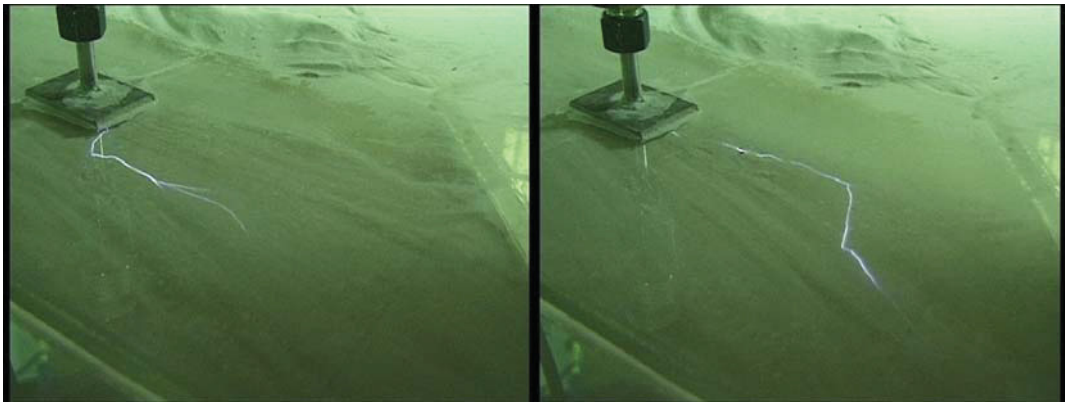

**Fig 4.4-1** Sparks as induced by static electricity from the Blitz.avi file on the enclosed CD

**Solution:**

- ✓ The low pressure difference sensors have been changed against sensors with electrical protection and standard mounting. (Prior installed sensors were mounted with a short rubber tube and the distance between the sensor and the surface of Plexiglas was very narrow).
- ✓ Thermocouples are replaced with PT-100 (RTD)
- ✓ Grounding of sensors (not effective)

### 4.4.2. Measuring errors of volumetric flow rates

At first the wrong installation of orifice plates caused the errors in the volumetric flow rates. Some of them were installed in the reverse direction and for some of them the opening diameters in the measurement program (HP Basic program) were wrongly specified. Theses problems could be detected easily with the measured values themselves or with the help of mobile flow meters.
The coding mistakes in the measurement program were not easy to find, as the differences between the flow meter values and the ones from the measurement program deviated only 10-20%, which was considered as measurement error caused by the measuring method. Although the possibility of wrong coding had been neglected for some months, just some small coding errors had been found and were corrected, until the fundamental error was found in the correlation.

**Solutions:**

- ✓ Comparison of measured values from alternative measuring methods with that from the measurement (data acquisition) program.

### 4.4.3. Sealing (gasket)

Copper or sand particles as bed material are very fine. Although the mean diameters are 68 and 100

respectively, naturally, much finer particles exist, in the particle size distribution. These particles are fluidized and move as a fluid. Especially under over-pressure in the chamber, small particles escape from the system throughout even any small gap, such as wrong bonded sealing rubbers, bolts and holes, by loose bolts, etc. Moreover, some pipe connections are sealed with adhesive aluminum tape or specialized tape. The adhesive surfaces which are not bonded correctly are exposed to particles continuously under high pressure, this might produce erosion and can cause leakage.

**Solutions:**

In the cold model, some parts are sealed with silicon. In the commercial beds with elevated temperature and higher pressure welded connection or proper gasket must be used.

- ✓ Assemble bolts with packing
- ✓ Tighten bolts and nuts (be careful of glass or Plexiglas)
- ✓ Good bondage, when the gaskets bond each other
- ✓ Fast stick without void in case of tape
- ✓ Examination before main process runs

### 4.4.4. Design mistakes

The height of the bed material inlet into the FHE from the siphon was as high as the charged level of bed material in the FHE. This caused the pipe blockage in the connection between the FHE and the siphon. Thereafter, some taps for compressed air were installed to fluidize bed material in the inclined entering chamber. However, this improvement alone was not sufficient. Hence, the design of the pipe had to be changed a little bit and the height of the inlet was raised; **Photo 4.4-1**.
The control valve which controls the entering amount of bed material from the siphon into the FHE was located as high as the FHE frame (**Photo 4.4-2**) and couldn't be operated. Thereafter the height level of the valve has been changed.

**Solution:**

- ✓ 3D-modeling or building a miniature can reduce these design mistakes

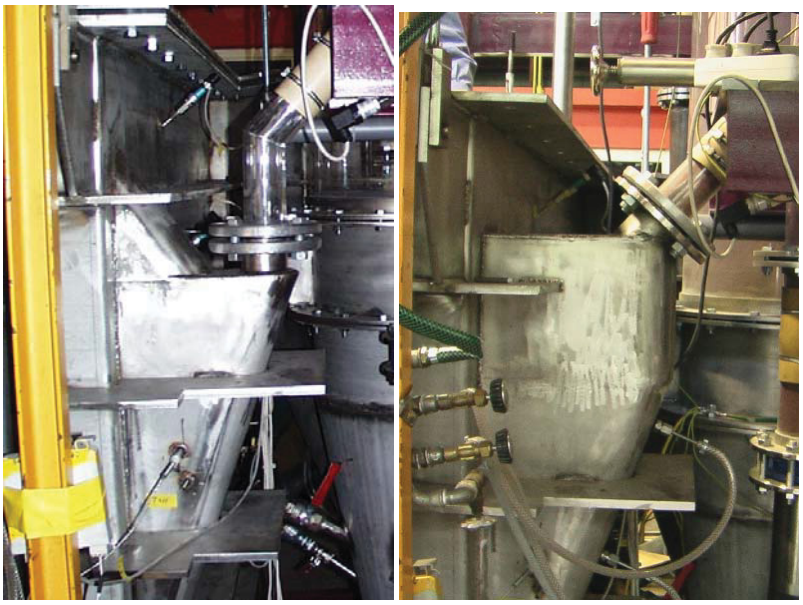

**Photo 4.4-1** Before (left) and after (right) changing of the pipe connection between siphon and FHE

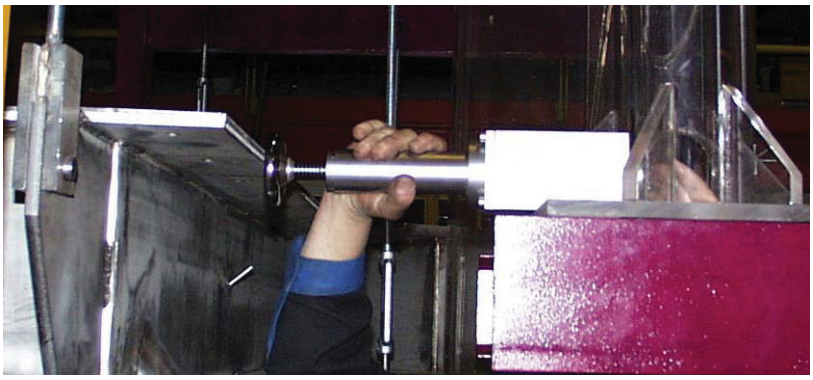

**Photo 4.4-2** The control valve for the feeding of the bed material from the siphon into the FHE; here seen in the original installation before changing the height level

# Conclusion

Throughout the “cold model project” the main experimental issues after construction of the model are the observation of solid behavior, the pressure profile in each part and its relationship with particle loading.
This solid behavior couldn't observed in the commercial hot bed or be just estimated in the computer simulation with considerable effort.

The overview of this project procedure is as following,

- Building the cold model
- Installation of measuring sensors and the data acquisition system
- System test with air (one phase)
- System test and preliminary experiments with sand
- Main experiments with Cu particles

The experimental results from main experiments (with Cu particles) are important for the commercial hot bed due to the scale law. The results can be summarized as follows:

From the observation of the solid particle behavior in the CFB as well as in the FHE, it is proven that the new designed siphon works acceptable. The behavior in the riser cannot be observed due to the dense annulus and clusters. However, the flow is investigated in the cyclone. Furthermore, a death zone between the weirs in the FHE and macroscopic flow of solid particles in the FHE is observed according to the various fluidizing conditions.

In the case of the constant amount bed material charged in the combustion chamber, the particle loading can increase just up to a critical point by only the increased superficial velocity.

The riser's pressure drop in the dense phase region as well as in the dilute region is related to the solid loading in gas. Therefore, it is proven that the circulating amount of solid can be predicted from the pressure drop in the riser.

Beside some of these experimental results, “Know-how” learned from building a two-phase flow pilot plant as well as the data acquisition system is also an excellent result on its own. Some problems which were encountered during building the cold model can now be circumvented or at least minimized in construction of a new model.

In a future step, detailed experiments for particle behavior in the FHE are planned according to the various weir shapes and locations. Our cold model will hopefully keep up contributing to the development and further improvements of commercial beds.

# References


1 H. Anderl & K. Kaufmann, 110 MW CFB boiler RV-Lenzing for incineration of waste materials (RDF) and sludge, Austrian Energy & Environment AG,(1999)

2 L.R. Glicksman, Scaling relationships for fluidized bed; Chemical Engineering Science, Vol.39, No.9, pp. 1373-1379, (1984)

3 D. Geldart, Powder Technol., 7, 285–292 (1973)

4 M. Pell & J.B. Durson, Gas-solid operations and equipment; Perry et al., Perry's Chemical Engineers' Handbook 7th Edition, 17-2 17-4, McGraw-Hill, (1999)

5 M. Stiess, Mechanische Verfahrenstechnik 2, pp. 351-352, Springer, (1997)

6 D. Geldart, Gas Fluidization Technology, John Wiley & Sons, (1986)

7 O. Molerus, Fluid-Feststoff-Strömungen-Strömungsverhalten feststoffbeladener Fluide und kohäsiver Schüttgütter, Springer, (1982)

8 J. R. Howard, Fluidized Bed Technology, Adam Hilger, (1989)

9 VDI-Wärmeatlas 7.Auflage, Lf2, (1984)

10 J.R. Grace & H. Bi, Introduction to circulating fluidized beds; J. R. Grace et al., Circulating Fluidized Beds, Blackie Academic & Professional, pp. 1-20, (1997)

11 L. Reh, Chemie- Ingenieur-Technik, 1, pp. 319–329, (1978)

12 J.R. Grace; Can. J. Chem. Eng., 64, pp. 353– 363, (1986)

13 M. Horio, Hydrodynamics; J.R. Grace et al., Circulating Fluidized Beds, Blackie Academic & Professional, pp. 21-85, (1997)

14 A.M. Squires, Contribution toward a history of fluidization; Proceedings Joint Meeting of Chemical Industrial Society China and AIChE, pp. 322-353, (1982)

15 J. Yeushalmi et al., The fast fluidized bed; Industrial and Engineering Chemistry, Process Design and Development, 15, pp. 47-53, (1976)

16 D. Shi, Fluiddynamik und Wärmeübergang in einer zirkulierenden Wirbelschicht. Dissertation, Eidgenössische Technische Hochschule Zürich, (1996)

17 L. Reh, Fluidized bed processing; Chemical Engineering Process 67, pp. 58-63, (1971)

18 J. Werther & B. Hirschberg, Solids motion and mixing; J.R. Grace et al., Circulating Fluidized Beds, Blackie Academic & Professional, pp. 119-148, (1997)

19 J.R. Grace & C. Brereton, End effects in circulating fluidized bed hydrodynamcis; A. Avidan (ed.) Circulating Fluidized Bed Technology IV, pp. 137-144, (1993)

20 M. Horio & R. Clift, A note on terminology: cluster and agglomerates; Powder Technology, 70, pp. 196,(1992)

21 T.M. Knowlton, Standpipes and return systems; J.R. Grace et al., Circulating Fluidized Bed, Blackie academic & Professional, pp. 214-260, (1997)

22 C.M. Eleftheriades & M.R. Judd, The design of downcomers joining gas-fluidized beds in multistage systems; Powder Technology, 21, 217, (1978)

23 D. Geldard & N. Broodryk, Studies on the behavior of cyclone diplegs; Presented at the Annual Meeting of the AIChE, Los Angeles, CA. November, 18-21, (2001)

24 M. Stiess, Mechanische Verfahrenstechnik 2, pp. 8-16, Springer, (1997)

25 E. Muschelknauz et al., Zykone zur Abscheidung von Feststoffen aus Gasen; VDI-Wärmeatlas 7.Auflage, Lja1-11, (1984)

26 L.R. Glicksman, Experimental verification of scaling relationships for fluidized beds; Chemical Engineering Science, Vol.39, No.9, pp. 1373-1379, (1984)

27 http://inventors.about.com/library/inventors/blbasic.htm

28 , , 340, , (2003)

29 M. Pell & J.B Durson, Gas-solid operations and equipment; Perry et al., Perry's Chemical Engineers' Handbook 7th Edition, 17-29, McGraw-Hill, (1999)

30 S. Yuu et al., The reduction of pressure drop due to dust loading in a conventional cyclone; Chemical Engineering Science, Vol. 33, pp. 1573-1580, (1978)

31 L. Reh, Chemie- Ingenieur-Technik, 1, 319–329, (1978)

32 M. Stiess, Mechanishce Verfahrenstechnik2, ,pp348,Springer, (1997)

33 M. Zöhrer, Progress Report , AEE, (2005)

34 http://www.ntb.ch/Pubs/sensordemo/sensordatenbank_main_publik.html

35 M.P. Boyce, Transport and storage of fluids, Perry et al, Perry's Chemical Engineers' Handbook 7th Edition, 10-8, McGraw-Hill, (1999)

36 , Transport and storage of fluids; Perry et al., Perry's Chemical Engineers' Handbook 7th Edition, 10-15, McGraw-Hill, (1999)

# Appendix

## Sensor connecting layout

| Mat. No. | Description | Level [m] | Symbol | Output-signal | Corr. Curve | IMP No. | Chan. No. | Mat. No. | Power No. |
|---|---|---|---|---|---|---|---|---|---|
| | **Temperatures** | | | | | | | | |
| 2 | Roots pump : outflow (169 Ohm shunt) | | T602 | 0-100 °C --> 4-20 mA | 1 | 1 | 2 | 2 | 4/10 |
| 3 | Booster : outflow (169 Ohm shunt) | | T701 | 0-100 °C --> 4-20 mA | 1 | 1 | 3 | 3 | 4/11 |
| 4 | Secondary air | | T702 | 0-100 °C --> 4-20 mA | 2 | 1 | 16 | 4 | 4/12 |
| 5 | riser : cylinder (169 Ohm shunt) | | T111 | 0-100 °C --> 4-20 mA | 1 | 1 | 1 | 5 | 4/9 |
| | | | | | | | | | |
| 8 | Ref. Temp. IMP 1 | | Ref_1 | °C | | 1 | 18 | 8 | |
| 9 | Ref. Temp. IMP 2 | | Ref_2 | °C | | 2 | 18 | 9 | |
| 10 | Ref. Temp. IMP 3 | | Ref_3 | °C | | 3 | 20 | 10 | |
| | | | | | | | | | |
| 11 | FHE : outflow | | T411 | 0-100 °C --> 4-20 mA | 2 | 1 | 4 | 11 | 4/5 |
| 12 | FHE : inflow | | T412 | 0-100 °C --> 4-20 mA | 2 | 1 | 5 | 12 | 4/6 |
| | | | | | | | | | |
| | **Static pressures:** | | | | | | | | |
| 20 | riser : wind box | | P101 | 0 - 250 mb --> 4-20 mA | 3 | 1 | 6 | 20 | 1/1 |
| 21 | riser : over gas distributing plate(c.chamber) | | P102 | 0 - 250 mb --> 4-20 mA | 3 | 1 | 7 | 21 | 1/2 |
| 22 | riser : conical part(c.chaber) | | P103 | 0 - 250 mb --> 4-20 mA | 3 | 1 | 8 | 22 | 1/3 |
| 23 | riser : conical part(c.chaber) | | P104 | 0 - 250 mb --> 4-20 mA | 3 | 1 | 9 | 23 | 1/4 |
| 24 | riser : conical part(c.chaber) | | P105 | 0 - 250 mb --> 4-20 mA | 3 | 1 | 10 | 24 | 1/5 |
| 25 | riser : cylinder | | P106 | 0 - 250 mb --> 4-20 mA | 3 | 1 | 11 | 25 | 1/6 |
| 26 | riser : cylinder | | P107 | 0 - 250 mb --> 4-20 mA | 3 | 1 | 12 | 26 | 1/7 |
| 27 | riser : cylinder end | | P108 | 0 - 250 mb --> 4-20 mA | 3 | 1 | 13 | 27 | 1/8 |
| 28 | seconadary air-1 | | P109 | 0 - 250 mb --> 4-20 mA | 3 | 1 | 14 | 28 | 3/3 |
| 29 | secondary air-2 | | P110 | 0 - 250 mb --> 4-20 mA | 3 | 1 | 15 | 29 | 3/5 |
| 30 | cyclone inlet | | P201 | 0-50 mb --> 1,841-8,034 V | 1 | 2 | 1 | 30 | 4/13 |
| 31 | cyclone outlet | | P202 | 0-50 mb --> 1,712-8,048 V | 1 | 2 | 2 | 31 | 4/14 |
| 32 | Sihpon : wind box | | P301 | 0 - 250 mb --> 4-20 mA | 3 | 2 | 3 | 32 | 3/7 |
| 33 | Siphon: Liftleg top | | P302 | 0 - 250 mb --> 4-20 mA | 3 | 2 | 4 | 33 | 3/8 |
| 34 | Siphon : Downleg (Profil) variable | | P303 | 0 - 250 mb --> 4-20 mA | 3 | 2 | 6 | 34 | 3/9 |
| 35 | Siphon : Downleg (Profil) | | P304 | - | - | - | - | 35 | |
| 36 | Siphon: Downleg (Profil) | | P305 | - | - | - | - | 36 | |
| 37 | Siphon: Downleg (Profil) Eintritt | | P306 | - | - | - | - | 37 | |
| 38 | FHE : Wind box | | P401 | 0 - 1000 mb --> 4-20 mA | 4 | 2 | 10 | 38 | 2/1 |
| 39 | FHE : Windbox | | P402 | 0 - 1000 mb --> 4-20 mA | 4 | 2 | 11 | 39 | 2/2 |
| 40 | FHE : Windbox | | P403 | 0 - 1000 mb --> 4-20 mA | 4 | 2 | 12 | 40 | 2/3 |
| 41 | FHE : empty chamber | | P404 | 0 - 1000 mb --> 4-20 mA | 4 | 2 | 13 | 41 | 2/4 |
| 42 | FHE : 1st heating chamber , top | | P405 | 0 - 1000 mb --> 4-20 mA | 4 | 2 | 14 | 42 | 2/5 |
| 43 | FHE : 1st heating chamber | | P406 | 0 - 1000 mb --> 4-20 mA | 4 | 2 | 15 | 43 | 2/6 |
| 44 | FHE : 1st heating chamber | | P407 | 0 - 1000 mb --> 4-20 mA | 4 | 3 | 1 | 44 | 2/7 |
| 45 | FHE : 1st heating chamber | | P408 | 0 - 1000 mb --> 4-20 mA | 4 | 3 | 2 | 45 | 2/8 |
| 46 | FHE : 1st heating chamber | | P409 | 0 - 1000 mb --> 4-20 mA | 4 | 3 | 3 | 46 | 2/9 |
| 47 | FHE : 2nd heating chamber | | P410 | 0 - 1000 mb --> 4-20 mA | 4 | 3 | 4 | 47 | 3/1 |
| 48 | Filter : outflow | | P501 | 0-50 mb --> 1,842-8,168 V | 1 | 3 | 5 | 48 | 4/15 |
| 49 | Rootsv pump : outflow | | P601 | 0 - 1000 mb --> 4-20 mA | 4 | 3 | 6 | 49 | 3/2 |
| | | | | | | | | | |

| | | | | | | | | | |
|---|---|---|---|---|---|---|---|---|---|
| | **Differential pressures:** | | | | | | | | |
| 55 | primary air | 4,2 m, VW | Dp112 | 0 - 50 mb --> 4-20 mA | 5 | 3 | 7 | 55 | 4/1 |
| 56 | secondary air-1 | 19 m, VW | Dp113 | 0 - 50 mb --> 4-20 mA | 5 | 3 | 8 | 56 | 3/4 |
| 57 | secondary air-2 | | Dp114 | 0 - 50 mb --> 4-20 mA | 5 | 3 | 9 | 57 | 3/6 |
| 58 | FHE : empty chamber | | Dp413 | 0 - 50 mb --> 4-20 mA | 5 | 3 | 10 | 58 | 4/2 |
| 59 | FHE : 1st heating chamber | | Dp414 | 0 - 50 mb --> 4-20 mA | 5 | 3 | 11 | 59 | 4/3 |
| 60 | FHE : 2nd heating chamber | | Dp415 | 0 - 50 mb --> 4-20 mA | 5 | 3 | 12 | 60 | 4/4 |
| | | | | | | | | | |
| | | | | | | | | 0 | |
| | **Calculation:** | | | | | | | | |
| 70 | primary air | | F112 | m³/h | - | - | - | 70 | |
| 71 | secondary air-1 | | F113 | m³/h | - | - | - | 71 | |
| 72 | secondary air-2 | | F114 | m³/h | - | - | - | 72 | |
| 74 | FHE : 1st heating chamber | | F414 | m³/h | - | - | - | 74 | |
| 75 | FHE : 2nd heating chamber | | F415 | m³/h | - | - | - | 75 | |

## Calculation of pressure drop in the cylcone

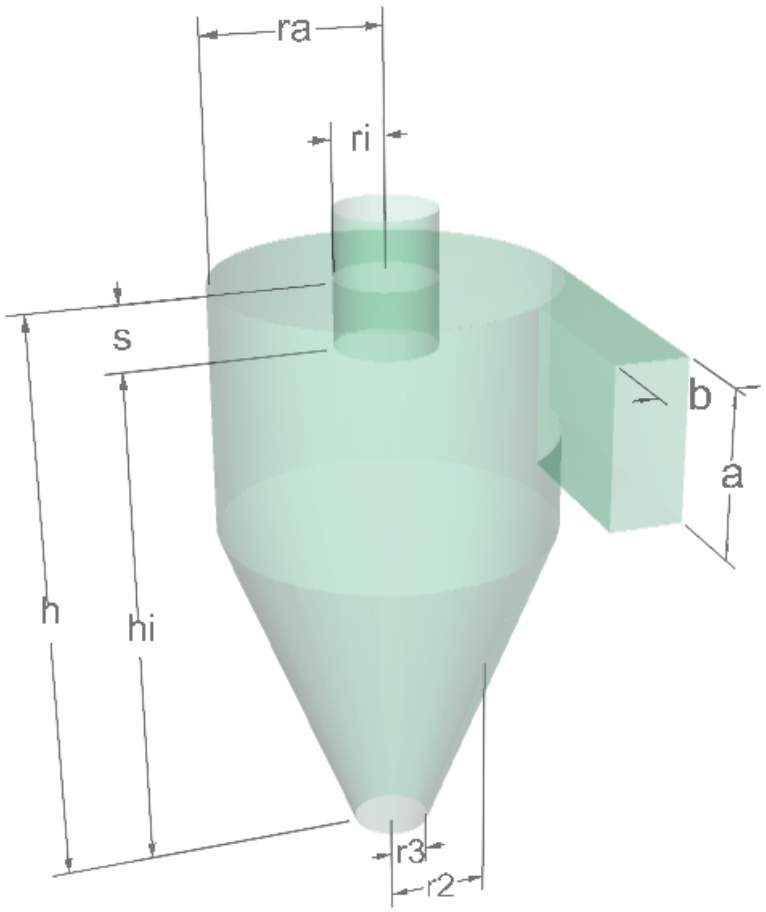


**Fig.** Nomenclature for the cyclone

### Geometrical values of the cyclone

| | Nomenclature | Values [m] |
|---|---|---|
| Radius of vortex tube | $r_i$ | 0.0975 |
| Radius of vessel | $r_a$ | 0.24 |
| Width of inlet | b | 0.105 |
| Height of inlet | a | 0.325 |
| Radius of particle outlet | $r_3$ | 0.055 |
| Height of cyclone | h | 1.02 |
| Mean inlet radius | $r_e(=r_a-b/2)$ | 0.1875 |
| Radius of cone at half height | $r_2(=(r_3+r_a)/2)$ | 0.1475 |
| Total surface area of cyclone | $A_R$ | 1.1551 |
| Relative width of cyclone inlet | $\beta(=b/r_a)$ | 0.4375 |

## Experimental data

| | $\dot{V}_g$ [m³/h] | $\dot{V}_g$ [m³/s] | $u_e$ [m/s] | $\dot{m}_g$ [kg/s] | $\dot{m}_p$ [kg/s] | $\mu_e(\dot{m}_g/\dot{m}_p)$ [] |
|---|---|---|---|---|---|---|
| 40/50/109/0 | 737.02 | 0.20 | 1.13 | 0.24 | 0.00 | 0.00 |
| 40/75/109/0 | 1071.43 | 0.30 | 1.64 | 0.35 | 0.00 | 0.00 |
| 40/100/109/0 | 1433.16 | 0.40 | 2.20 | 0.47 | 0.00 | 0.00 |
| 40/120/109/0 | 1716.16 | 0.48 | 2.63 | 0.56 | 0.00 | 0.00 |
| 40/50/109/25 | 730.72 | 0.20 | 1.12 | 0.24 | 0.03 | 0.14 |
| 40/75/109/25 | 1100.01 | 0.31 | 1.69 | 0.36 | 0.30 | 0.85 |
| 40/100/109/25 | 1456.92 | 0.40 | 2.24 | 0.48 | 0.58 | 1.21 |
| 40/120/109/25 | 1746.88 | 0.49 | 2.68 | 0.57 | 0.66 | 1.16 |
| 40/50/109/50 | 740.78 | 0.21 | 1.14 | 0.24 | 0.21 | 0.86 |
| 40/75/109/50 | 1103.02 | 0.31 | 1.69 | 0.36 | 0.60 | 1.67 |
| 40/100/109/50 | 1473.20 | 0.41 | 2.26 | 0.48 | 0.81 | 1.69 |
| 40/125/109/50 | 1765.03 | 0.49 | 2.71 | 0.58 | 0.91 | 1.57 |
| 40/50/109/75 | 751.92 | 0.21 | 1.15 | 0.25 | 0.26 | 1.06 |
| 40/75/109/75 | 1104.49 | 0.31 | 1.70 | 0.36 | 0.86 | 2.39 |
| 40/100/109/75 | 1461.76 | 0.41 | 2.24 | 0.48 | 1.54 | 3.21 |
| 40/120/109/75 | 1732.26 | 0.48 | 2.66 | 0.57 | 1.66 | 2.93 |
| 40/50/109/100 | 718.34 | 0.20 | 1.10 | 0.23 | 0.23 | 0.98 |
| 40/75/109/100 | 1112.34 | 0.31 | 1.71 | 0.36 | 1.03 | 2.82 |
| 40/100/109/100 | 1470.83 | 0.41 | 2.26 | 0.48 | 1.89 | 3.94 |
| 40/120/109/100 | 1754.11 | 0.49 | 2.69 | 0.57 | 2.03 | 3.54 |

Where

| | |
|---|---|
| $\dot{V}_g$ | volumetric flow rate of gas |
| $u_e$ | superficial velocity at cyclone inlet |
| $\dot{m}_g$ | mass flow rate of gas calculated from $\dot{V}_g$ |
| $\dot{m}_p$ | mass flow rate of particle in inflow |
| $\mu_e$ | particle loading ratio |

## Coefficient

From the equations for expansion/contraction coefficient (α)

$$\alpha = \frac{1-\sqrt{1+4\left[\left(\frac{\beta}{2}\right)^2-\frac{\beta}{2}\right]\sqrt{1-\frac{1-\beta^2}{1+\mu}\left(2\beta-\beta^2\right)}}}{r_a}$$

and the friction coefficient for a simplified calculation;

μ<1 $\lambda = 0.005(1+2\sqrt{\mu})$

μ>1 $\lambda = 0.005(1+3\sqrt{\mu})$

Note that $\lambda_0$ is 0.005 for assumption

The calculated data are following:

| | α | λs |
|---|---|---|
| 40/50/109/0 | 0.601662 | 0.005 |
| 40/75/109/0 | 0.601662 | 0.005 |
| 40/100/109/0 | 0.601662 | 0.005 |
| 40/120/109/0 | 0.601662 | 0.005 |
| 40/50/109/25 | 0.654924 | 0.0088 |
| 40/75/109/25 | 0.790728 | 0.0142 |
| 40/100/109/25 | 0.825449 | 0.0215 |
| 40/120/109/25 | 0.821153 | 0.0211 |
| 40/50/109/50 | 0.792423 | 0.0143 |
| 40/75/109/50 | 0.856138 | 0.0244 |
| 40/100/109/50 | 0.856827 | 0.0245 |
| 40/125/109/50 | 0.850507 | 0.0238 |
| 40/50/109/75 | 0.812316 | 0.0204 |
| 40/75/109/75 | 0.886693 | 0.0282 |
| 40/100/109/75 | 0.908938 | 0.0319 |
| 40/120/109/75 | 0.902264 | 0.0307 |
| 40/50/109/100 | 0.805515 | 0.0149 |
| 40/75/109/100 | 0.899565 | 0.0302 |
| 40/100/109/100 | 0.922335 | 0.0348 |
| 40/120/109/100 | 0.915477 | 0.0332 |

**Required velocities for the calculation of pressure drop in the cyclone**

The equation for the gas velocity in a cyclone inlet($v_e$):

$$v_e = \frac{\dot{V}}{ab}$$

The tangential velocity at $r_a$ can be calculated with gas velocity:

$$u_a = \frac{v_e r_e / r_a}{\alpha}$$

The tangential velocity at $r_i$ :

$$u_i = \frac{u_a r_a / r_i}{1 + \frac{\lambda}{2}\frac{A_R}{\dot{V}} u_a \sqrt{r_a / r_i}}$$

and mean axial velocity in a vortex tube:

$$v_i = \frac{\dot{V}}{\pi r_i^2}$$

Then,

| | $v_e$ | $u_a$ | $u_i$ | $v_i$ |
|---|---|---|---|---|
| 40/50/109/0 | 6.00 | 7.79 | 12.85 | 6.86 |
| 40/75/109/0 | 8.72 | 11.32 | 18.68 | 9.97 |
| 40/100/109/0 | 11.67 | 15.15 | 24.99 | 13.33 |
| 40/120/109/0 | 13.97 | 18.14 | 29.92 | 15.96 |
| 40/50/109/25 | 5.95 | 7.10 | 12.03 | 6.80 |
| 40/75/109/25 | 8.95 | 8.85 | 15.84 | 10.23 |
| 40/100/109/25 | 11.86 | 11.22 | 20.33 | 13.55 |
| 40/120/109/25 | 14.22 | 13.53 | 24.47 | 16.25 |
| 40/50/109/50 | 6.03 | 5.94 | 10.65 | 6.89 |
| 40/75/109/50 | 8.98 | 8.19 | 12.67 | 10.26 |
| 40/100/109/50 | 11.99 | 10.93 | 16.90 | 13.70 |
| 40/125/109/50 | 14.37 | 13.20 | 20.55 | 16.42 |
| 40/50/109/75 | 6.12 | 5.89 | 9.53 | 6.99 |
| 40/75/109/75 | 8.99 | 7.92 | 11.75 | 10.27 |
| 40/100/109/75 | 11.90 | 10.23 | 14.57 | 13.60 |
| 40/120/109/75 | 14.10 | 12.21 | 17.63 | 16.11 |
| 40/50/109/100 | 5.85 | 5.67 | 10.08 | 6.68 |
| 40/75/109/100 | 9.05 | 7.86 | 11.41 | 10.35 |
| 40/100/109/100 | 11.97 | 10.14 | 14.01 | 13.68 |
| 40/120/109/100 | 14.28 | 12.18 | 17.11 | 16.32 |

Finally the pressure drop occurs both in the vessel and in the vortex tube.
Therefore, from the equations (1.6-2) and (1.6-3),

$$\Delta p_e = -\lambda \frac{A_R}{0.9\dot{V}} \frac{\rho_g}{2} (u_a u_i)^{3/2}$$

and

$$\Delta p_i = -\left[ 2 + 3\left(\frac{u_i}{v_i}\right)^{4/3} + \left(\frac{u_i}{v_i}\right)^2 \right] \frac{\rho_g}{2} v_i^2$$

From the equation for the total pressure drop in the cyclone (1.6-1) is :

$$\Delta p_{total} = \Delta p_e + \Delta p_i$$

**Calculated pressure drop:**

| | $\Delta p_e$ | $\Delta p_i$ | Δp total [Pa] | Δp total [mbar] |
|---|---|---|---|---|
| 40/50/109/0 | 18.47 | 344.21 | 362.68 | 3.63 |
| 40/75/109/0 | 39.04 | 727.41 | 766.45 | 7.66 |
| 40/100/109/0 | 69.85 | 1301.50 | 1371.35 | 13.71 |
| 40/120/109/0 | 100.16 | 1866.26 | 1966.41 | 19.66 |
| 40/50/109/25 | 25.70 | 314.01 | 339.71 | 3.40 |
| 40/75/109/25 | 58.24 | 601.94 | 660.18 | 6.60 |
| 40/100/109/25 | 138.22 | 1016.29 | 1154.51 | 11.55 |
| 40/120/109/25 | 198.04 | 1467.86 | 1665.91 | 16.66 |
| 40/50/109/50 | 26.41 | 272.46 | 298.88 | 2.99 |
| 40/75/109/50 | 63.65 | 464.74 | 528.40 | 5.28 |
| 40/100/109/50 | 113.47 | 827.52 | 941.00 | 9.41 |
| 40/125/109/50 | 163.85 | 1207.65 | 1371.50 | 13.72 |
| 40/50/109/75 | 30.99 | 241.35 | 272.33 | 2.72 |
| 40/75/109/75 | 62.31 | 428.36 | 490.67 | 4.91 |
| 40/100/109/75 | 107.90 | 700.39 | 808.29 | 8.08 |
| 40/120/109/75 | 151.96 | 1005.06 | 1157.02 | 11.57 |
| 40/50/109/100 | 24.43 | 248.85 | 273.28 | 2.73 |
| 40/75/109/100 | 62.74 | 417.95 | 480.69 | 4.81 |
| 40/100/109/100 | 108.84 | 676.76 | 785.60 | 7.86 |
| 40/120/109/100 | 155.05 | 986.45 | 1141.49 | 11.41 |

## Target values for the Cu particle tests

| the ratio of primary air in the total supplied fluidization air in CFB | load factor | Normal volumetric flow rate [Nm³/h] | | | | | |
|---|---|---|---|---|---|---|---|
| | | CFB total | primary air | secondary air-1 | secondary air-2 | FHE | Siphon |
| 30 | 50 | 721 | 216 | 62 | 319 | 109 | 12 |
| | 75 | 1082 | 325 | 108 | 529 | 109 | 12 |
| | 100 | 1443 | 433 | 151 | 738 | 109 | 12 |
| | 120 | 1731 | 519 | 186 | 906 | 109 | 12 |
| 40 | 50 | 721 | 289 | 53 | 259 | 109 | 12 |
| | 75 | 1082 | 433 | 90 | 439 | 109 | 12 |
| | 100 | 1443 | 577 | 127 | 619 | 109 | 12 |
| | 120 | 1731 | 692 | 156 | 762 | 109 | 12 |
| 50 | 50 | 721 | 361 | 41 | 200 | 109 | 12 |
| | 75 | 1082 | 541 | 72 | 349 | 109 | 12 |
| | 100 | 1443 | 721 | 102 | 499 | 109 | 12 |
| | 120 | 1731 | 866 | 127 | 619 | 109 | 12 |

| the ratio of primary air in the total supplied fluidization air in CFB | load factor | Operating volumetric flow rate [Bm³/h] | | | | | | velocity [m/s] |
|---|---|---|---|---|---|---|---|---|
| | | CFB total | primary air | secondary air-1 | secondary air-2 | FHE | Siphon | In the riser |
| 30 | 50 | 838 | 223 | 69 | 337 | 102 | 15 | 1.3 |
| | 75 | 1257 | 334 | 114 | 559 | 102 | 15 | 1.9 |
| | 100 | 1676 | 446 | 160 | 780 | 102 | 15 | 2.5 |
| | 120 | 2011 | 535 | 196 | 957 | 102 | 15 | 3 |
| 40 | 50 | 838 | 297 | 56 | 274 | 102 | 15 | 1.3 |
| | 75 | 1257 | 446 | 95 | 464 | 102 | 15 | 1.9 |
| | 100 | 1676 | 594 | 134 | 653 | 102 | 15 | 2.5 |
| | 120 | 2011 | 713 | 165 | 805 | 102 | 15 | 3 |
| 50 | 50 | 838 | 371 | 43 | 211 | 102 | 15 | 1.3 |
| | 75 | 1257 | 557 | 76 | 369 | 102 | 15 | 1.9 |
| | 100 | 1676 | 743 | 108 | 527 | 102 | 15 | 2.5 |
| | 120 | 2011 | 891 | 134 | 653 | 102 | 15 | 3 |

## VBA source code

```
Private Sub CommandButton2_Click()                    'coded by Mark Read
Dim a As String
Dim c
Dim Zeichen1
Dim interval
Dim start, finish

restart:                                    'return point

Worksheets("Input").Activate                        'activate table "Input"
Worksheets("Input").Range("a7").Select              'put cursor in "A7"
Open "c:\Hpbasic\Daten\Exceldat" For Input As #1    'Open HP-Basic file for reading
Open "c:\Hpbasic\Daten\Exceldat2" For Output As #2          'Open new file for writing

Do While Not EOF(1)                                 'loop until data end
   Zeichen1 = Input(1, #1)                  'read one letter

   Select Case Zeichen1
   Case ","
      Zeichen1 = "."
      Print #2, Zeichen1;                   'write character on SAME line
   Case ";"
      Zeichen1 = ""
      Print #2, Zeichen1                    'write character on NEW line
   Case Else
      Print #2, Zeichen1;                   'value or text - write on SAME (;) line
   End Select
Loop                                        'go back to "do"

Close #1                                            'close input file
Close #2                                            'close output file
Open "c:\Hpbasic\Daten\Exceldat2" For Input As #2            'open new file for reading
For c = 1 To 80                                     'loop through data
```

See the ‘source.txt’ file on the enclosed CD for the Basic source code.